QUALITY BY DESIGN FOR CONTINUOUS POWDER MIXING

by

PATRICIA MARIBEL PORTILLO

A Dissertation submitted to the

Graduate School-New Brunswick

Rutgers, The State University of New Jersey

In partial fulfillment of the requirements

For the degree of

Doctor of Philosophy

Graduate Program in Chemical and Biochemical Engineering

Written under the direction of

Professors Marianthi G. Ierapetritou and Fernando J. Muzzio

And approved by

_____

_____

_____

_____

New Brunswick, New Jersey

May, 2008

ABSTRACT OF THE DISSERTATION

Quality by Design for Continuous Powder Mixing

By PATRICIA MARIBEL PORTILLO

Dissertation Directors:
Marianthi G. Ierapetritou and Fernando J. Muzzio

The main target of our research is to investigate powder mixing, particularly continuous mixing. Continuous mixing is considered as an efficient alternative to batch mixing processes that in principle allows for easier on-line control and optimization of mixing performance. In order to illustrate the benefits of this process we have demonstrated the effectiveness of continuous mixing for powders. A number of operating and design parameters including processing angle, rotation rate, fill level, convective design, APAP concentration, and residence time have been investigated to consider their effects on mixing performance and on the content uniformity. Statistical analysis has been applied to examine the significance of the effects of processing parameters and material properties on the mixing rate. In addition to mixing experiments, the particle trajectory within a continuous mixer has been studied for different cohesion levels, flowrates, and rotation rates using Positron Emission Particle Tracking (PEPT). The approach was beneficial in providing particle trajectories and, as a result, allowing us to obtain axial dispersion coefficients quantitatively. The experimental methods have been

used to verify computational approaches as well as study some important areas that are difficult to examine experimentally such as online homogeneity measurements.

Notably, powder-mixing models are restricted due to computational limitations and obstacles associated with correlating simulation-time to real-time. We have developed efficient modeling approaches that will enable the simulation, optimization, and control of mixing processes. One method is compartment modeling, a method that discretizes the blender into finite regions. We have adapted the approach to mixing processes (v-blender, a horizontal drum, and continuous blenders). Another approach we propose is the use of a hybrid methodology that utilizes compartment modeling and the Discrete Element Method. The effectiveness of the methodology will be demonstrated by modeling particle mixing under the influence of an impeller in the continuous blender, which for usual modeling methods typically lead to extremely high computational costs.

Acknowledgement and Dedication

This work was made possible by the financial support of the Nanopharmaceutical IGERT Fellowship and the NSF Engineering Research Center on Structured Organic Particulate Systems. I would not have been able to complete this work without the guidance and resources provided by both of my advisors Marianthi G. Ierapetritou and Fernando J. Muzzio. Marianthi and Fernando have both been role models to me and have been responsible for my growth as a researcher. I wish to thank Marianthi for her supervision in the beginning and always being supportive when I was in need. I am very grateful to Fernando for also taking the time to improve my work as well as the opportunities to go Birmingham, England, attend NSF meetings, and participate in NSF advocacy with congressional staff. From the summer of 2005, I have had the pleasure to work with several undergraduates whom I would like to acknowledge: Warren Schmidt, Roentgen Hau, Hiral Parikh, Shiny Eapen, and Maggie Feinberg. I also would like to thank my committee members: Professor Benjamin Glasser for his time, careful review of my work, and suggestions. Professor Jonathan Seville for allowing me to work in the PEPT laboratory at the University of Birmingham and taking the time to be a part of my defense committee. I would also like to acknowledge the following graduate students and post-docs for teaching me particular methods and their helpful advice: Ipsita Banerjee, Aditya Bindal, Mobeen Faqih, Amit Mehrotra, Bodhi Chaudhuri, and Andy Ingram. Margaret Julius for her wonderful friendship in graduate school and Hong Yang for her great company in the lab.

I want to thank my parents, Julio and Sandra Portillo for never pressuring me, their unconditional support, and being the best parents anyone can ask for. Thanks to my brother, Julio Portillo Jr., for constantly fixing my old used cars, without him I would not

have transportation or a good sense of humor. My grandmother, Vidalia Ruano for her love and constantly helping so I could study. Undoubtedly, I would not have been able to get this degree without the support of my husband, Tom Brieva. He pursued me to go to graduate school, helped me along the way, and advised me to think independently. I am very thankful to God for giving me the ability to go to school and blessing me with these people and great opportunities in my life.

TABLE OF CONTENTS

Lists of Tables

List of Illustrations

Chapter 1

Introduction

1.1 Motivation

The main target of our research is to investigate continuous mixing as an effective method for powder mixing. Continuous mixing is considered as an efficient alternative to batch mixing processes that allows for on-line control and optimization of mixing performance. Toward this objective we have identified the following specific aims:

Specific Aim 1: Demonstrate the effectiveness of continuous mixing for powders using a continuous mixing process. A number of operating and design parameters including residence time, rotation rate, processing angle, convective design, and feed variability, will be investigated to consider their effects on mixing performance.

Specific Aim 2: Apply a quality by design approach using statistical analysis to examine the impact of all the processing parameters and minimize the number of parameters to be examined in detail. This allows the design parameters to be focused on minimizing in-homogeneities in the system output stream.

Specific Aim 3: Develop efficient modeling approaches that will enable the simulation of powder mixing processes. Notably, powder mixing models are restricted due to computational limitations and obstacles associated with correlating simulation-time to real-time. Thus, we are proposing the use of a compartment model and a hybrid methodology that utilizes compartment modeling to simulate the areas within the mixing system that do not require a detailed description and the Discrete Element Method for the areas where a more comprehensive description is needed (for example areas around the impeller). The effectiveness of the proposed methodologies will be demonstrated by

modeling mixing within continuous blenders, which for pre-existing modeling methods typically lead to extremely high computational costs.

1.2 Powder Mixing

Powder mixing has been the subject of substantial research, motivated by applications in a variety of industrial sectors including pharmaceuticals, food, ceramics, catalysts, metals, and polymer manufacturing. Understanding mixing mechanisms and identifying critical process and material parameters is often a crucial step during process development. In the pharmaceutical context, inefficient blending can lead to increased variability of the active component, threatening the health of patients. Content uniformity problems have four main root causes: (i) Weight variability in the finished dose, which is often related to flow properties of the powder stream, (ii) poor equipment design or inadequate operation, (iii) particle segregation (driven by differences in particle properties), and (iv) particle agglomeration, driven by electrostatics, moisture, softening of low melting point components, etc.

A perennial concern in pharmaceutical process development is the scale-up of mixing operations. Process scale-up can drastically reduce production costs, but in order to change scale reliably, the effects of powder manufacturing processing parameters on the properties of intermediate and finished product properties must be known. In many cases, for a new powder formulation, processing conditions are thoroughly examined at small scales during process development. However, the design and scale up of blending operations is essentially multivariate: when the blending process is transferred to a larger scale for manufacturing purposes, the relative magnitudes of shear, dispersion, and convective forces can be altered.

This issue is particularly important because several critical variables such as shear rate and total strain, which are known to affect blend microstructure (and, consequently, degree of ingredient agglomeration, blend flow properties, and finished product hardness and dissolution) are usually not addressed by any of the usual criteria during blender scale-up. This can lead to failures during scale-up; for example, if the intensity of shear (per revolution of blender) increases during scale-up, a frequent undesired result is blend over-lubrication. In engineering mechanics, shear rate is a measure of the rate of shear deformation (deformation is a change in shape) due to an applied force. Shear rate is calculated as the magnitude of the velocity gradient in a flowing material. Process parameters such as rotation rates affect the shear rate since a powder experiences faster shear in a given time interval. The rate of which powder is blended affects the velocity gradient in the blender and was found to change degree of homogeneity (Arratia *et al.*, 2006). The effect of the velocity gradient is also affected by the powder cohesion, because interparticle forces vary the powder bed density by dilation, affecting subsequent tableting and capsule filling stages.

1.3 Batch Mixing

One of the most common processes used in the pharmaceutical industry is batch mixing in tumbling blenders. Optimization of the blending process requires an understanding of mechanisms and critical variables. Although powder cohesion and mixer size and geometry may not be modifiable due to other constraints, operating conditions such as rotation rate and fill level are often easier to modify. Thus, an understanding of interactions among variables is essential.

V-blenders, tote-blenders, and double-cone blenders are examples of batch blenders that vary in geometric design. For these systems, variables such as mixer size and fill level can affect mixing behavior (Alexander *et al.*, 2001; Alexander *et al.*, 2003; Sudah *et al.*, 2002a). Mixing in tumbling blenders is often limited by component segregation, usually caused by variations in particle characteristics such as size or shape (Alexander *et al.*, 2004). The effects of tote size have previously been examined, and it has been shown that the mixing performance was more significantly affected for cohesive than a free-flowing pharmaceutical formulations (Sudah *et al.*, 2002b). A number of process problems are caused by cohesive phenomena, for example, when inter-particle forces result in API agglomeration. In previous experimental studies Top/Bottom and Left/Right starting configurations of the API and excipients affected the mixing rate (Muzzio *et al.*, 2004).

Brone and coworkers (1998) examined the effect of changing the rotation rate from 8 to 24 rpm for glass beads in a V-blender. This study illustrated that for such free flowing materials, increasing the rotation rate did not change the mixing mechanism but did reduce the total mixing time. In addition, Sudah and coworkers (2002b) varied the rotation rate from 5 to 15 rpm for art sand in a rectangular tote blender, demonstrating that in earlier stages of the mixing process (up to 64 revolutions of the blender) the mixing rate (per revolution) was not affected by rotation rate, but the effect of rotation rate affected the asymptotic variance plateau (total achievable homogenization). The studies also showed that for a cohesive blend, rotating the vessel at 10 rpm resulted in the smallest asymptotic variance, suggesting the presence of competing mechanisms. Later

on, Arratia and coworkers (2006) examined the effects of blender fill level, finding that for a Bohle-Bin blender, the higher the fill level, the slower the mixing rate.

Thus, in summary, the main variables known to affect mixing performance include: (1) the design of the mixing system, (2) its size, (3) the fill level employed, (4) the blender loading mode, (5) the speed of rotation of the blender, and (6) the material properties of the ingredients being mixed (particle size, shape, and density, etc.) typically affecting either the nature of the flow and the mixing rate through cohesive interactions, or the final homogeneity through segregation tendencies.

1.4 Continuous Mixing

Powder mixing is crucial for many processing stages within the pharmaceutical, catalysis, food, cement, and mineral industries, to name a few. A significant problem hindering process design is the paucity of information about the effects of changing process parameters on mixing efficiency (Laurent and Bridgwater, 2002d). The main target of this research is to investigate continuous mixing, examining the effects of different process and design parameters. Interestingly, continuous processing has been utilized extensively by petrochemical, food, and chemical manufacturing but has yet to reach the pharmaceutical industry to a meaningful extent. Recent research efforts indicate that a well-controlled continuous mixing process illustrates the capability of scale-up and ability to integrate on-line control ultimately enhancing productivity significantly (Muerza *et. al*, 2002; Marikh *et. al*, 2005).

Previous studies on continuous mixing include the work for zeolite rotary calciners (Sudah *et al.*, 2002c), chemical processes (SiC or Irgalite and $Al(OH)_3$) (Weinekötter and Reh, 1994), food processes (Couscous/Semolina) (Marikh *et al.*, 2005),

and a pharmaceutical system ($CaCO_3$ - Maize Starch) (Kehlenbeck and Sommer, 2003). Prior work points to the fact that a batch system that can be run in continuous mode can be expected to possess similar mixing mechanisms (Williams, 1976; Pernenkil and Cooney, 2006). This is because in continuous blending systems, a net axial flow is superimposed on the existing batch system to yield a continuous flow.

Williams and Rahman (1971a) proposed a numerical method to predict the Variance Reduction Ratio (VRR), a performance measurement of continuous mixing. The method utilizes results obtained from a residence time distribution test for an "ideal" and "non-ideal" mixer. The ideality of the mixer was defined by a mixing efficiency proposed by Beaudry (1948). Unlike the mixing apparatus presented in this work, the mixing mechanism was the horizontal drum rotating. In another publication Williams and Rahman (1971b) investigated their numerical method using a salt/sand formulation of different compositional ratios. They validated the predicted VRR with experiments and suggested that the results where comparable although replicating the experiments varied by 10-20%. They also illustrated that the drum speed and VRR were directly correlated, but as the speed escalated over 120 revolutions per minute the VRR began to descend as drum speed increased. Williams (1976) reviewed the previous work examining the mixing performance using variance reduction ratio (VRR) and recognized that additional work was needed considering different materials.

Harwood *et al.* (1975) studied the performance of seven continuous mixers as well as the outflow sample size effect of sand and sugar mixtures. Their objective was to develop a method to predict mixing performance by applying an impulse disturbance. They investigated the mixing performance of different convective mixers and sample

sizes, although no correlations were proposed. Weinekötter and Reh (1995) introduced purposely-fluctuated tracers into the processing unit in order to examine how well the unit eliminated the feeding noise. In chapter 2 we examined a number of parameters including residence times, rotation rate, processing angle for two continuous mixers. Chapter 3 applied statistical analysis to the experimental results to determine the influence of the parameters on residence time and content uniformity.

Other studies have focused on the flow patterns formed by the different convective mechanisms within horizontal mixers. Laurent and Bridgwater (2002a) examined the flow patterns by using a radioactive tracer, which generated the axial and radial displacements as well as velocity fields with respect to time. Using the same approach, chapter 4 focuses particle mobility within a continuous mixer. Marikh *et al.* (2005) focused on the characterization and quantification of the stirring action that takes place inside a continuous mixer of particulate food solids where the hold up in the mixer was empirically related to the flow rate and the rotational speed.

1.5 Powder Mixing Models

Many industrial sectors rely heavily on granular mixing to manufacture a large variety of products. In the pharmaceutical industry, it is very important to ensure homogeneity of the product. The pharmaceutical industry is one of the most representative examples, where homogeneity is cited to ensure product quality and compliance with strict regulations. Modeling can play an important role in improving mixing process design by reducing mixing time as well as manufacturing cost, and ensuring product quality. The main difficulty in modeling powder-mixing processes is that granular materials are complex substances that cannot be characterized either as

liquids or solids (Jaeger and Nagel, 1992). Moreover, granular mixing can be described by multiple mixing regimes due to convection, dispersion, and shear (Gayle *et al.*, 1958). Fan *et al.* (1970) reviewed a number of publications where powder mixing is modeled in an attempt to reduce the production cost and improve product quality.

The existing approaches used to simulate granular material mixing processes can be categorized as 1) heuristic models, 2) models based on kinetic theory, 3) particle dynamic simulations, and 4) Monte Carlo simulations (Riley *et al.*, 1995). Geometric arguments and ideal mixing assumptions are some common features of heuristic models. Although these models can generate satisfactory results, they are restricted to batch processes and are case dependent (Hogg *et al.*, 1966; Thýn and Duffek, 1977). Kinetic–theory-based models are used to simulate mixtures of materials with different mechanical properties (size, density and/or restitution coefficient), where each particle group is considered as a separate phase with different average velocity and granular energy. These models typically address shear flow of binary and ternary mixtures based on the kinetic theory of hard and smooth spherical particles (Jenkins and Savage, 1983; Iddir *et al.*, 2005; Lun *et al.*, 1984). The main shortcoming of these models is that they focus on the microscopic interactions between particles, neglecting the effects due to convection and diffusion.

Particle dynamic simulations, which apply molecular dynamic concepts to study liquids and gases, are extensively used to simulate powder mixing (Zhou *et al.*, 2004; Yang *et al.*, 2003; Cleary *et al.*, 1998). A discrete element method (DEM) examines the interactions between solid particles with different physical properties, monitoring the movement of every single particle in the system. DEM proceeds by dividing the particles

in the system into discrete entities defined by their size and geometric location. The model is able to predict the collision probability of particle-particle interaction with every particle within the grid and neighboring grid. The collisions caused by the forces of the process are solved using the spring latch model Walton and Braun (1986). The main limitations of particle dynamic simulations are (a) the maximum number of particles required to model the system is restricted due to the computational complexity of the involved calculations, and (b) the lack of realistic particle morphology (Wightman *et al.*, 1998; Bertrand *et al.*, 2005).

Monte Carlo (MC) simulations begin with an initially random configuration, which is driven to an energetically feasible equilibrium. One limitation of such an approach is that it cannot provide information about time-dependent characteristics, since it does not follow a realistic dynamic trajectory.

In order to model granular mixing processes accurately and efficiently, we explore compartment modeling. Compartment modeling has been utilized in bioprocesses to study the effects of mixing in large-scale aerated reactors (Vrábel *et al.*, 1999) and stirred reactors (Cui *et al.*, 1996) with satisfactory results (both qualitatively and quantitatively). Curiously, this approach has not been used to model powder mixing. The main idea of compartment modeling is to spatially discretize the system into a number of homogeneous subsections containing a fixed number of particles. Discretizing also the time domain, a number of particles are allowed to flow from each compartment to the neighboring ones at each time step.

The main advantages of compartment modeling are that (a) it incorporates all associated forces responsible for particle movement within the vessel, using a flux term

that can be experimentally determined and (b) it allows the simulation of a large number of particles. Although the exact particle position cannot be determined the changes in composition can be captured by including the flow of particles entering and exiting each compartment. Chapters 5 will focus more on the details required and results obtained from Compartment Modeling for batch mixing processes and chapter 6 for continuous mixing processes. In cases where Compartment Modeling cannot be solely used, the hybrid methodology may serve as an alternative, the details of this approach can be found in chapter 7. In order to validate mixing models experimental information is needed, so in the next chapter we will identify and examine some process parameters and material effects for continuous mixers.

Chapter 2

Continuous Mixing Experiments

In this chapter, the two continuous mixing systems, the feeding mechanisms, and blend formulations are described. A number of studies illustrating the effects of the operating parameters, processing angle and rotation rate, on the residence time and mixing performance of the continuous mixers are examined. The effects of design parameters are discussed, and the effect of material properties on the mixing performance are investigated.

2.1 Continuous Mixer 1

Among emerging technologies for improving the performance of blending operations, continuous mixing (and continuous processing in general) currently commands enormous interest at Pharmaceutical companies. Continuous processing has numerous known advantages, including reduced cost, increased capacity, facilitated scale up, mitigated segregation, and more easily applied and controlled shear. However, development of a continuous powder blending process requires venturing into a process that has a large and unfamiliar parametric space.

2.1.1 Description

The continuous blender device used in this dissertation is shown in Figure 2.1.1. The mixer has a 2.2 KW motor power, rotation rates range from 78 revolutions per minute (RPM) at a high speed to 16 RPM at a low speed. The length of the mixer is .74 meters and the diameter is .15 meters. An adjustable number of flat blades are placed within the horizontal mixer. The length of each blade is .05 m and the width is .03.

Convection is the primary source of mixing, the components have to be radially mixed which is achieved by rotation of the impellers (Weinekötter and Reh, 1995). The convective forces arising from the blades drive the powder flow. As the blades rotate, the powders are mixed and agglomerates are broken up. The powders are fed at the inlet and removed from the outlet as illustrated in Figure 2.1.1. The powder is discharged through a weir in the form of a conical screen. This feature ensures that the agglomerates are hindered from leaving the mixer. Thus, by varying the mesh of this screen, different degrees of micro-homogeneity can be accomplished. The particulate clusters become lodged in the screen, were they are broken up by the last impeller, the one closest to the outflow, before exiting the blender.

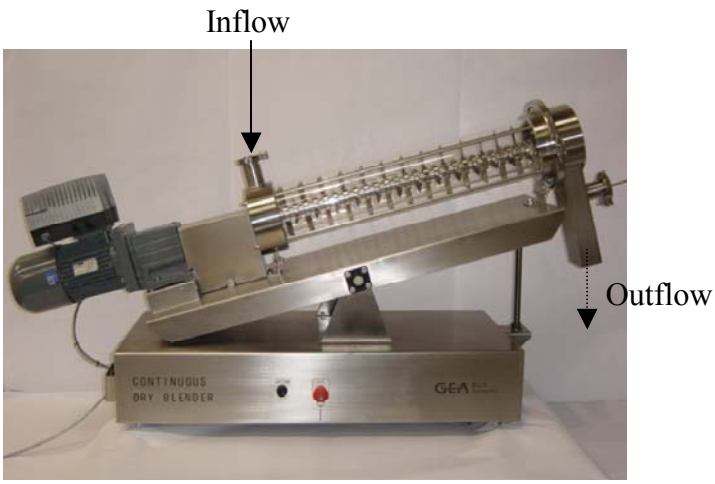

Figure 2.1.1: GEA Buck Systems Continuous Dry Blender

2.1.2 Feeding Mechanisms/Blend Formulations

Independent of the mixing performance, the outflow concentration may fluctuate due to the inflow composition variability. Thus it is crucial to ensure that the variability that exists in the feeding system be minimized so that the fluctuations that arise are handled within the mixer. In the system used in this study, the powder ingredients are fed using two vibratory powder feeders. The two vibratory feeders were manufactured by

Eriez and feed powder directly into the mixer inlet. Built-in dams and powder funnels were used to further control the feed rate of each feeder. Case studies consist of one active and one excipient.

Model blends have been formulated using the following materials: DMV Ingredients Lactose (100) (75-250mm), DMV International Pharmatose® Lactose (125) (55mm), and Mallinckrodt Acetaminophen (36mm). The compositions of the formulations used are as follows:

Formulation 1: Acetaminophen 3%, 97% Lactose 100.

Formulation 2: Acetaminophen 3%, 97% Lactose 125.

The formulation is split into two inflow streams both at the same mass flowrate. One flow stream supplies a mass composition of 6% Acetaminophen and 94% of Lactose and the other stream consists entirely of 100% Lactose. Both feeders are identical and process powders with a total a mass rate of 15.5 g/s with a standard deviation of 2.53 g/s. After the feed is processed, the material entering the mixer should contain: 3% Acetaminophen and 97% Lactose.

2.1.3 Continuous Mixer Characterization

The main mechanisms responsible for blending in a continuous mixer are the powder flow and the particle dispersion. Dispersion is the main driver for axial mixing, and the magnitude is dependent on the power input. In the case studies presented in this work two methods are used to characterize mixing, the residence time and the degree of homogeneity as described in the next sections.

2.1.3.1 Residence Time

The residence time distribution is an allocation of the time different elements of the powder flow remain within the mixer. To determine the residence time distribution, the following assumptions are made: (a) the particulate flow in the vessel is completely mixed, so that its properties are uniform and identical with those of the outflow as also noticed by Berthiaux *et al.* (2004) in their recent work; (b) the elements of the powder streams entering the vessel simultaneously, move through it with constant and equal velocity on parallel paths, and leave at the same time (Danckwerts, 1953).

In this study the residence time is measured as follows:

A quantity of a tracer substance is injected into the input stream; virtually instantaneous samples are then taken at various times from the outflow.

After the injection, the concentrations of the injected material in the exit stream samples are analyzed using Near Infrared (NIR) Spectroscopy (EL-Hagrasy *et al.*, 2001). Sample concentrations are expected to change since the tracer is fed at one discrete time point and not continuously.

The residence time distribution is determined both as a function of time and number of blade passes. The average number of blade passes is used to measure the shear intensity the powder experiences and its effect on blending and is measured using the following equation: $\eta=\omega\times\tau$ where η is the number of blade passes, ω is the impeller's rotation rate, and τ the mean residence time. The mean residence time is determined using the mass-weighted average of the residence time distribution.

2.1.3.2 Homogeneity

The effect of processing parameters on the homogeneity of the output steam is determined by analyzing a number of samples retrieved from the outflow as a function of time. The samples are analyzed to calculate the amount of tracer (in our case Acetaminophen) present in the sample using Near Infrared (NIR) Spectroscopy. The homogeneity of samples retrieved from the outflow is measured by calculating the variability in the samples tracer concentration. The Relative Standard Deviation (RSD) of tracer concentration measures the degree of homogeneity of the mixture at the sample:

$$RSD = \frac{\sqrt{\sum_{i=1}^{n} \frac{(X_i - \bar{X})^2}{n-1}}}{\bar{X}} \qquad (1)$$

where X_i is the sample tracer concentration retrieved at time point t_i; n is the number of samples taken; and $\bar{X}$ is the average concentration over all samples retrieved. Lower RSD values mean less variability between samples, which implies better mixing.

Another important characteristic of the mixer is to what extent variability of feed composition can be eliminated within the unit. In order to measure this characteristic, the Variance Reduction Ratio is used, which is defined as VRR = $\frac{\sigma_{in}^2}{\sigma_{out}^2}$, where σ_{in}^2 is the inflow variance calculated from samples collected at the entrance of the mixer, using the following equation:

$$\sigma^2 = \frac{1}{n}\sum_{i=1}^{n}(X_i - \bar{X})^2 \qquad (2)$$

σ_{out}^2, the outflow variance, is calculated collecting samples from outflow of the mixer and using equation 2. VRR is discussed in Danckwerts (1953) and Weinekötter and Reh

(2000). The larger the VRR, the more efficient the mixing system, since inflow fluctuations are reduced. As will be shown in the next section, both metrics (RSD and VRR) lead to the same conclusion regarding which parameters result in better mixing performance.

2.1.4 First Continuous Mixer – Results

The first continuous mixer used in this study has two operating parameters, processing angle and impeller rotation rate. The mixer's function is to simultaneously blend two or more inflow streams radially as the powder flows axially. Adjusting the mixer processing angle modifies the axial flow whereas the impeller's rotation rate results in higher shear rate, which affects the degree of material dispersion throughout the mixer. The following sections examine the effects of these two operating parameters in mixing performance of the mixer.

2.1.4.1 Processing Angle

Residence Time

Since axial flow is affected by adjusting the processing angle it is reasonable to assume that the residence time distribution will also be changed. The residence time distribution of Acetaminophen was determined for three processing angles (shown in Figure 2.1.2) and two rotation rates. The residence time distribution curves are shown in Figures 2.1.3a for the higher RPM and 3b at the lower RPM.

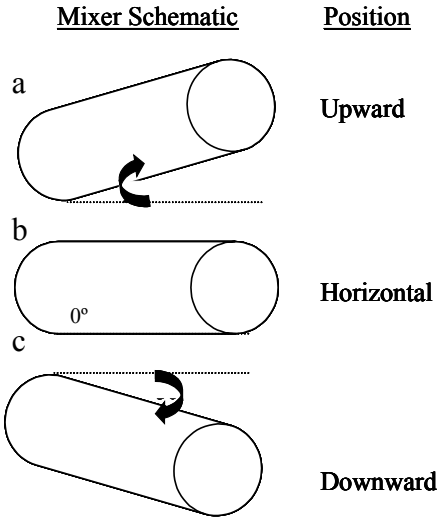

Figure 2.1.2: Mixer Schematic at three different processing positions

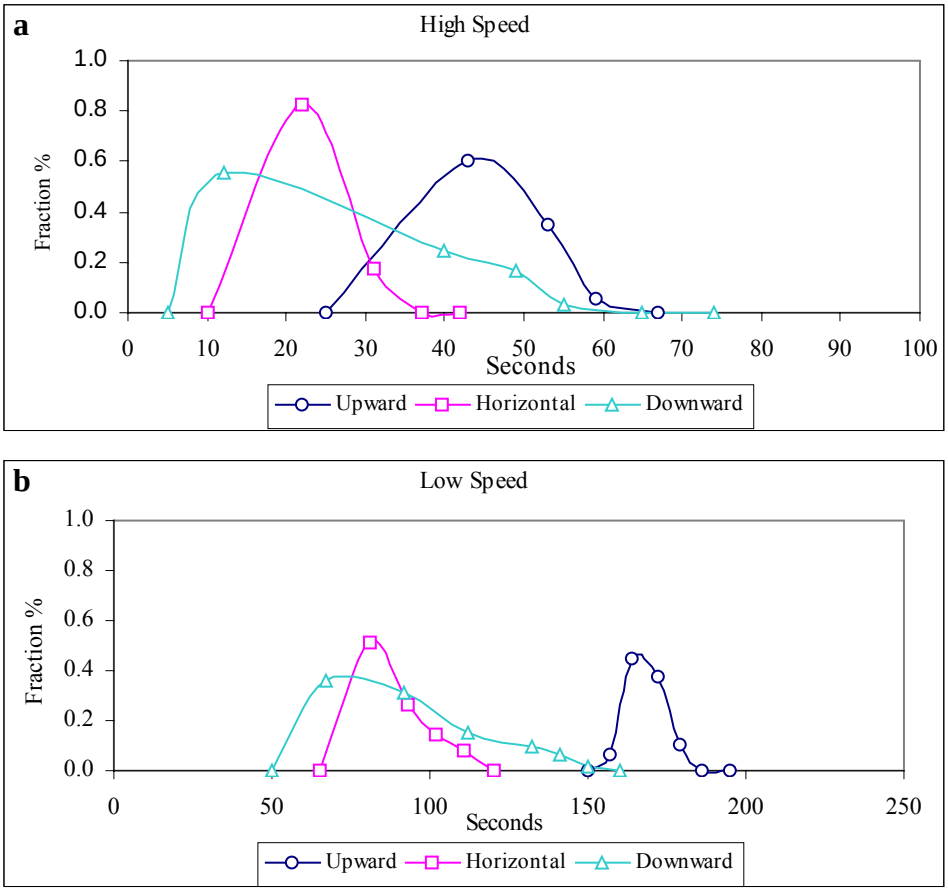

Figure 2.1.3 Residence Time Distribution plots from Acetaminophen tracer particles of Vessel as a function of Position and Rotation Rate: (a) High Speed (b) Low Speed

At the upward processing angle shown in Figure 2.1.2a, an upward angle of 30° is used. Mixing occurs due to the convective forces induced by the series of impellers. The

additional processing time incurred due to the gravitational forces results in larger strain being applied as a result powder flow is retained for a longer period of time within the mixer (shown in Figure 2.1.3a and 2.1.3b).

At the horizontal position, the mixer operates at a 0° incline (as shown in Figure 2.1.2b). Powder flow is neither promoted nor hindered by gravitational forces along the drums axial direction. Particles are moving downstream due to the convective mechanism caused by the impellers and mixing is solely based on radial mixing. The horizontal processing angle distribution curve has similar slope to that of the upward angle, with the exception that the distribution exists in a lower time range.

In the downward angle the mixer is positioned at a -30° incline (Figure 2.1.2c). The convective motion and gravitational forces promote particles shifting downstream along the mixer, referred to as axial mixing (Gupta *et al.*, 1991). The result is a broaden residence time distribution profile for the downward angle as shown in Figure 2.1.3a for the high rotation rate and 3b lower rotation rate. The wider residence time distribution, the larger the difference between each powder flow time element, as a result for the determination of the mean residence time the geometric mean is used (Kenney and Keeping, 1962).

The mean residence time is the average time the powder remains within the mixer. As previously mentioned in Section 2.1.3.1, the mean residence time is determined using the weighted average of the residence time distributions. The mean residence time is affected by processing angle, due to changing gravitational forces. Figure 2.1.4 illustrates the Acetaminophen residence time for both the high and low impeller rotation rates at all three processing angles. Increasing the processing angle to

the upward slope increases the mean residence time since additional gravitational forces are acting on the powder, hindering the powder's axial transport. The downward angle shows the lowest mean residence time due to the additional force that results in accelerating flow, whereas the horizontal position results in intermediate mean residence time as expected.

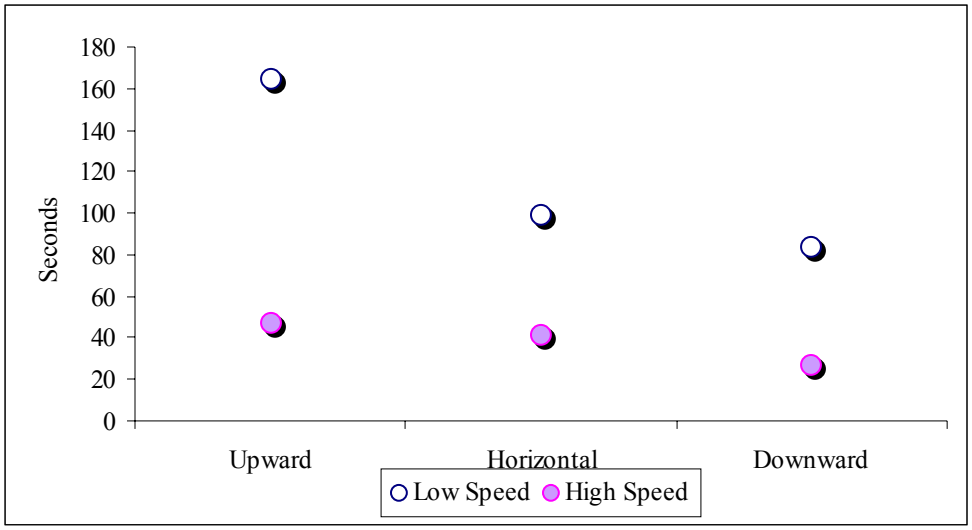

Figure 2.1.4: Mean Residence Time as a function of Seconds for Acetaminophen tracer particles of Vessel as a function of Processing Position at a Low and High Impeller Rotation Rate

Homogeneity

In order to characterize and quantify the effects of processing angle in mixer homogeneity, the outflow variability is examined in this section. It is also important to mention that a built-up of powder deposits is observed, presumably by electrostatic agglomeration at the bottom of the mixer and between the blades. Samples were retrieved from the powder outflow and dead zones within the mixer. Notably the concentration of Acetaminophen was always larger within the mixers dead zones than the powder outflow. The loss of Acetaminophen within the mixer dead zones prevent from obtaining the target concentration at the powder outflow.

Table 2.1.1 illustrates the processing conditions of the three experimental settings used. Each case is examined at the three processing angles previously discussed. Table 2.1.2 displays the RSD and VRR of 3 independent experiments conducted with varying processing angles. The results shown in Table 2.1.2 illustrate that the upward position gives the best mixing performance in terms of RSD and VRR. The upward position results in the lowest RSD and highest VRR, as shown in Table 2.1.2. At the lower position, the highest RSD and lowest VRR is obtained, the intermediate values are obtained for the horizontal processing angle. In comparison to the other three operating positions the upward processing angle is the most effective and the operating condition with the longest residence time.

Table 2.1.1: Experiments Processing Conditions

Experiment	Pure Lactose fed in one Feeder	Processing Speed	Blade Angle	No. of Blades
1	125	High	15°	29
2	100	Low	45°	29
3	100	High	45°	34

Table 2.1.2: Experiments illustrating the RSD and VRR profile as a function of processing position

Experiment	RSD_{Upper}	$RSD_{Horizontal}$	RSD_{Lower}	VRR_{Upper}	$VRR_{Horizontal}$	VRR_{Upper}
1	.010	.027	.030	8.99	3.45	3.13
2	.076	.098	.116	1.20	.936	0.794
3	.038	.048	.071	2.42	1.93	1.30

2.1.4.2 Rotation Rate

Residence Time

Figures 2.1.5a, b, and c show that increasing the impeller rotation rate reduces the powder's residence time distribution range for all processing angles. However, the effect of impeller speed does more than just change the residence time. At high speeds, the

powder experiences greater shear forces, promoting mixing in the radial direction, for all processing angles.

The residence time distribution of Acetaminophen was determined for three processing angles (shown in Figure 2.1.2) and two rotation rates. The high impeller rotation rate signifies a rate of 78 RPM (revolutions per minute) and a low impeller rotation rate of 16 RPM, the residence time distributions for the upward angle is illustrated in Figure 2.1.5a, the horizontal 2.1.5b, and for the downward 2.1.5c. As shown in Figures 2.1.5a, b, and c independent of the processing angle at the high impeller rotation rate the distributions shift to the right and range from 5 to 75 (s), a narrower span than at the low impeller gyration rate of 50 to 200 (s). Clearly, at the lower speed, the powder remains within the system for a longer time period.

Another factor that changes is the rate at which the powder leaves the unit, which is captured as the slope of the residence time distribution. As illustrated in Figures 2.1.3 a and b, both processing angle and impeller rotation rate affect the slope, the lower impeller rotation rates elucidate higher slopes as does the upward processing angles. The higher slope signifies that the different elements of the powder tend to leave closer together in time. The effects of rotation rate on the mean residence time are shown in Figure 2.1.4. The figure illustrates that independent of impeller rotation rates the processing angle affects the mean residence time. At both rotation rates, the upward angle is the longest followed by the horizontal and downward angle.

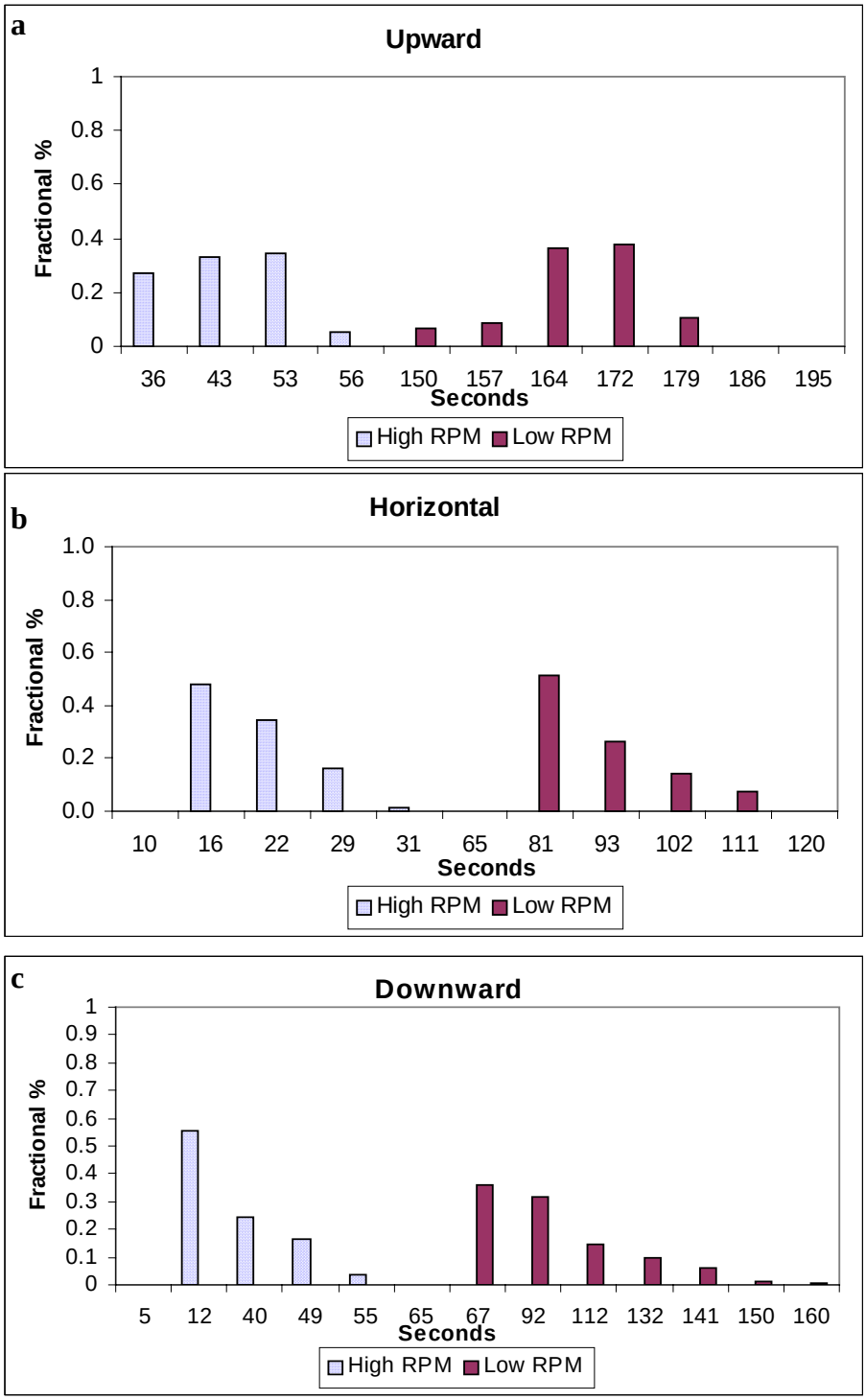

Figure 2.1.5: Residence Time Distribution at High RPM and Low RPM (a) Upward (b) Horizontal (c) Downward

Varying impeller rotation rate and processing angle also modify the number of blade passes. As discussed in Section 2.2.3.1, the average number of revolutions the powder flow experiences during its residence time in the mixer is dependent on the processing angle and the impeller rotation rate. Although at a higher RPM powder remains within the mixer for a shorter time (Figure 2.1.5), the actual number of blade passes the powder is subject to be greater as shown in Figure 2.1.6 than at the lower impeller RPM. This occurs because the number of blade passes is dependent on the powder residence time and impeller rotation rate. In the upward processing angle the powder experiences additional blade passes than at the horizontal or downward angle. Residence time and the number of blade passes both increase as the processing angle slope moves toward the positive incline.

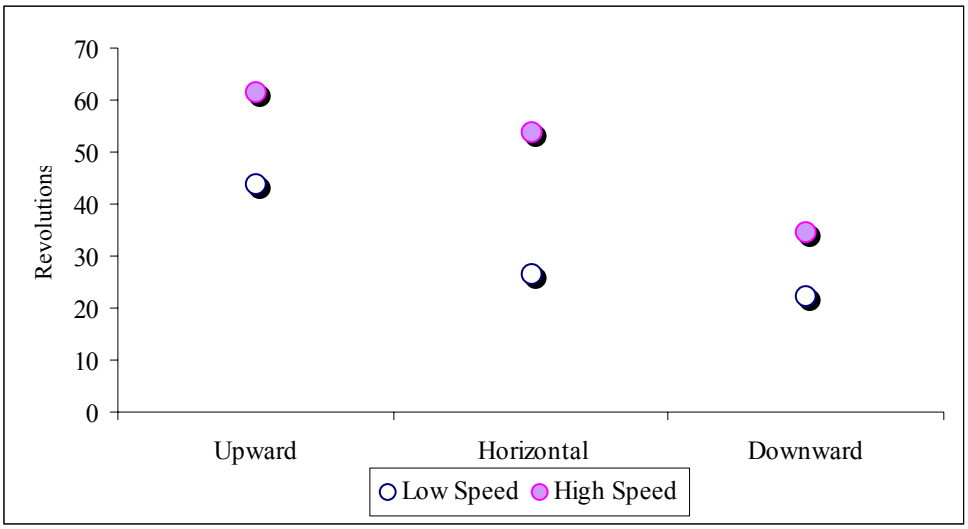

Figure 2.1.6 Residence Time as a function of Revolutions for Acetaminophen tracer particles of Vessel as a function of Processing Position at a Low and High Impeller Rotation Rate.

Homogeneity

In this section the effects of the varying residence time on the mixing performance are presented. As previously discussed, the average number of revolutions the powder flow experiences during its residence time in the mixer is dependent on the processing angle and the impeller rotation rate. Figures 2.1.5a, b, and c show that increasing the impeller rotation rate reduces the powder's residence time distribution range for all processing angles. However, the effect of impeller speed does more than just change the residence time. At high speeds, the powder experiences greater shear forces shown in Figure 2.1.6, promoting mixing in the radial direction, for all processing angles. As shown in Figure 2.1.7 the variability of powder composition is greater when the system uses the higher impeller rotation rate, independent of processing angle. Table 2.1.3 illustrates additional experiments using different convective designs where the effect of rotation rate was examined for the three previously described processing angle. The results shown in Table 2.1.4 again illustrate that the lower RSD values are obtained for the low impeller RPM than for the higher RPM. This is surprising, since as discussed before the higher rotation rate results in a greater number of blade passes during the residence time. One explanation for this result is that this effect is due to triboelectric forces. Electrostatic forces have not been extensively studied in pharmaceutical powder processing but have been recently noticed by other researchers (Bailey, 1984; Dammer *et al.*, 2004). Electrostatic forces are created from the accumulation of surface charges that are developed when the powders are continuously stirred or shaken with other powders and/or surfaces. This might explain why at the higher rotation rate there are larger powder deposits within the mixer that result in larger variability between the samples.

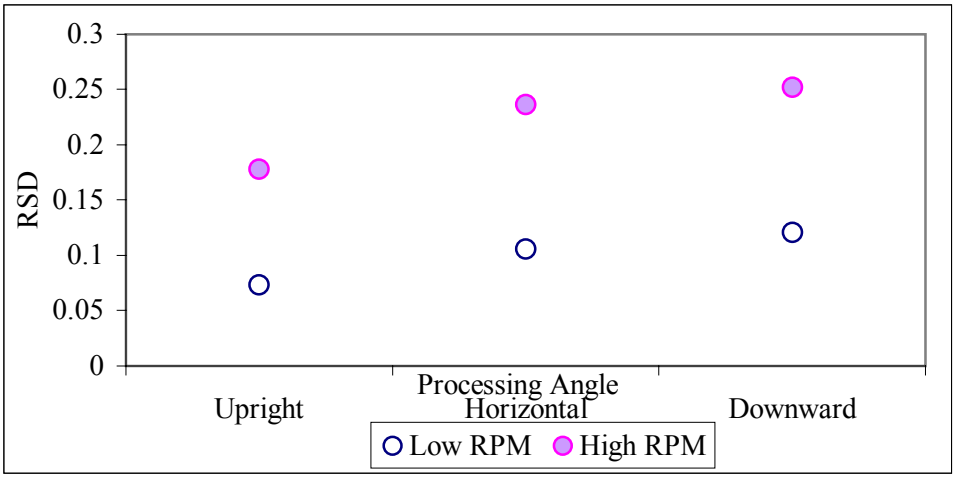

Figure 2.1.7: RSD plots for experiments conducted at two different speeds (High and Low Speed) and at the following processing angles **(**Downward, Horizontal, Upward). The experiments used 29 blades at a 45° degree angle.

Table 2.1.3: Experiments Processing Condition*s*

Experiment	Pure Lactose fed in one Feeder	Processing Speed	Blade Angle	No. of Blades
4	100	Both	45º	29
5	100	Both	45º	34
6	100	Both	60º	29

Table 2.1.4: Experiments illustrating the RSD profile as a function of processing position

Experiment	*Speed*	RSD_{Upper}	$RSD_{Horizontal}$	RSD_{Lower}
4	Low	0.073	0.082	0.106
	High	0.178	0.236	0.251
5	Low	0.051	0.063	0.097
	High	0.090	0.124	0.160
6	Low	0.063	0.080	0.106
	High	0.128	0.181	0.217

Design Parameters

There are several design parameters that affect the mixing performance of the continuous convective mixer. Shear is induced by blade motion and, as a result, modifying the blade design affects the shear intensity and powder transport. In this study the effect of changing the number of blades, blade spacing, and blade angle is consider.

In addition the effects of increasing the mixing time by incorporating a recycle stream back into the continuous mixer is investigated in section 2.1.4.4.

2.1.4.3 Convective Design

2.1.4.3.1 Number of Blades

In the experiments described in this section, the mixer was initially mounted with the original number of blades, 29. In a separate set of experiments five more blades were added into the mixing vessel to minimize the formation of stagnant zones in the mixer and to increase the intensity of transport mechanisms in the axial direction. A larger number of blades increase the rate of energy dissipation, and thus the shear forces in the mixer. In cases were the feed is agglomerated, increasing the intensity of mixing mechanism can reduce the size of the agglomerates, thus increasing the homogeneity of the powder outflow. However, a completely different outcome might be observed if agglomerates form within the mixer, possibly due to the development of electrostatic effects as discussed in the previous section. In such a case, increasing shear and/or the total metal surface within the mixer might lead to an increase in the formation of agglomerates (Laurent and Bridgwater, 2002a).

Based on our previous experience with Acetaminophen (a material that agglomerates readily) both effects might be present in our system. The effect of blending powders using 29 and 34 blades at a 45º blade angle was studied for high and low impeller rotation rate. As shown in Figures 2.1.8a and b, increasing the number of blades did improve the outflow homogeneity since the RSD is decreased with the addition of blades independent of processing angle and impeller rotation rate.

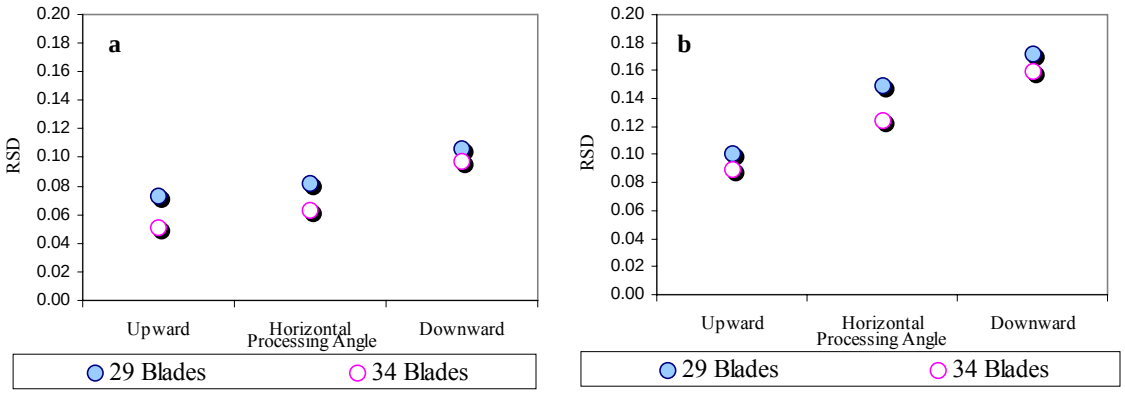

Figure 2.1.8: RSD from experiments conducted with 29 and 34 blades at an a) low speed and b) high speed

2.1.4.3.2 Blade Angle

Another important convective design parameter investigated is the blade angle, which affects powder transport (as shown by Laurent and Bridgwater, 2002b). The purpose of the impeller is to propel the powder within the vessel. The motion of the particulates is affected by the blade angle. Varying the blade angle affects the particle's spatial trajectory, thus altering the radial and axial dissipation. Laurent and Bridgwater (2002b) illustrated that increasing the blade angle promoted additional dispersion forces leading to increasing radial mixing (Laurent and Bridgwater, 2002b). In this study all 29 blades within the mixer were positioned to a specified blade angle. Figure 2.1.9 displays the results derived from varying the blade angle keeping all other processing parameters constant. The five blade angles examined were 15°, 45°, 60°, 90° and 180°. Since the dispersion of material is reduced from a 60° to 15° angle, it is not surprising to observe that the RSD of the outflow stream is the highest for the lower 15° angle followed by the 45° angle design, and the lowest at the higher 60° angle, which is experimentally validated in Figure 2.1.9. However, there are limitations in further increasing the angle to 90°. This is mainly because at the 90° angle there is not enough axial transport to transfer

the material out of the blender at the upward processing angle. Figure 2.1.10, depicts an axial and radial view of the blades at a 90º angle and at the 180º degree angle. At the 90º angle the distances between the blades decreases to the point where axially the neighboring blades are right next to each other. At the 180º (or 0º) angle the 1.2" blade widths are perpendicular to the axis of rotation (y-axis). As shown in Figure 2.1.9, at the 180° angle, axial powder transport only occurred at the downward position mainly due to the gravitational forces acting on the particles. The RSD are higher for the 90º and 180º angles mainly due to the hindrance of the axial transport. Consequently based on the results obtained for different blade angles, the 60º blade angle performed better in terms of the investigated mixing characteristics.

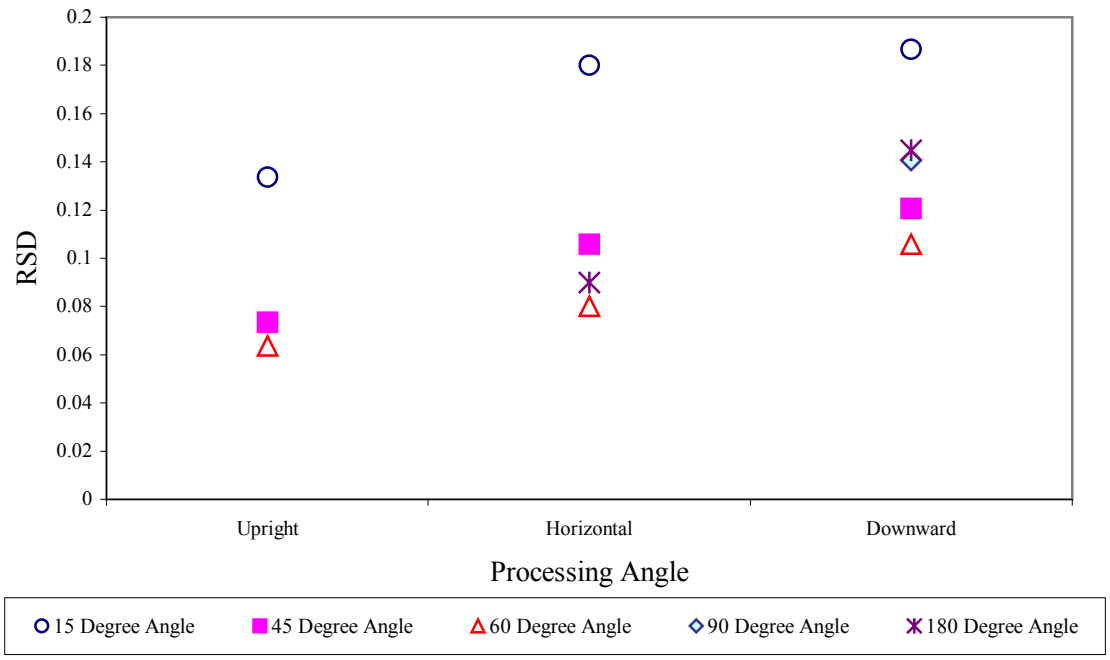

Figure 2.1.9: RSD plot from experimental data from a Baffle Angle of 15° to 180° at a low speed.

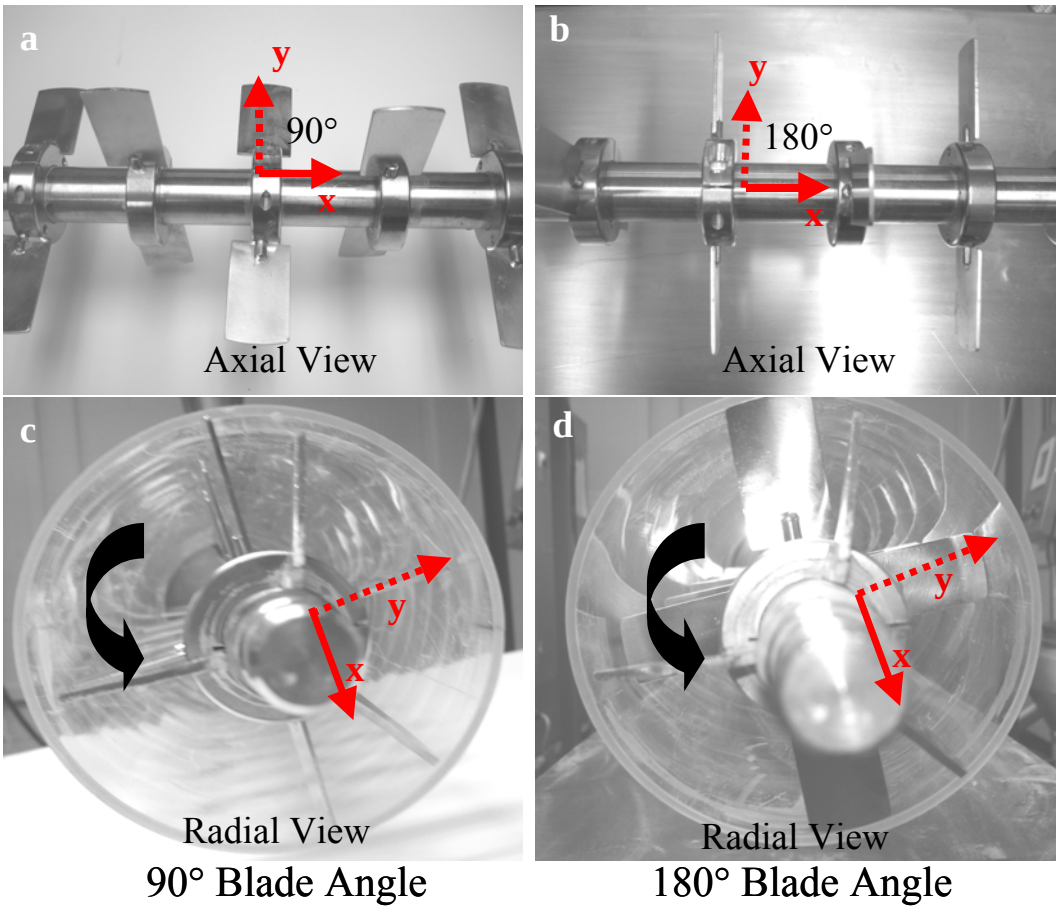

Figure 2.1.10: Schematic of blade angles at the axial view a) 90ºand b) 180º angle. Radial view is c) 90º angle and d) 180º angle.

2.1.4.4 Powder Recycle

One of the main benefits of transitioning from batch to continuous mixing is the number of adjustable parameters that facilitate integration capability with several other manufacturing processes such as mixing, encapsulation, milling, and coating in series. However, in an integrated system, lags and recycles are often part of the overall dynamics. The effects of recycling are considered using the scheme shown in Figure 2.1.11. The material used (Acetaminophen formulation) is reprocessed into the same continuous mixer using the same processing parameters, 15°-29 blades, horizontal processing angle, and high impeller rotation rate.

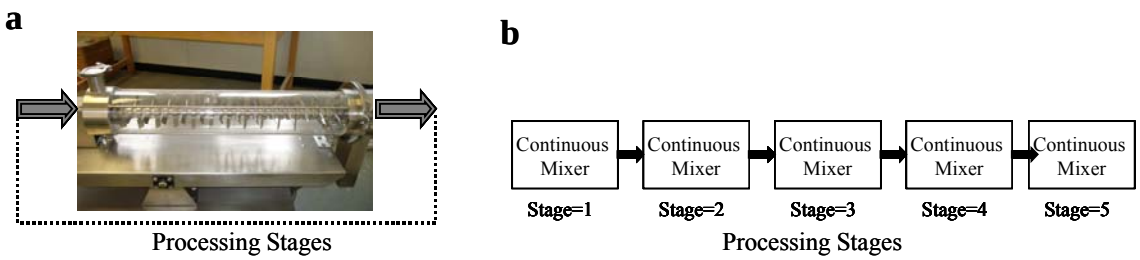

Figure 2.1.11: Schematic illustrating the addition of mixing processing stages a) Visual Depiction of the powder leaving and re-entering the mixer b) Illustration of the number of processing stages examined.

The recycle is implemented as follows: powder is collected in a cylinder and once the cylinder fill level is reached the material is poured into the inflow of the continuous mixer. As the number of recycles increases the, total mixing time increases. At the end of each processing stage samples are withdrawn from the outflow and analyzed using NIR. The RSD at each stage is calculated, as expected the results show a RSD decreasing profile as illustrated in Figure 2.1.12.

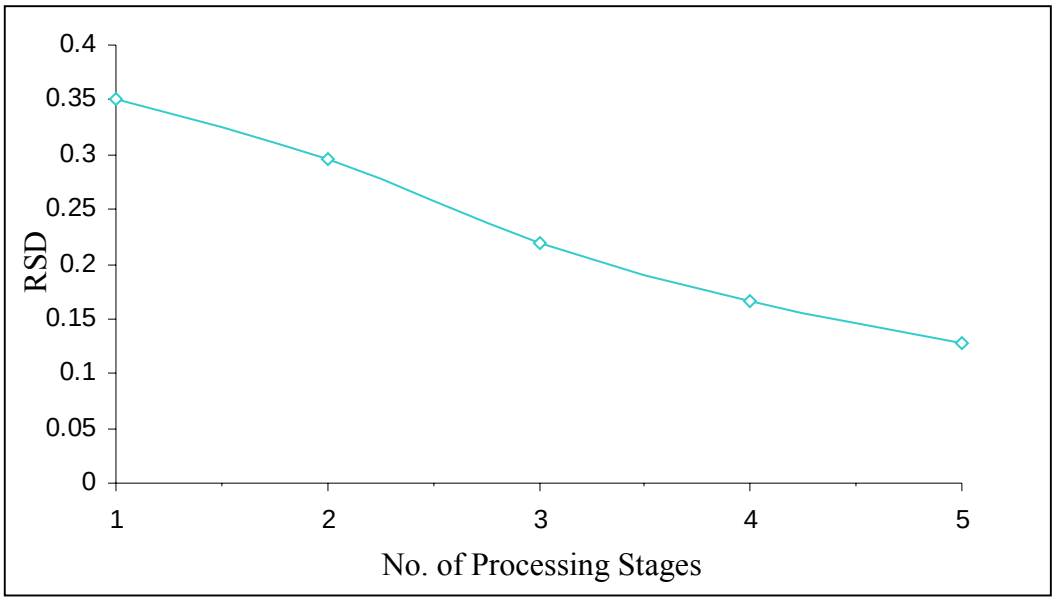

Figure 2.1.12: RSD profile of an Acetaminophen formulation as a function of processing stages.

2.1.4.5 Material Properties

Particle characteristics also affect mixing efficiency (Porion *et al.*, 2004). Mixing is affected particularly by variations in particle size distributions, which impact both the flow properties and segregation tendencies of powder blends (Alexander *et al.*, 2001; Liss *et al.*, 2004; Conway *et al.,* 2005). Particle size also affects the relative importance of triboelectric forces within powders, since the average charge per unit mass and the Coulomb forces decrease with increasing particle size (Dammer *et al.*, 2004). As discussed in section 2.2.2, two vibratory feeders were utilized to deliver powder into the continuous mixer. One fed a pre-blend mixture of powder containing Lactose and Acetaminophen and the other fed pure Lactose. To investigate the effects of powder cohesion in mixing, the particle size of one of the powders is decreased since typically, the smaller the particle size, the higher the cohesion level (Orband and Geldart, 1997). Two grades of Lactose varying in particle size are utilized, Lactose 100 (130 μm) and Lactose 125 (55 μm). Figure 2.13 illustrates the results of mixing with the two different grades of Lactose. The experiments used 29 blades with 15° angle at a low rotation rate for all processing angles. As shown in Figure 2.1.13, decreasing the particle size did not affect the mixing performance of the process at either low or high speed. Cohesive materials readily form powder agglomerates. However, when the agglomerates come in contact with the crossing slip planes created by the passing blades, the particulate clusters breakup and disperse (Liss *et al.*, 2001). As a result, the more cohesive Lactose does not affect the mixing performance and an advantage of utilizing convective mixers for cohesive mixtures certainly exists.

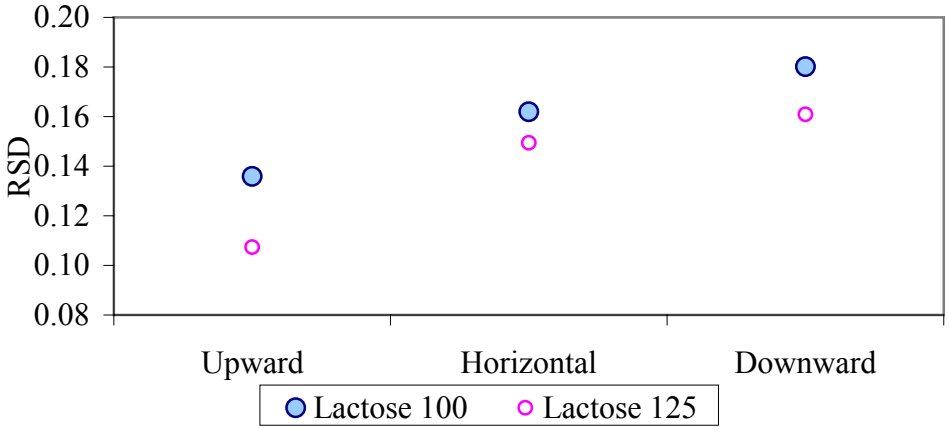

Figure 2.1.13: RSD plots for experiments conducted at low speed and at the following processing angles **(**downward, Horizontal, Upward) for two different cohesion levels high cohesion Lactose 125 and low cohesion Lactose 100.

2.2 Continuous Mixer 2

Experimental work published so far focuses on operating conditions such as rotation rate, mixing inclination, and flowrate. While many types of continuous mixers have been built, and many more can easily be conceived, only a few geometric designs have been examined in the literature. A second continuous blender with a different geometric design was examined for a broader set of operating conditions.

2.2.1 Description

The mixing system examined in this section is manufactured by GEA Buck Systems and shown in Figure 2.2.1. The blender varies in diameter and length from the first blender (Figure 2.1.1). The first blender has a diameter that is 3 fold that of the second blender (Figure 2.2.1). Moreover, the first blender has an axial vessel than is 2.4 times longer than the second blender. Geometric parameters of each blender are shown in Table 2.2.1. Figure 2.1.10 and 2.2.2 shows the blade design for each of the continuous mixers. Other then geometrical differences, the systems work similarly, except that the smaller mixer is capable of much higher impeller speeds. The blenders have three main adjustable parameters that determine the degree of operational flexibility (operational space): the vessel angle, impeller rotation rate, and the blade pattern.

Figure 2.2.1: 2nq Continuous Mixer

Figure 2.2.2: Convective Design of the Continuous Mixer

Table 2.2.1: Continuous Mixing geometrical descriptions

Mixer	Diameter (m)	Length (m)	No. of Blades	Blade length (m)	Blade Type	Speed (RPM)
1	0.15	0.74	0-34	0.05	Rectangular with a circular tip	16-87
2	0.05	0.31	0-14	0.02	Triangular with a circular tip	16-340

2.2.2 Results

2.2.2.1 Effect of Vessel Angle

The preceding section illustrated that the mixing inclination was the most significant parameter among variations in rotation rate and cohesion. In this section, the second, smaller continuous blender with a different geometric design is examined for a broader set of operating conditions. We first provide an individual discussion of the observed effects of the main parameters, followed by a full statistical analysis of the data set.

The effects of vessel angle on the content uniformity of the outgoing powder are shown in Figure 2.2.3a for experiments using 3%APAP and the rest consisting of Lactose 125M at a rate of 50 RPM, at a total flow rate of 16 grams per second**.** This figure illustrates the results from 5 different mixing angles. Results indicate that the higher the vessels angle from the horizontal position, the better the content uniformity. This can be an effect of the larger residence time the powder experiences at higher inclinations. Residence times at each vessel angle are shown in Figure 2.2.3b. Clearly both residence time and content uniformity are affected by the vessel angle; the data suggests that more

effective mixing occurs at the upward angle, which, as shown in Figure 2.2.3b corresponds to the highest residence time.

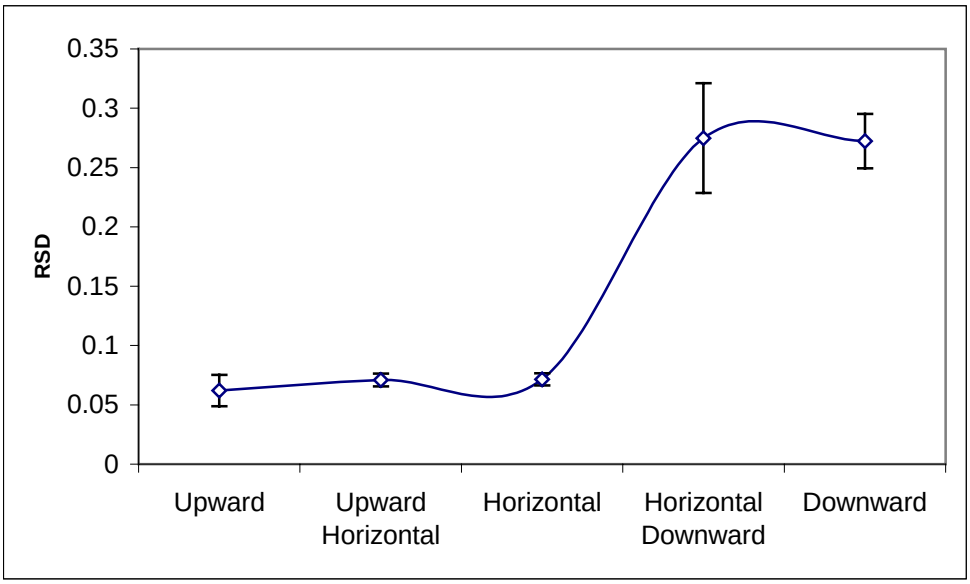

Figure 2.2.3a RSD versus Mixing Angles at 50 RPM using Lactose 125M

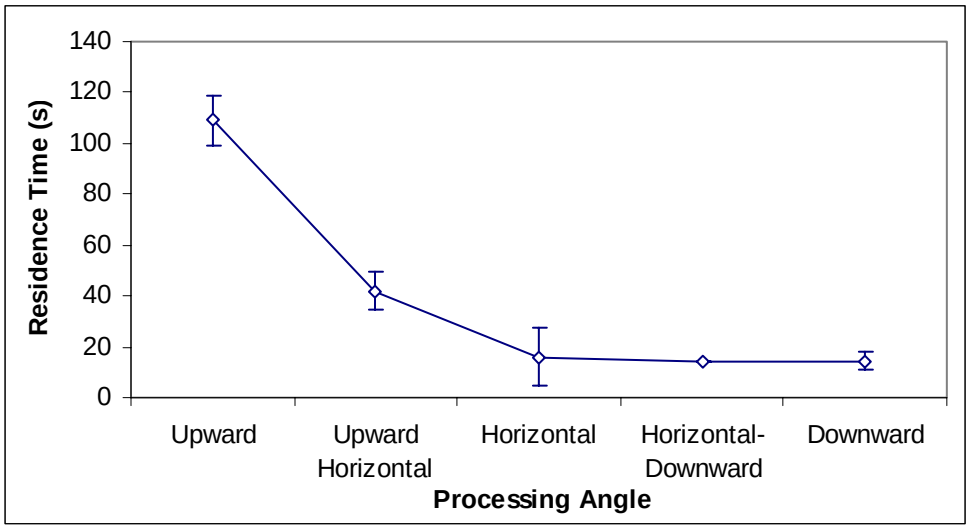

Figure 2.2.3b Residence Time versus Mixing Angles at 50 RPM using Lactose 125M

2.2.2.2 Effect of Rotation Rate

As discussed for the first mixer, the rotation rate of the blades determines the rate of shear and the intensity of material dispersion throughout the mixer, potentially affecting mixing performance. For the second mixer we examine six different levels of

impeller speed (or process shear rate) at the horizontal vessel position for a Lactose 125M blend. The RSD results are shown in Figure 2.2.4a and indicate that, once again, better content uniformity is observed at the lower shear rates. This might be a result of the effect of rotation rate on residence time, shown in Figure 2.2.4b, which illustrates to be higher at lower rotation rates (since the total strain the powder experiences is proportional to the total number of blade passes). However the total number of blade passes is actually larger for the highest shear rate. Figure 2.2.5 shows the number of passes as a function of RPM, confirming that at higher shear rates the powder experiences a greater total amount of strain. In fact, the relationship between the total number of blade passes and rotation rate can be considered a fairly linear function with a regression coefficient of .94. As shown in Table 2.2.1, both total strain (total blade passes) and shear rate (RPM) affect the content uniformity in a similar manner.

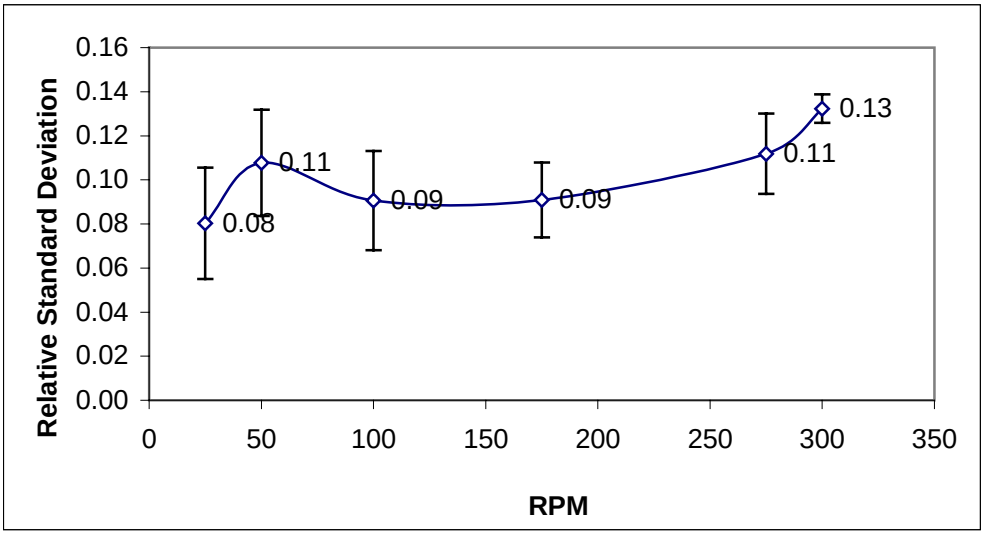

Figure 2.2.4a RSD versus Rotation Rate (RPM) at a horizontal mixing angle for Lactose 125M

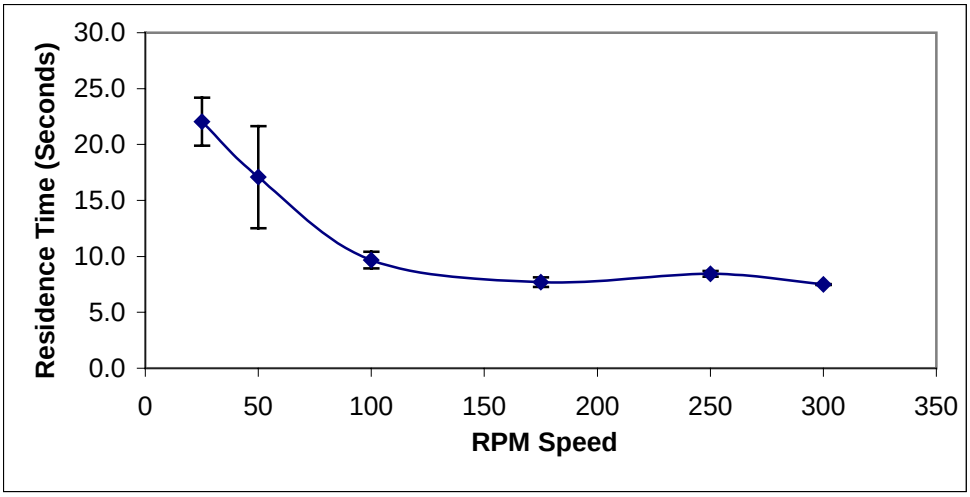

Figure 2.2.4b Residence Time (seconds) versus Rotation Rate (RPM)

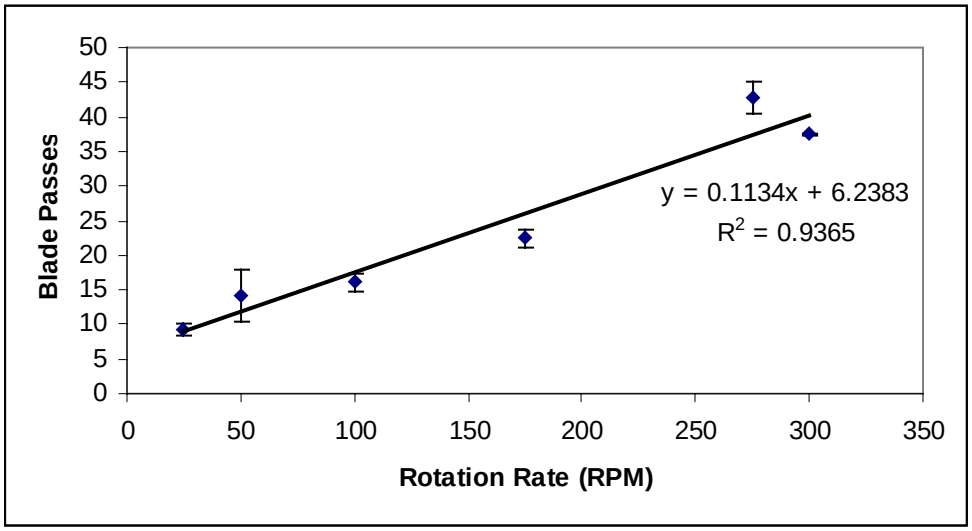

Figure 2.2.5 Number of blade passes Lactose 125 M experiences as a function of rotation (RPM)

Table 2.2.2: The content uniformity as a function of rotation rate and blade passes

RPM	Blade Passes	RSD
25	9	8.03E-02
50	16	1.08E-01
100	22	9.06E-02
175	14	9.09E-02
275	43	1.12E-01
300	37	1.32E-01

2.2.2.3 Effect of Powder Cohesion

In addition to operating conditions such as rotation rate and mixing inclination, material properties have shown to affect the blending performance of batch mixing systems (Muzzio *et al.*, 2004). For a continuous convective system, Harwood *et al.* (1975) examined the same formulation composed of sand and sugar for several convective continuous mixing systems, varying cohesion by sifting the materials into different particle sizes ranges, but failed to observe a significant effect. Bridgwater and coworkers (1993) for a closed convective mixing system found that the motion of varying size of tracer particles from 2 to 4 mm, processing at 4 Hz showed no discernible effect in terms of particle trajectories. The case studies presented in this work examine the mixing performance between two different Lactose materials that vary in cohesion. Table 2.2.2 illustrates the results obtained from mixing Milled Acetaminophen with Lactose 100 and Lactose 125, at the horizontal mixing inclination. The new results presented here reveal that an effect indeed exists, although of moderate intensity.

In fact, the effects of cohesion can be system-dependent. Since cohesion can affect the degree of variability in the flow rate delivered by a powder feeder, it should be expected that cohesion could have impact on the performance of the integrated system, including feeders, mixers, and downstream finishing equipment. However, the differences in relative standard deviation between the two powders are small. The lack of a large observed effect could be due to the fact that shear rates are typically higher in convective systems than in tumblers (in fact convective blenders are often used for cohesive materials because they impart more shear), and it is possible that for both materials considered here, cohesion is simply to small to affect the outcome of the

convective mixing process to a large degree. However, an ANOVA can be helpful in order to determine whether or not the small-observed effect of cohesion is statistically significant.

Table 2.2.3: Continuous Mixing RSD Results from Lactose 100 and Lactose 125.

RPM	RSD	
	Lactose 100	Lactose 125
25	0.060±.014	0.080±.025
50	0.108±.024	0.117±.016
75	0.051±.024	0.087±.022
125	0.070±.024	0.079±.032

2.3 Summary and Conclusions

Continuous mixing has been an area of particular interest for many industries including pharmaceutical manufacturing. The results indicate that the powder's residence time and number of blade passes it experiences was affected by rotation rate and processing angle. Although at all the processing angles, the underlying normal forces the powder experiences fluctuate. Interestingly, what was observed is that the upward processing angle and low impeller rotation rate are the optimal processing settings, and these parameters result in the longest residence time. On the other hand, high sample variability is observed for the short residence times that are associated with the downward processing angle and high impeller rotation rate. This suggests that one of the main variables affecting mixing performance is residence time.

The results also illustrated the importance of blade design in mixing performance that is in agreement with the previous studies of Laurent and Bridgwater (2002a,b,c) that have demonstrated that blade structure has a significant effect on altering flow patterns, thereby affecting mixing performance. In our case study it was found that the addition of blades and the increase of the blade angle until it reaches a limit improved mixing performance. Particle properties have also been known to affect mixing performance.

However, in these studies, decreasing the particle size of one of the materials did not show a clear affect on the mixing performance (based on the RSD of the samples obtained at the outflow). In this case, an ANOVA can be helpful in order to further determine whether the effect of cohesion is or is not statistically significant. As a result in the next chapter, we will apply statistical analysis to the experimental results found in this chapter.

Chapter 3

Statistical Analysis

A statistical analysis on the effects of mixing angle, rotation rate, and cohesion for the mixers discussed in chapter 2 is considered in this chapter. The method examines the effects these parameters have on mixing performance and residence time, variations between the two mixers will be seen. A 4-way ANOVA is used to determine the significance of the differences between the two mixers; rotation rate will illustrate to be the least significant parameter.

3.1 Introduction

As part of their product development process, pharmaceutical companies carry out intensive research efforts focused on examining and optimizing the production of homogeneous solid mixtures. Minimizing variability in powder blends is critical to pharmaceutical (and many other) manufacturing operations because blend uniformity has direct impact on product quality and performance. Deviations from desired mixing performance, which often lead to batch failures, usually trigger costly process investigations and corrective actions required to maintain regulatory compliance (Muzzio *et al.*, 2002). Unfortunately, powder flow and powder mixing are topics that are far from being well understood. Often, powder mixing processes are designed ad-hoc, based on a limited set of experimental information. Not surprisingly, the need to understand blending has been a central focus of regulatory interest in the past 15 years, and remains a key target of QbD and PAT efforts. In the recently issued Q8(R1) guidance, the FDA has recently published their current thinking on using QbD methods to identify critical

quality attributes (CQAs), stating that product quality should be studied and controlled by systematically identifying the material attributes and process parameters that can affect the products CQA.

Among emerging technologies for improving the performance of blending operations, continuous mixing (and continuous processing in general) currently commands enormous interest at pharmaceutical companies. Continuous processing has numerous known advantages, including reduced cost, increased capacity, facilitated scale up, mitigated segregation, and more easily applied and controlled shear.

However, development of a continuous powder blending process requires venturing into a process that has a large and unfamiliar parametric space. While continuous blending processes have been used in other industries, in general such applications operate at much larger flow rates and have less demanding homogeneity requirements than typical pharmaceutical applications. Experimental work published so far has focused on operating conditions such as rotation rate, mixer inclination angle, and flowrate. While several types of continuous mixers have been built, and many more can easily be conceived, only a few geometric designs have been examined in the literature.

For example, in chapter 2 we examined a continuous mixing process and examined a set of operating and design parameters that were found to affect the content uniformity of the final product. The case studies illustrated in chapter 2 demonstrated that the powder's residence time and content uniformity were affected by operating conditions (rotation rate and mixing angle). A second continuous blender was examined for a broader set of operating conditions. However, many more conditions remain to be examined, and for many interesting designs, performance has never been quantitatively

examined in the literature. Thus, substantial work is necessary in order to develop the prior knowledge needed to enable companies to design continuous processes with confidence and economy.

Given the magnitude of the task ahead, some consideration should be paid up front to the design of the methodology used to gather shareable information, and the statistical methods to be used to quantify performance and establish significance of various parameters. Due to the large experimental data set that arises from the various parameters, we propose systematic application of design of experiments and statistical analysis (specifically, analysis of variance - ANOVA) to examine the significance of main factors and their interactions.

A reasonable starting point is to consider the system response that is of most interest. A natural approach would be to extend to continuous mixers the methods typically used for batch processes, where a mixing index (typically, a Relative Standard Deviation, also known as the Coefficient of Variability) is computed at the "end" of the blending process based on samples extracted with a thief. Several other indexes have been used to quantify the mixing performance of particle processes; for example, Lacey (1943) developed a mixing index that considers several variances. Approximately thirty-five other mixing indices can be found in the excellent review by Fan and coworkers (1970), which outlines the criteria for selecting an index based on the different degrees of content uniformity that can be achieved. These measurements have been applied to many systems, including various rotating horizontal cylinders (Wightman and Muzzio, 1998), V-blenders (Brone *et al.*, 1997, 1998; Alexander *et al.*, 2003, 2004; Lemieux *et al.*, 2007), double cones (Brone and Muzzio, 2000), bin blenders (Sudah *et al.*, 2002b;

Arratia *et al.*, 2006), and ribbon blenders (Muzzio *et al.*, in press), and continuous blenders (Marikh *et al.*, 2005; Harwood *et al.*, 1975).

Although indices can be used to quantify whether design and operating parameters and/or material properties affect mixing performance, by themselves they are poor tools when it comes to revealing which effects are more influential. For the typical number of samples used to characterize batch processes, RSDs are very "noisy", and statistically significant differences between process responses for different parametric settings can be established only rarely.

Rollins and coworker (1995) presented a theoretical discussion on the advantage of the ANOVA technique for Monte Carlo simulations. ANOVA's have also been used for particle processing such as nano-particle wet milling (Hou *et al*., 2007). Walker and Rollins (1997) examined how well ANOVAs perform for detecting mixture in-homogeneity with several non-normal distributions. They found that the Kruskal-Wallis test was not superior to the ANOVA technique even when the assumption of normality was broken. Given that ANOVA is the essential tool used in design of experiments, which is one of the essential toolkit components of a modern QbD approach, it seems fitting to introduce the ANOVA technique for the characterization of developing technologies intended to be used in modern pharmaceutical manufacturing processes.

3.2 Statistical Analysis

A randomized experimental design was used to examine the four variables (mixer type, mixing angle, rotation rate, and powder cohesion), as well as their interactions. For each mixer, we initially examine a three-way ANOVA considering mixing angle, speed, and type of powder. Initially, all factors and interactions are considered, subsequently

reducing the statistical model to remove the non-significant effects. It is important to mention that we examine some of these variables in more detail in order to illustrate the effect of mixing performance and residence times. On the first mixer, a full factorial design is used, for the second a fractional factorial design, and when we examine the variability between both mixers a full factorial design that is built using only portion of the data. The levels examined for the factorial design consider 3 mixing angles and 2 rotation rates (16 RPM and 76 RPM) for the first mixer, reflecting speed limitations in the device. A broader set of conditions is considered for the second mixer, including 5 mixing angles and 9 rotation rates up to 300 RPM. The section on rotation rate illustrates the effect of increasing the speed further for the second continuous mixer. For both systems, 2 different Lactose powders, Lactose 100M and Lactose 125M, a slightly more cohesive powder, are examined.

The methodology used in this study begins with the full statistical model for the three-way ANOVA of each mixer:

$$y_{jkl} = \mu + \alpha_j + \beta_k + \alpha\beta_{jk} + \gamma_l + \alpha\gamma_{jl} + \beta\gamma_{kl} + \alpha\beta\gamma_{jkl} + \varepsilon_{jkl}$$

In the above equation, the single-symbol terms in the model refer to the overall average μ and the main effects; α for mixing angle, β for rotation rate, γ for powder cohesion. The terms with combination of symbols represent the interactions between main factors, and ε represents the error term. Data was analyzed under the usual assumptions of normality and independence. Since n=1 for the first mixer, not all interactions can be examined simultaneously. Multivariate analysis requires assuming that some interactions do not exist in order to release degrees of freedom to construct an error term.

As terms are found to be non-significant ($p>0.2$) the initial model, in subsequent models non-significant terms are eliminated in order to form a new ANOVA. This step is repeated until all the effects left are considered significant ($p<0.05$).

The same analysis is performed for the 4-way ANOVA, where the additional main effect is η for the mixer

$$y_{ijkl} = \mu + \eta_i + \alpha_j + \eta\alpha_{ij} + \beta_k + \eta\beta_{ik} + \alpha_j\beta_k + \alpha\beta_{jk} + \gamma_l + \eta\gamma_{il} + \alpha\gamma_{jl} + \beta\gamma_{kl} + \eta\alpha\beta_{ijk} + \eta\beta\gamma_{ikl} + \alpha\beta\gamma_{jkl} + \alpha\beta\gamma\eta_{ijkl} + \varepsilon_{ijkl}$$

Analysis of Variance (ANOVA) is a standard statistical procedure where the variability in a data set is properly calculated for each main effect and for each interaction retained for a given statistical model. An ANOVA table includes the different treatments examined. The degrees of freedom, df, for each treatment reflects the number of different levels, g. An appropriately formed F-statistic (or F-ratio), is computed for each effect and interaction, and the value obtained is compared to a critical value corresponding to a certain (pre-selected) probability that the observed "effects" be in fact due to chance. Results can be used for comparing models and, during post-ANOVA processing, to establish which groups within a data set typically represent the response of the system for a given set of treatment conditions) are actually different than others. Moreover, the p-value is defined as the probability of obtaining a result at least as extreme as a given data point, under the null hypothesis.

Many equivalent commercial software packages exist for conducting ANOVA analysis of data sets. The Sums of Squares were determined by giving the relative variance of powder streams for each experiment in SAS version 9.1. The p-value was calculated using M.S. Excel's p-dist function. The smaller the p-value, the larger the component has a significant contribution to the main effect.

The p-value is an indication of significance. A p-value lower than 0.05 is usually taken to mean that the effect is significant, because the probability that observed differences corresponding to different levels of the independent variable (or, for interactions, the combinations of levels of 2 or more variables) be due to chance are lower than p. Thus, it is concluded that groups of observations for different levels of independent variables are significantly different from each other, and that the variable therefore has a statistically significant effect, and as a result, that the null hypothesis (that results for different levels are not different from each other) can be rejected with high probability ($p>0.95$) of correctness. An example of a null hypothesis in this study would be that the mean variability of the content uniformity for different levels of cohesion be the same, i.e., that the levels of cohesion of the powder considered in the study do not have a statistically significant effect on the homogeneity of samples.

Values of p greater than 0.05 do not mean that the null hypothesis is "true", they simply mean that, given the amount of data available, we cannot assert with sufficient confidence that they are actually different from each other (i.e., that an effect actually exists). Moreover, given a certain data set, p values are customarily used to rank the relative significance of the multiple variables and their interactions. This practice is somewhat misleading, since the relative values of p can (and do) depend on the number of levels of a given variable that are explored, the number of replications, etc., and therefore, comparisons (and statistically based conclusions in general) should always be considered under the caveat "given available data".

3.3 Results

The results presented in chapter 2 described the mixing performance and residence time of the first continuous mixer. In this study we supplement the results in chapter 2 with new results obtained for the second continuous mixer. A summary of results for both systems is presented in Table 3.8. In the next section we compare the performance of both mixers and examine the significance of the various model parameters and their interactions.

3.3.1. Statistical Analysis for Continuous Mixer 1

As mentioned before, the three parameters specifically examined for the first mixing vessel (Figure 2.1.1) are vessel angle, impeller rotation rate, and blend cohesion. The three mixing angles that were examined were an upward, horizontal, and downward inclination. Two impeller rotation rates (16 and 76 RPM) were examined, and two different grades of lactose; Lactose 100M and Lactose 125M. The Hausner ratio illustrated that Lactose 100M was less cohesive than Lactose 125M. The results are summarized in Table 3.1 using the compositional variance of powder samples taken at the discharge of the mixer as the main response. For each treatment combination, about 20 samples approximately 3 grams in weight were examined. Results readily showed that all the parameters play an important role on the mixing performance. In what follows, the statistical analysis will be split into two parts one considers three main effects (mixing angle, rotation rate, and cohesion) on homogeneity and the effects of mixing angle and rotation rate on residence time.

3.3.1.1 Homogeneity

Here we briefly recount three previous observations: (1) Between the two different rotation rates, on average, lower compositional variances are found for the lower rotation rates. (2) A more cohesive powder did show different results than the less cohesive powder. Interestingly, performance did not seem to improve when cohesion was reduced. (3) The inclination of the vessel played a critical role on the content uniformity. In order to establish the statistical significance of these observations, the results were analyzed using ANOVA.

Table 3.1: Continuous Mixer 1 Experimental Variance Results obtained from varying materials, process inclination, and rotation rate (RPM).

Observation	Processing Angle	Speed	Cohesion	R.Var
1	Upward	16	Lactose 100	0.0037
2	Horizontal	16	Lactose 100	0.0057
3	Downward	16	Lactose 100	0.0063
4	Upward	75	Lactose 100	0.0081
5	Horizontal	75	Lactose 100	0.0093
6	Downward	75	Lactose 100	0.0129
7	Upward	16	Lactose 125	0.0021
8	Horizontal	16	Lactose 125	0.0031
9	Downward	16	Lactose 125	0.0032
10	Upward	75	Lactose 125	0.0017
11	Horizontal	75	Lactose 125	0.0061
12	Downward	75	Lactose 125	0.0083

Initially, the statistical model used is:

$$y_{jkl} = \mu + \alpha_j + \beta_k + \alpha\beta_{jk} + \gamma_l + \alpha\gamma_{jl} + \beta\gamma_{kl} + \alpha\beta\gamma_{jkl} + \varepsilon_{jkl}$$

For n=1 this model is not fully solvable; in particular, the three-way interaction is confounded with the error. Since the three-way interaction is the least likely to be significant, we neglect this term, (i.e., we assume that the three way interaction is not significant) and use the degrees of freedom of the three-way interaction to form an error term, which results in the following model:

$$y_{jkl} = \mu + \alpha_j + \beta_k + \alpha\beta_{jk} + \gamma_l + \alpha\gamma_{jl} + \beta\gamma_{kl} + \varepsilon_{jkl}$$

For this model, the standard ANOVA table is shown in Table 3.2, where the sources are vessel angle, impeller rotation rate, and powder cohesion grades. Three angles, two rotation rates, and two different powders that vary in cohesion were studied. As mentioned in the statistical analysis section, main effects are listed in order of increasing p-values, where the lowest p-value is the (statistically) most significant factor affecting the variance for the data set at hand. In this case, the impeller rotation rate is the most significant factor, followed by powder cohesion; the least significant being vessel angle.

Table 3.2: 3-way ANOVA on the blend uniformity variance for Continuous Mixer 1 considering the treatments as: mixing angle, rotation rate, cohesion, and their interactions.

Source	DF	SS	MS	F	p
Mixing Angle	2	2.87E-05	1.43E-05	11.71	0.079
Rotation Rate	1	4.14E-05	4.14E-05	33.83	0.028
Cohesion	1	3.85E-05	3.85E-05	31.44	0.030
Process Angle*Rotation Rate	2	7.67E-06	3.84E-06	3.13	0.242
Process Angle*Cohesion	2	7.10E-07	3.55E-07	0.29	0.775
Rotation Rate*Cohesion	1	3.97E-06	3.97E-06	3.24	0.214
Error	2	2.45E-06	1.23E-06		

The interactions are fairly insignificant with p-values greater than .2. Thus, we re-examine the main effects using a 3-way ANOVA neglecting the interactions. The resulting model is shown below:

$$y_{jkl} = \mu + \alpha_j + \beta_k + \gamma_l + \varepsilon_{jkl}$$

The ANOVA, for this model is shown in Table 3.3. Clearly, all the main effects remain significant, displaying very small values of p. The two most significant factors are rotation rate and cohesion. The least significant factor, although still very significant, is the mixing angle.

Table 3.3: 3-way ANOVA on the blend uniformity variance for Continuous Mixer 1 considering the treatments as: mixing angle, rotation rate, cohesion.

Source	DF	SS	MS	F	p
Mixing Angle	2	2.87E-05	1.43E-05	6.78	0.023
Rotation Rate	1	4.14E-05	4.14E-05	19.60	0.003
Cohesion	1	3.85E-05	3.85E-05	18.22	0.004
Error	7	1.48E-05	2.11E-06		

3.3.1.2 Residence Time

In chapter 2, we showed that the residence time of powder in the blender was affected by rotation rate and vessel angle. Here we examine the effect of rotation rate and processing angle on the residence time. The 12 observations used are shown in Table 3.4, the resulting statistical model is:

$$y_{jk} = \mu + \alpha_j + \beta_k + \alpha\beta_{jk} + \varepsilon_{jk}$$

The resulting ANOVA results are shown in Table 3.5. Clearly both main effects are significant, whereas the interaction can be considered insignificant with a p-value of 0.30.

Table 3.4: Continuous Mixer 1 Residence time as a function of rotation rate and processing inclination for Lactose 100.

Observation	Processing Angle	Rotation Rate (RPM)	Residence Time (s)
1	Upward	16	164
2	Upward	16	225
3	Horizontal	16	99
4	Horizontal	16	156
5	Downward	16	84
6	Downward	16	116
7	Upward	75	47
8	Upward	75	77
9	Horizontal	75	42
10	Horizontal	75	48
11	Downward	75	27
12	Downward	75	35

Table 3.5: 2-way ANOVA for residence time of the first continuous mixer examining mixing angle, rotation rate, and their interactions.

Source	DF	SS	MS	F	p
Mixing Angle	2	8176.2	4088.1	5.454436	0.04468
Rotation Rate	1	26885.3	26885.3	35.87098	0.000974
Mixing Ange * Rotation F	2	2238.2	1119.1	1.493129	0.297658
Error	6	4497	749.5		

In order to further examine the significance of the two main effects, the interaction term is eliminated, and the resulting model is:

$$y_{jk} = \mu + \alpha_j + \beta_k + \varepsilon_{jk}$$

The ANOVA shown in Table 3.6 for this model clearly shows both process parameters are significant where rotation rate is partly more influential than mixing angle. As expected, lower shear rates and vessel inclinations resulted in longer residence times, which have also been noticed in rotary calciners (Sudah *et al.*, 2002c).

Table 3.6: 2-way ANOVA for residence time of the first continuous mixer examining mixing angle, and rotation rate.

Source	DF	SS	MS	F	p
Mixing Angle	2	8176.2	4088.1	4.855802	0.041623
Rotation Rate	1	26885.3	26885.3	31.93408	0.000481
Error	8	6735.2	841.9		

3.3.2 Statistical Analysis (Second Continuous Mixer)

In this section, an ANOVA analysis is conducted taking into account the effects of processing inclination, rotation rate, and cohesion on the homogeneity measurements of the second continuous mixer, followed by an investigation on the effects of mixing angle and rotation rate on the residence time. The approach is essentially the same as the one used for the first mixer.

3.3.2.1 Homogeneity

In this section, we examine the effect on blend homogeneity of the three parameters previously mentioned: processing inclination, rotation rate, and cohesion. As shown in Figures 2.2.3a and 2.2.4a, we have obtained a larger number of experimental results for the second mixer than for the first mixer for one grade of lactose. Five mixing angles and seven rotation rates were considered where the mixing experiment was duplicated 2-5 times; the result was a total of 55 experimental observations. Table 3.7 lists all the observations from the main effects (mixing angle, rotation rate, and powder cohesion).

Initially, the full model is used:

$$y_{jkl} = \mu + \alpha_j + \beta_k + \alpha\beta_{jk} + \gamma_l + \alpha\gamma_{jl} + \beta\gamma_{kl} + \alpha\beta\gamma_{jkl} + \varepsilon_{jkl}$$

Table 3.7: Continuous Mixer 2 Experimental Variance Results obtained from varying materials, process inclination, and rotation rate.

Observation	Processing Angle	Speed	Cohesion	R.Var	Observation	Processing Angle	Speed	Cohesion	R.Var
1	Upward	16	Lactose 100	0.006472	29	Horizontal	50	Lactose 125	0.012283
2	Horizontal	16	Lactose 100	0.020664	30	Horizontal	100	Lactose 125	0.007117
3	Downward	16	Lactose 100	0.013822	31	Horizontal	100	Lactose 125	0.010181
4	Upward	75	Lactose 100	0.004582	32	Horizontal	100	Lactose 125	0.006808
5	Horizontal	75	Lactose 100	0.010068	33	Horizontal	125	Lactose 125	0.016352
6	Downward	75	Lactose 100	0.011729	34	Horizontal	125	Lactose 125	0.005961
7	Upward	16	Lactose 125	0.003981	35	Horizontal	125	Lactose 125	0.004086
8	Horizontal	16	Lactose 125	0.004452	36	Horizontal	125	Lactose 125	0.00094
9	Downward	16	Lactose 125	0.006016	37	Horizontal	125	Lactose 125	0.014357
10	Upward	75	Lactose 125	0.001404	38	Horizontal	125	Lactose 125	0.004079
11	Horizontal	75	Lactose 125	0.011	39	Horizontal	175	Lactose 125	0.002537
12	Downward	75	Lactose 125	0.016232	40	Horizontal	175	Lactose 125	0.005838
13	Upward	50	Lactose 125	0.003274	41	Horizontal	175	Lactose 125	0.006226
14	Upward	50	Lactose 125	0.005742	42	Horizontal	175	Lactose 125	0.018245
15	Upward-Horizontal	50	Lactose 125	0.003995	43	Horizontal	275	Lactose 125	0.009789
16	Upward-Horizontal	50	Lactose 125	0.006523	44	Horizontal	275	Lactose 125	0.015561
17	Horizontal	50	Lactose 125	0.006282	45	Horizontal	300	Lactose 125	0.016316
18	Horizontal	50	Lactose 125	0.005164	46	Horizontal	300	Lactose 125	0.018742
19	Horizontal-Down	50	Lactose 125	0.098037	47	Horizontal	25	Lactose 100	0.002483
20	Horizontal-Down	50	Lactose 125	0.057224	48	Horizontal	25	Lactose 100	0.004858
21	Downward	50	Lactose 125	0.082521	49	Horizontal	50	Lactose 100	0.011611
22	Downward	50	Lactose 125	0.072285	50	Horizontal	50	Lactose 100	0.013591
23	Horizontal	25	Lactose 125	0.00879	51	Horizontal	50	Lactose 100	0.011036
24	Horizontal	25	Lactose 125	0.005947	52	Horizontal	75	Lactose 100	0.001136
25	Horizontal	25	Lactose 125	0.004858	53	Horizontal	75	Lactose 100	0.004599
26	Horizontal	25	Lactose 125	0.00361	54	Horizontal	125	Lactose 100	0.002825
27	Horizontal	50	Lactose 125	0.01323	55	Horizontal	125	Lactose 100	0.007639
28	Horizontal	50	Lactose 125	0.008261					

As previously discussed, blend variance appears to change as a function of all these parameters. However, the question that remains is whether the observed effects are

indeed significant. Table 3.8 illustrates the three-way ANOVA, where since n>1, it can be solved for all interactions. Results show that mixing angle is the most significant contributor to the observed differences in blend variance. The following significant parameter is rotation rate, followed by cohesion, which is not significant for the available data, and is characterized by very high p-value of 0.70. Only the interaction between angle and rate is significant; all interactions involving cohesion are also clearly non-significant. Using this information we simplify the model as:

$$y_{jkl} = \mu + \alpha_j + \beta_k + \alpha\beta_{jk} + \varepsilon_{jkl}$$

The results of this statistical model are shown in Table 3.9. All three terms remain significant ($p<0.0001$), showing a lower value of p than in the full model. One remaining question is whether differences between the mixers are significant. Later on, a 4-way ANOVA will consider the results from both mixers, and reassess the significance of other parameters when considering both datasets. Prior to that, in the next section we examine the behavior of the powder residence time in the second mixer.

Table 3.8: Three-Way ANOVA on the blend uniformity variance for the second Continuous Mixer considering the treatments as: mixing angle, rotation rate, cohesion as well as 2-way and 3-way interactions.

Source	DF	SS	MS	F	p
Mixing Angle	4	1.23E-02	3.06E-03	64.42	0.000
Rotation Rate	8	1.72E-03	2.15E-04	4.52	0.001
Cohesion	1	7.16E-06	7.16E-06	0.15	0.701
Process Angle*Rotation Rate	4	4.37E-03	1.09E-03	22.95	0.000
Process Angle*Cohesion	2	5.18E-06	2.59E-06	0.05	0.947
Rotation Rate*Cohesion	4	1.55E-04	3.86E-05	0.81	0.528
Process Angle*Rotation*Cohes	2	6.99E-05	3.50E-05	0.74	0.488
Error	29	1.38E-03	4.76E-05		

Table 3.9: Two-way ANOVA for variance of the second continuous mixer examining mixing angle, rotation rate, and 2-way interactions.

Source	DF	SS	MS	F	p
Mixing Angle	4	1.23E-02	3.06E-03	72.04	0.000
Rotation Rate	8	1.72E-03	2.15E-04	5.06	0.000
Process Angle*Rotation Rate	4	4.37E-03	1.09E-03	25.67	0.000
Error	38	1.62E-03	4.25E-05		

3.3.2.2 Residence Time

In chapter 2 we found a direct correlation between improved mixing and higher residence times. As shown in Figures 2.2.3b and 2.2.4b, both angle and rotation rate affect the residence time. In the experiments reported here, five mixing angles and seven rotation rates where considered, each experiment was duplicated, resulting in a total of 24 observations, the details are shown in Table 3.10. Above, we considered whether the low significance of rotation rate on mixing is a result of rotation rate not statistically affecting residence time. Not enough data exists to determine the interaction of rotation rate and mixing angle but the main effects can be examined using the following statistical model:

$$y_{jk} = \mu + \alpha_j + \beta_k + \varepsilon_{jk}$$

The 2-way ANOVA for this model is shown in Table 3.11, where we consider the sources of mixing angle and rotation rate on residence time. The results clearly show that mixing angle has a more significant effect on residence time, with a p-value <0.001, but the effect of rotation rate is significant only to a lower degree, exhibiting a p-value of 0.07.

Table 3.10: Continuous Mixer 2 Experimental Residence Time Results obtained from varying materials, process inclination, and rotation rate.

Observation	Mixing Angle	Speed (RPM)	Residence Time (s)
1	Upward	50	102
2	Upward	50	115.9
3	Upward-Hori	50	36.6
4	Upward-Hori	50	47.1
5	Horizontal	50	8.02
6	Horizontal	50	24.2
7	Horizont-Down	50	14.3
8	Horizont-Down	50	14.4
9	Downward	50	17
10	Downward	50	12
11	Horizontal	25	23.6
12	Horizontal	25	20.5
13	Horizontal	50	20.3
14	Horizontal	50	13.84
15	Horizontal	100	9.14
16	Horizontal	100	10.2
17	Horizontal	125	11.9
18	Horizontal	125	9.48
19	Horizontal	175	8
20	Horizontal	175	7.39
21	Horizontal	275	9
22	Horizontal	275	8.63
23	Horizontal	300	7.53
24	Horizontal	300	7.47

Table 3.11: 2-way ANOVA for residence time of the second continuous mixer examining mixing angle and rotation rate.

Source	DF	SS	MS	F	p
Mixing Angle	4	14076	3519	140.76	1.46E-10
Rotation Rate	6	395	65.83333	2.633333	0.067641
Error	13	325	25		

3.3.3 Four-way ANOVA

Now that we have examined the mixing inclination, rotation rate, and cohesion for each individual mixer, we are in a position to conduct a general analysis that also examines the effect of the different mixers. This is an interesting approach when conducting design space studies and we wish to include in the study the effect of blender size. For batch rotating mixing systems, the scale-up of a mixer affects the shear rate primarily due to the fact that its dependence on the surface area. For free flowing

powders this may be dismissed; however for cohesive mixtures, a reduction in shear can lead to a decrease of the mixing rate (Muzzio *et al.*, 2004). As previously mentioned, convective blenders impart high shear conditions particularly beneficial for cohesive materials, which may otherwise agglomerate. More intense shear can break and disperse agglomerates, enhancing homogeneity on a finer scale. The observations used for the statistical model are shown in Table 3.12. Initially the model is:

$$y_{ijkl} = \mu + \eta_i + \alpha_j + \eta\alpha_{ij} + \beta_k + \eta\beta_{ik} + \alpha_j\beta_k + \alpha\beta_{jk} + \gamma_l + \eta\gamma_{il} + \alpha\gamma_{jl} + \beta\gamma_{kl} + \eta\alpha\beta_{ijk} + \eta\beta\gamma_{ikl} + \alpha\beta\gamma_{jkl} + \alpha\beta\gamma\eta_{ijkl} + \varepsilon_{ijkl}$$

Using the 4-way interaction as the error, since n=1, results with the following model:

$$y_{ijkl} = \mu + \eta_i + \alpha_j + \eta\alpha_{ij} + \beta_k + \eta\beta_{ik} + \alpha_j\beta_k + \alpha\beta_{jk} + \gamma_l + \eta\gamma_{il} + \alpha\gamma_{jl} + \beta\gamma_{kl} + \eta\alpha\beta_{ijk} + \eta\beta\gamma_{ikl} + \alpha\beta\gamma_{jkl} + \varepsilon_{ijkl}$$

Table 3.12: Variance observations as a function of Mixer, Processing Angle, Speed, and Cohesion.

Observation	Mixer	Mixing Angle	Speed	Cohesion	R.Var	Observation	Mixer	lixing Angl	Speed	Cohesion	R.Var
1	1	Upward	16	Lactose 100	0.0037	35	2	Horizontal	25	Lactose 125	0.00879
2	1	Horizontal	16	Lactose 100	0.0057	36	2	Horizontal	25	Lactose 125	0.005947
3	1	Downward	16	Lactose 100	0.0063	37	2	Horizontal	25	Lactose 125	0.004858
4	1	Upward	75	Lactose 100	0.0081	38	2	Horizontal	25	Lactose 125	0.00361
5	1	Horizontal	75	Lactose 100	0.0093	39	2	Horizontal	50	Lactose 125	0.01323
6	1	Downward	75	Lactose 100	0.0129	40	2	Horizontal	50	Lactose 125	0.008261
7	1	Upward	16	Lactose 125	0.0021	41	2	Horizontal	50	Lactose 125	0.012283
8	1	Horizontal	16	Lactose 125	0.0031	42	2	Horizontal	100	Lactose 125	0.007117
9	1	Downward	16	Lactose 125	0.0032	43	2	Horizontal	100	Lactose 125	0.010181
10	1	Upward	75	Lactose 125	0.0017	44	2	Horizontal	100	Lactose 125	0.006808
11	1	Horizontal	75	Lactose 125	0.0061	45	2	Horizontal	125	Lactose 125	0.016352
12	1	Downward	75	Lactose 125	0.0083	46	2	Horizontal	125	Lactose 125	0.005961
13	2	Upward	16	Lactose 100	0.006472	47	2	Horizontal	125	Lactose 125	0.004086
14	2	Horizontal	16	Lactose 100	0.020664	48	2	Horizontal	125	Lactose 125	0.00094
15	2	Downward	16	Lactose 100	0.013822	49	2	Horizontal	125	Lactose 125	0.014357
16	2	Upward	75	Lactose 100	0.004582	50	2	Horizontal	125	Lactose 125	0.004079
17	2	Horizontal	75	Lactose 100	0.010068	51	2	Horizontal	175	Lactose 125	0.002537
18	2	Downward	75	Lactose 100	0.011729	52	2	Horizontal	175	Lactose 125	0.005838
19	2	Upward	16	Lactose 125	0.003981	53	2	Horizontal	175	Lactose 125	0.006226
20	2	Horizontal	16	Lactose 125	0.004452	54	2	Horizontal	175	Lactose 125	0.018245
21	2	Downward	16	Lactose 125	0.006016	55	2	Horizontal	275	Lactose 125	0.009789
22	2	Upward	75	Lactose 125	0.001404	56	2	Horizontal	275	Lactose 125	0.015561
23	2	Horizontal	75	Lactose 125	0.011	57	2	Horizontal	300	Lactose 125	0.016316
24	2	Downward	75	Lactose 125	0.016232	58	2	Horizontal	300	Lactose 125	0.018742
25	2	Upward	50	Lactose 125	0.003274	59	2	Horizontal	25	Lactose 100	0.002483
26	2	Upward	50	Lactose 125	0.005742	60	2	Horizontal	25	Lactose 100	0.004858
27	2	Upward-Horizontal	50	Lactose 125	0.003995	61	2	Horizontal	50	Lactose 100	0.011611
28	2	Upward-Horizontal	50	Lactose 125	0.006523	62	2	Horizontal	50	Lactose 100	0.013591
29	2	Horizontal	50	Lactose 125	0.006282	63	2	Horizontal	50	Lactose 100	0.011036
30	2	Horizontal	50	Lactose 125	0.005164	64	2	Horizontal	75	Lactose 100	0.001136
31	2	Horizontal-Down	50	Lactose 125	0.098037	65	2	Horizontal	75	Lactose 100	0.004599
32	2	Horizontal-Down	50	Lactose 125	0.057224	66	2	Horizontal	125	Lactose 100	0.002825
33	2	Downward	50	Lactose 125	0.082521	67	2	Horizontal	125	Lactose 100	0.007639
34	2	Downward	50	Lactose 125	0.072285						

Table 3.13: Four-way ANOVA considering the treatments as: Mixer, Mixing Angle, Rotation Rate, Cohesion, and their interactions.

Source	DF	SS	MS	F	p
Mixer	1	5.43E-04	5.43E-04	11.41	0.002
Mixing Angle	4	1.12E-02	2.81E-03	59.11	0.000
Rotation Rate	8	1.75E-03	2.18E-04	4.59	0.001
Cohesion	1	3.06E-05	3.06E-05	0.64	0.429
Mixer*Mixing Angle	2	1.03E-03	5.15E-04	10.82	0.000
Mixer*Rotation Rate	1	1.62E-05	1.62E-05	0.34	0.564
Mixer*Cohesion	1	1.51E-05	1.51E-05	0.32	0.630
Mixing Angle*Rotation Rate	4	4.36E-03	1.09E-03	22.94	0.000
Mixing Angle*Cohesion	2	5.45E-06	2.73E-06	0.06	0.944
Rotation Rate*Cohesion	4	8.07E-05	2.02E-05	0.42	0.790
Mixer*Mix.Angle*Rotation R	2	1.51E-05	7.56E-06	0.16	0.854
Mixer*Mix.Angle*Coh.	2	5.10E-06	2.55E-06	0.05	0.948
Mixer*Rotation R.*Coh.	1	7.75E-05	7.75E-05	1.63	0.212
Mix.Angle*Rotation R.*Coh.	2	5.00E-05	2.50E-05	0.53	0.597
Mixer*Mix.Angle*Rot*Coh	2	0.00002224	1.11E-05	2.34E-01	0.793
Error	29	1.38E-03	4.76E-05		

The Four-way ANOVA for this model is shown in Table 3.13; the sources are the mixer, processing inclination, rotation rate, and cohesion. The ANOVA showed that the cohesion is the least significant factor. Mixing angle, rotation rate, followed by mixer, are the most significant parameters. The interaction between the three effects (cohesion, mixing angle, and mixer) was also the most influential out of the interactions. The least influential main effect was cohesion. All other interactions with the exception of the two-way interactions of mixing angle with rotation rate and cohesion, were also fairly insignificant with p-values greater than 0.2. Further examining the effects of the three most significant factors we neglect the main effect of cohesion and all of its interactions, which results in the following model:

$$y_{ijkl} = \mu + \eta_i + \alpha_j + \gamma_l + \eta\alpha_{ij} + \alpha\gamma_{jl} + \varepsilon_{ijkl}$$

The ANOVA for this statistical model is shown in Table 3.14. The ANOVA illustrates that mixer, processing angle, and cohesion are significant. Harwood (1975) observed that the mixing performance of several different convective continuous mixers depended on the formulation. This might lead to an assumption that convective continuous mixers will have the performance variations due to material properties, where the convective design and blender geometry may be important parameters to define. Previously we found that cohesion was an important parameter that statistically affected the mixing performance. Clearly in this work we found that cohesion did affect blend performance.

Table 3.14: Three-way ANOVA considering the treatments as: Mixer, Mixing Angle, and Cohesion.

Source	DF	SS	MS	F	p
Mixer	1	5.43E-04	5.43E-04	1.51E+01	3.227E-04
Mixing Angle	4	1.12E-02	2.81E-03	78.06	3.744E-20
Rotation Rate	8	1.75E-03	2.18E-04	6.06	2.394E-05
Mixer*Mixing Angle	2	1.03E-03	5.15E-04	1.43E+01	1.419E-05
Mixing Angle*Rotation Rate	4	4.36E-03	1.09E-03	30.30	1.744E-12
Error	47	1.69E-03	3.60E-05		

3.4 Summary and Conclusion

A majority of the existing continuous mixing work examines the effect of the convective system and rotation rate on the mixing behavior and residence time. In this work we extend this work by applying statistical analysis to investigate the effects of rotation rate, cohesion, and mixing inclination. Several ANOVAs were presented in this chapter; a 3-way ANOVA for the first mixer showed that all processing and material parameters did influence performance. In the 3-way ANOVA for the second mixer the mixing angle played a more significant role on mixing than the rotation rate. Cohesion

did not have a significant effect on homogeneity when we examined two different cohesion levels.

Given the difference in size and convective design of the blenders presented, dissimilarity between the results was to be expected. A 4-way ANOVA examined the main effects of: processing conditions, material parameters, and the mixers. The result illustrated that the mixer variability was a significant parameter and the more influential parameters were the mixing angle followed by rotation rate. Cohesion showed to be the least significant factor, with a p-value of 0.429 in the 4-way ANOVA.

Residence time was also examined and clearly illustrated to be influenced by rotation rate and mixing angle for both mixers. For the first continuous mixer we examined two different speeds and 3 mixing angles, for that case study the most significant factor was rotation rate. On the other hand for the smaller mixer, 5 mixing angles and 7 rotation rates were examined and mixing angle showed to be the more influential parameter.

The objective of this chapter was to apply a statistical method to characterize the significance of design, operation, and material parameters. Future work in continuous mixing will determine the most significant parameters and further increase the number of levels examined for that parameter. We will further investigate the effects of rotation rate and cohesion on residence time, axial dispersion, and other important parameters using PEPT in the next chapter.

Chapter 4

Positron Emission Particle Tracking

In this chapter we first present, the properties of the materials used, processing units, and the experimental setup are discussed. An example of the particle trajectories obtained from PEPT for a continuous mixing process is shown. The residence time, axial dispersion coefficient, and path length at different processing parameters such as impeller rotation rate and different mass flowrates are determined and discussed. Statistically the variations between the axial dispersion coefficients of the two materials examined will be minor.

4.1 Introduction

The study of granular materials is a complex field that often exhibits poorly understood phenomena both in nature (Wang *et al.*, 2002) and in industrial applications (Mehrotra *et al.*, 2007). The motion of granular materials is affected by the particle properties such as size and morphology (Jullien and Meakin, 1990), particle interactions (Hutton *et al*., 2004), and physical surroundings such as vessel design (Moakher *et al*., 2000). Several tracking techniques have been used in order to understand granular motion: MRI (Metcalfe *et al.*, 1998), X-ray tomography (Powell and Nurck, 1996), impedance tomography (Williams and Xie, 1993) and positron emission particle tomography (PEPT). PEPT is used in this chapter to examine a continuous powder mixer.

PEPT is a non-invasive tomographic technique derived from medical applications of Position Emission Tomography (PET) (Yang *et al.*, 2007). In PEPT, the motion of a

single positron-emitting particle within the flow of a typical bulk granular material is followed. The technique yields spatial coordinates of the particle as a function of time. The method has been examined at the University of Birmingham for several blending systems: solid flow in the riser of a Circulating Fluidised Bed (Van de Velden *et al.*, 2007), rotating drums (Lim *et al.*, 2003; Ingram *et al.*, 2005), and a V-Blender (Kuo *et al.*, 2005). The system may track one, two, and up to three particles within the vessel at a time (Yang *et al.*, 2006; Yang *et al.*, 2007). The method has been found useful to determine velocity distributions, shear gradients, occupancy diagrams (Laurent and Bridgwater, 2002b; Laurent and Bridgwater, 2002c). However, previous publications investigating mixing vessels using PEPT examined closed systems. Here, PEPT is used for the first time to examine continuous flow and mixing processes.

While continuous powder mixing has been used for decades in food and cement industries, interest in the topic has been renewed by a recent emphasis placed on continuous pharmaceutical manufacturing applications. Two important questions that need to be addressed are (1) what are the critical parameters and (2) how to select values of these parameters that ensure content uniformity. Previous work on continuous mixing has identified impeller speed (Marikh *et al*., 2005), blender inclination (Portillo *et al.*, 2008), powder flowrate (Marikh *et al.*, 2005), and the convective design (Harwood *et al.*, 1975) as important variables. Prior work has mainly examined the effect of content uniformity and residence time using tracer injection studies. No published experimental work has examined the motion of a particle along the axial length of the mixer and the effects that cohesion, rotation rate, and flowrate have on residence time, axial dispersion, and on estimated total particle path length traveled by the particles.

4.2 Material Properties and Experimental Equipment

4.2.1 Powder Properties

The two materials examined were both common pharmaceutical ingredients that varied in cohesion grade: edible lactose (Dairy Crest) and free flowing lactose (Mallinckrodt). Following recently published work, cohesion was characterized by measuring the extent of dilation of the powder flowing under unconfined conditions. In general, dilation increases with cohesion, this was further explained by Faqih *et al.* (2006), who developed a method where common pharmaceutical ingredients such as lactose dilated up to 30%. The changes in powder dilation are illustrated in Figure 4.2 for the two materials used in this study. Clearly edible lactose has a higher dilation. In addition, a flow index that is proportional to the yield strength of the dilated powder was measured using the GDR (gravitational displacement rheometer). The higher the flow index, the more cohesive the powder and the worse the flow properties (Faqih *et al*., 2006). As shown in Table 4.1, the edible lactose displays a higher dilation, a larger flow index values and a larger Hausner ratio. All of these results agree in indicating that the more cohesive powder was the edible lactose in comparison to the free flowing lactose.

Table 4.1: Density properties of Edible and Fast Flow Lactose

Material	Bulk Density	95 %Confidence Interval	Tapped Density	95 %Confidence Interval	Hausner Ratio	Flow Index
F. Flow Lactose	0.626	[.615, .637]	0.704	[.692, .716]	1.125	24.9
Edible Lactose	0.629	[.612, .646]	0.981	[.963, .998]	1.559	34.8

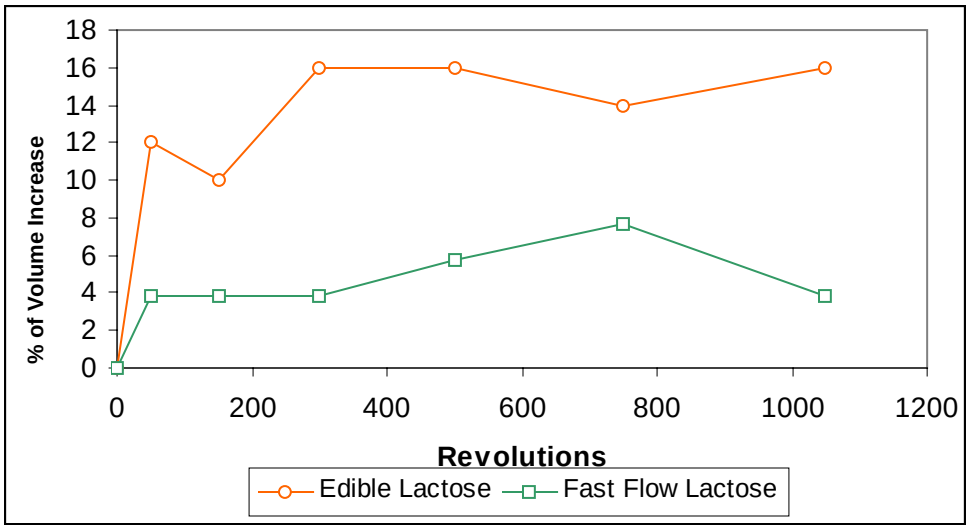

Figure 4.1 Dilation results for Edible and Fast Flow Lactose

4.2.2 Vibratory Feeder

The feeding system used was a vibratory mechanism (Eriez, Erie, PA). Vibration speed, dam height, and spring thickness are the parameters used within the feeder to change flow rate. The feeding flow rate is also dependent on the powders bulk density; therefore at the same processing conditions, flowrates vary as a function of bulk density as shown for the two materials in Table 4.2. The average mass flowrates and confidence intervals shown in Table 4.2 were obtained from three trials. Free Flowing Lactose was also studied for two additional flowrates used for a flowrate study.

Table 4.2: Flowrates used in the inflow of the continuous mixer for Edible and Fast Flow Lactose

Material	Flowrates (g/s)	95% Confidence Interval (g/s)
Edible Lactose	8.300	[7.76, 8.85]
F. Flow Lactose	6.804	[6.59, 7.02]
F. Flow Lactose	4.139	[3.90, 4.38]
F. Flow Lactose	8.415	[8.02, 8.81]

4.2.3 Continuous Mixer

The continuous mixer examined here is manufactured by Buck Systems in Birmingham, England. The mixer is 0.31 meters long and the radius is 0.025 meters. The

continuous mixer was inclined at an upward angle of 17°. The mixer's rotation rate spans from 17 RPM to 340 RPM. The mixer contains flat triangular blades with a 37° angle. As material enters the mixer, the powder crosses the pathway of several impellers. The convective system of the continuous blender studied is illustrated in Figure 4.2. As the blades rotate, the powders are mixed and agglomerates are broken up. Convection is the primary source of mixing in the cross-sectional direction. Dispersion is the main source of mixing in the axial direction, which is superimposed on the axial transport effect of the bulk flow, which conveys the powder toward the exit of the blender.

Figure 4.2 Detail of the impeller design in the continuous blender used for PEPT experiments

4.3 Measurement technique

4.3.1 Method

PEPT has been reviewed in several existing papers and in this work we briefly summarize the method. A more detailed explanation on the technique can be found in Parker *et al.* (1997) and in Jones *et al.* (2007). PEPT tracks a single radioactive tracer (130 μm resin tracer is composed of silica glass and is irradiated with F_{18} radioisotope) as a function of time. During radioactive decay, a high-energy positron is emitted, an electron nearby annihilates the positron and two almost collinear gamma rays are generated. The PEPT camera consists of two symmetric plates that detect the gamma rays between them. If both gamma rays are absorbed by a detector element on each plate,

then two lines can be drawn between the detector elements (one line for each gamma ray) on which the tracer is expected to lie. The intersection of the multiple pairs of lines gives the location of the tracer. Unfortunately, due to the scattering of gamma rays, erroneous locations might be shown. In order to filter erroneous locations, a position is considered accurate if the location is repeated 100 times and dismissed if found a lower number of times. Consequently, the results are averaged (x,y,z) points that estimate the location of the tracer between the plates.

4.3.2 Particle Trajectories

In this section we discuss the details of obtaining one particle trajectory of the resin particle within Edible Lactose for the processing conditions (170 RPM, 8.3 g/s Flowrate, ~23 % Fill Level). The occupancy diagram for the particle along the radial view of the vessel is shown in Figure 4.3a. Figure 4.3b illustrates the corresponding velocity gradients using a radial view. The corresponding trajectory of the particle along the radial area depicts the particle moving within a ring area, never occupying the center due to the presence of the shaft.

If a vertical line slices the vessel from top to bottom into two adjoining semicircles, the right semicircle illustrates a greater degree of radial dispersion along the radial axis. This occurs because when the particle exists in the left region, movement occurs due to the impeller lifting up the particles whereas at the right the particles are falling mainly due to gravity. The particle trajectory at the axial view of the vessel is shown in Figure 4.4a, the velocity view is Figure 4.4b, and the 3-dimensional schematic is shown in Figure 4.5. All illustrations show that the particle follows a spiral path, due to the combination of axial transport and blade rotations. Computation of the residence

time, axial dispersion coefficient, and total particle length will be discussed in the next section.

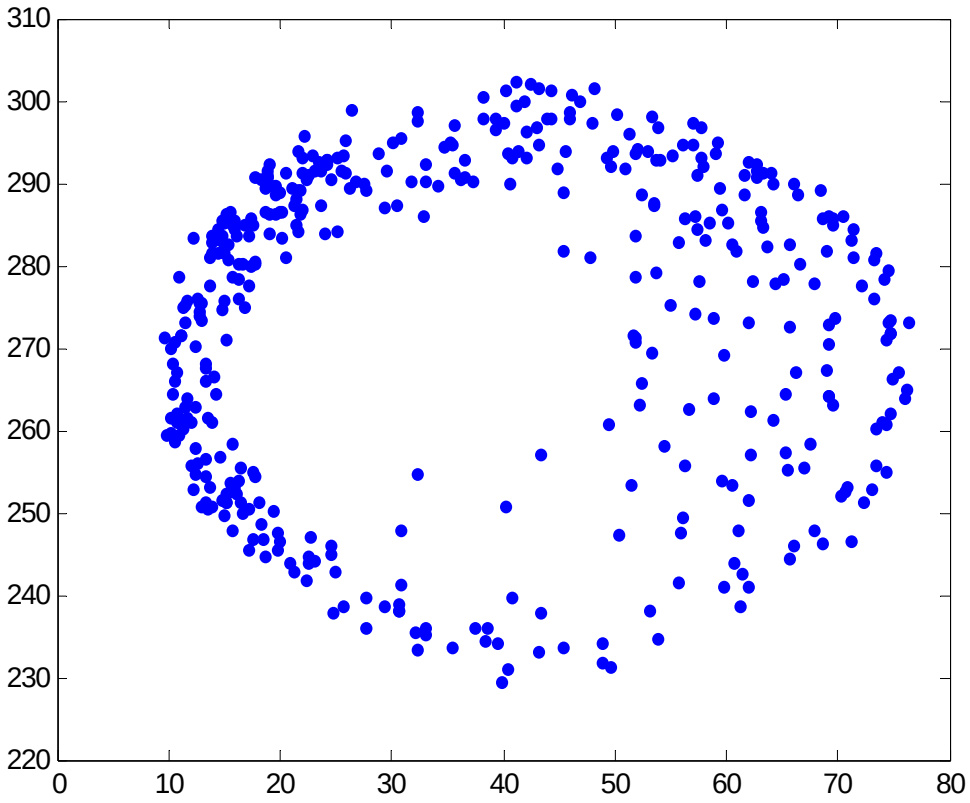

Figure 4.3a Radial view of PEPT particle trajectory in the continuous blender operated at 170 RPM, 8.3 g/s flowrate, for edible lactose at ~23 % fill level

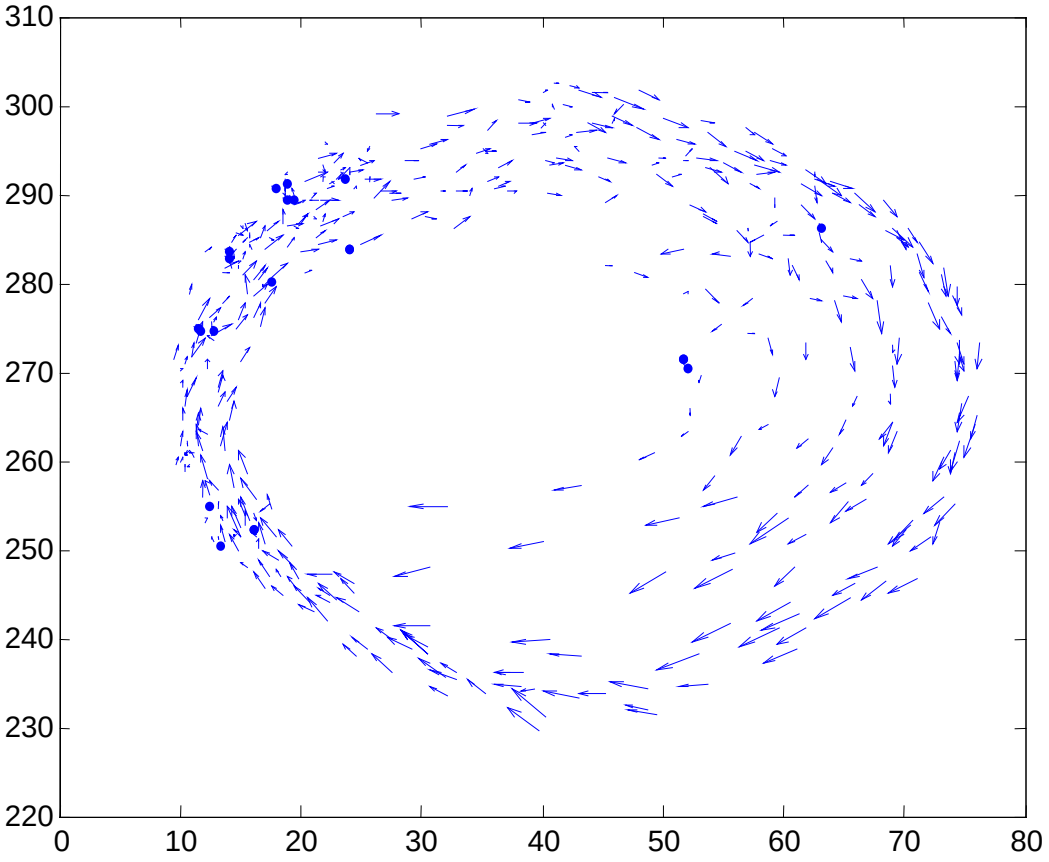

Figure 4.3b Radial view of PEPT particle velocity plot in the continuous blender operated at 170 RPM, 8.3 g/s flowrate, for edible lactose at ~23 % fill level

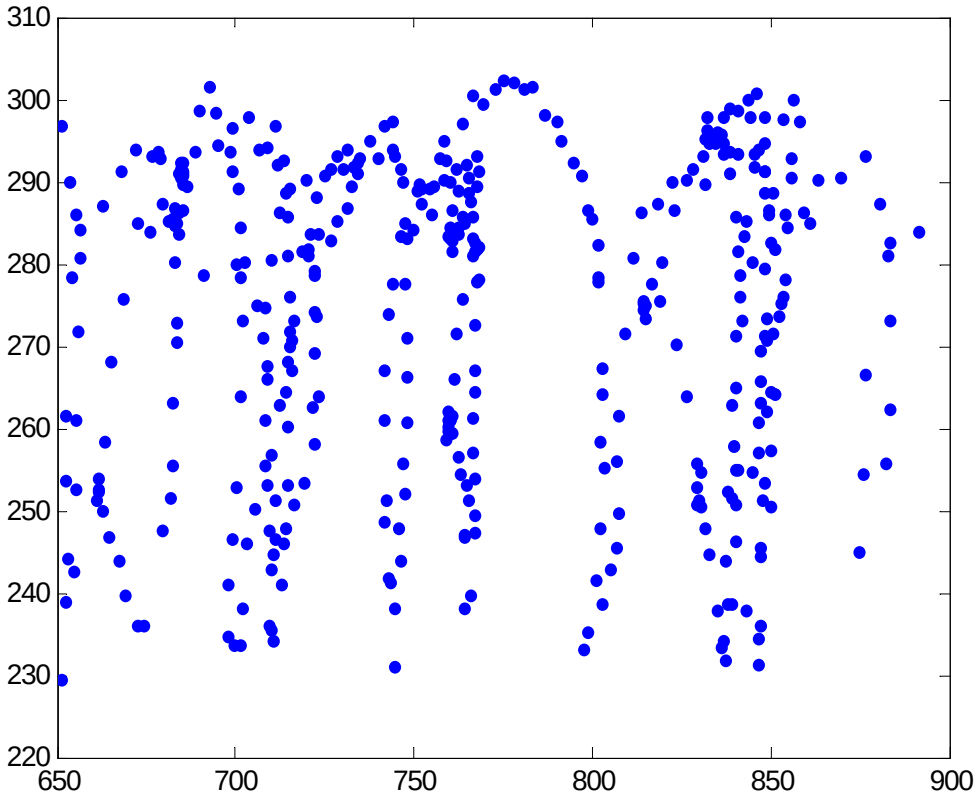

Figure 4.4a Axial view of PEPT particle trajectory in the continuous blender operated at 170 RPM, 8.3 g/s flowrate, for edible lactose at ~23 % fill level.

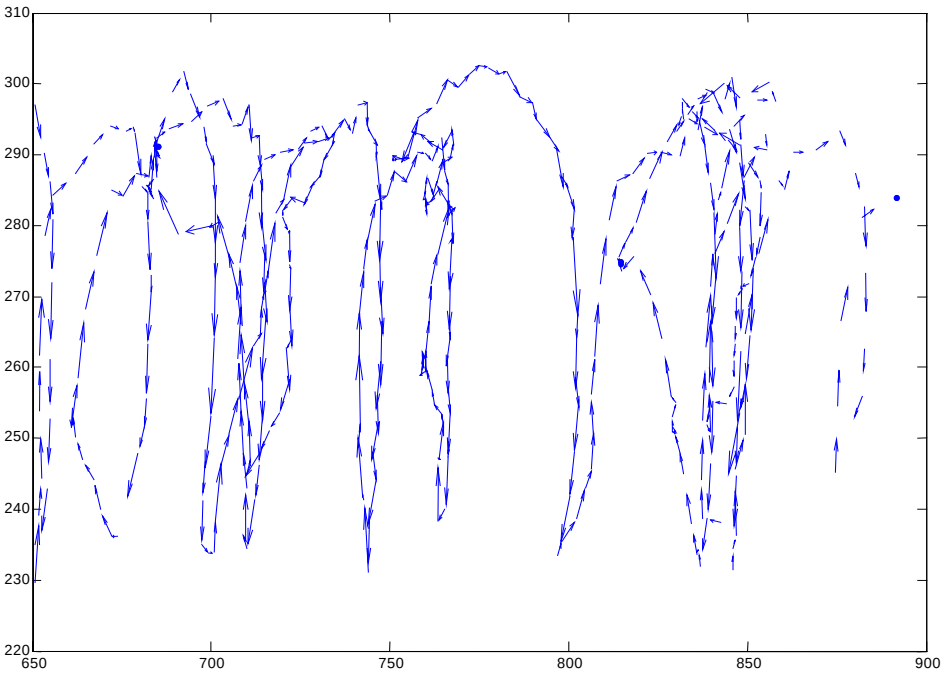

Figure 4.4b Axial view of PEPT particle velocity plot in the continuous blender operated at 170 RPM, 8.3 g/s flowrate, for edible lactose at ~23 % fill level

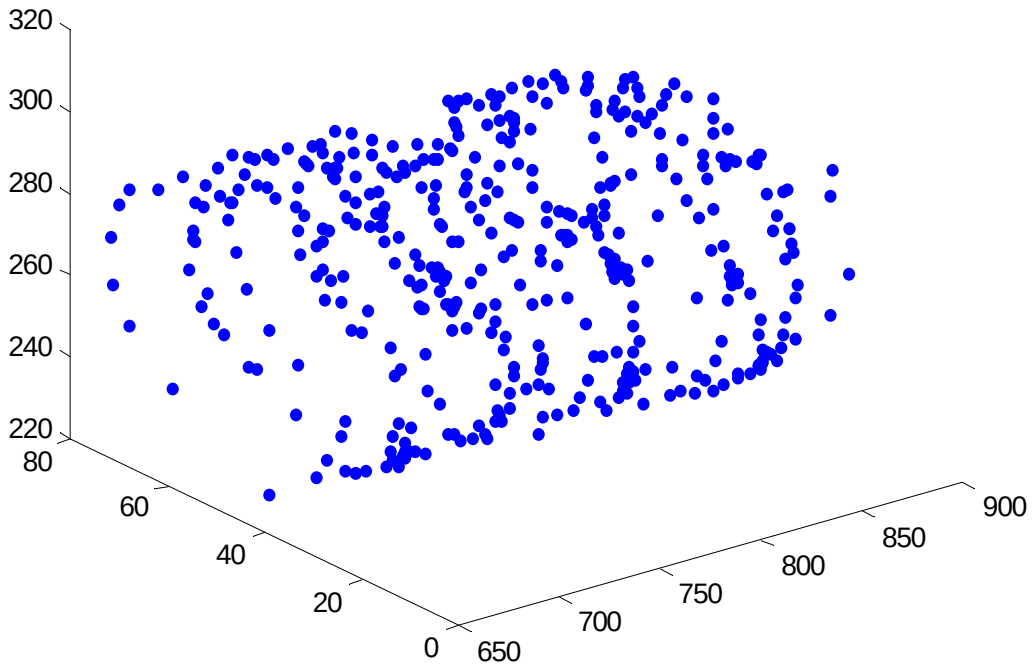

Figure 4.5 3-D view of PEPT particle trajectory in the continuous blender operated at 170 RPM, 8.3 g/s flowrate, for edible lactose at ~23 % fill level.

4.4 Results

4.4.1 Particle Residence Time

The residence time was calculated for each particle trajectory at the given processing conditions. Residence time is used to determine the strain and is an indirect indicator of the axial transport velocity the particle experiences within the vessel at varying processing and bulk material conditions. Several particle trajectories were recorded for each set of operating conditions (speed, powder, and flowrate). The average residence time was calculated from all the trajectories. The experimental work presented in chapter 2 using Danckwerts' RTD approach (1953) has measured residence times for continuous blending (Portillo *et al.*, 2008), where a large number of tracer particles were injected at the entrance of the mixer and the residence time distribution was obtained as

the powder appeared at the mixer outflow. The mean residence time can than be derived from the distribution using the preferred mathematical mean approach.

In addition, the time a particle enters and departs an axial interval within the vessel has been examined using PEPT by Broadbent and coworkers (1995). In this work we refer to such a measurement as the spatial residence time. This measurement was particularly useful considering the horizontal cylinder is at an upward 17° degree incline and the residence time along the inclined cylinder can be determined and analyzed to determine whether the spatial residence time changes along the axis as the inclination increases, for example if the depth of the powder bed is position-dependent. Here, spatial residence times are determined and the variability between the spatial residence times at different axial positions are statistically examined in order to determine if the residence time along the axial length is affected by the inclination.

4.4.2 Effect of Impeller Rotation Rate

The convective motion within a mixer has been shown to affect blending and axial transport (Laurent and Bridgwater, 2002b,c) in continuous mixers. The issue has been examined in some detail for tumbling blenders. For blending of batch systems, homogenization of free flowing powders is often unaffected by the rate of the convective motion. On the other hand, cohesive powders have been affected by the vessel rotation rate (Sudah *et al.*, 2002a). For continuous mixing, on the other hand, the effect of agitation rate has been examined more sparsely. Williams and Rahman (1971a), obtained enhanced mixing results for lower rates of agitation. Moreover, in chapter 2 the rate of agitation for a continuous mixer found that mixing was best at the lower convective motion rates.

Intuitively, the rotation rate of the blades changes the rate of shear and the intensity of material dispersion throughout the mixer. The effect of the work performed by the agitator is examined here to determine its effect on powder axial transport. In chapter 2 we use Danckwerts RTD approach (1953), we reported that higher rotation rates resulted in lower residence times. In this study, the rotation rate was adjusted to three different impeller rotation rates (16, 75, 170 RPM). The quantitative measurements for the residence times at the three different rotation rates for free flowing lactose are illustrated in Table 4.3. In summary, the residence times correlated closely to those obtained using Danckwerts approach (1953), measuring noticeably higher residence times at lower impeller speeds (RPM).

Table 4.3: Average Residence Time for free flowing lactose at a flowrate of 6.8g/s at three different rotation rates

Rotation Rate	16 RPM	75 RPM	170 RPM
Average Residence Time	143	66	10
95 % Confidence Interval	[118,168]	[50, 82]	[9, 11]

4.4.3 Flowrate Comparison

Fill level is an important parameter that has been intensively studied for batch mixing systems (Sudah *et al.*, 2002b; Arratia *et al.*, 2006), where it has been shown that mixing is often best at 40-60% fill level and it worsens substantially at fill levels greater than 70%. Unlike batch mixers, for continuous mixers material is continuously fed into the vessel as a function of time. Thus, the fill level or powder hold-up is affected by the material flowrate and residence time, thereby correlating flowrate variations to fill level.

Three flowrates at two different rotation rates were examined. At a constant rotation rate, variations in flowrate changed the residence time. The results of the 6 different processing conditions are shown in Table 4.4. At 75 rpm we found that

increasing the flowrate resulted in lower residence times. Thus, high throughout resulted in greater transport velocity. On the other hand, at a higher rotation rate (170 rpm), increasing the throughput resulted in higher residence times. The controlling factor for these two effects of flowrate variations is likely to be the powder hold-up. As these two processing conditions change the powder hold-up within the vessel also changes, as shown in Figure 4.6; as the powder hold-up ratio increases, the residence time increases.

Broadbent and coworkers (1995) found the same trend when they examined several tracer particles that ranged from 2 to 8 mm in size using a convective mixing system in a closed vessel. The fill levels examined spanned from 10 to 70% and the resulting pattern was an increasing residence time with fill level. In summary, the effect of flowrate on the residence time is dependent on the processing agitator rate since both flowrate and agitator rate affect fill level.

Table 4.4: Residence Time as a function of flowrate

Flowrate (g/s)	RPM	Res. Time (s)	95% Confidence Interval
4.139	75	78	[89, 66]
6.804	75	66	[82, 50]
8.415	75	44	[52, 36]
4.139	170	9.5	[10, 8.5]
6.804	170	10	[11, 9]
8.415	170	15	[17, 13]

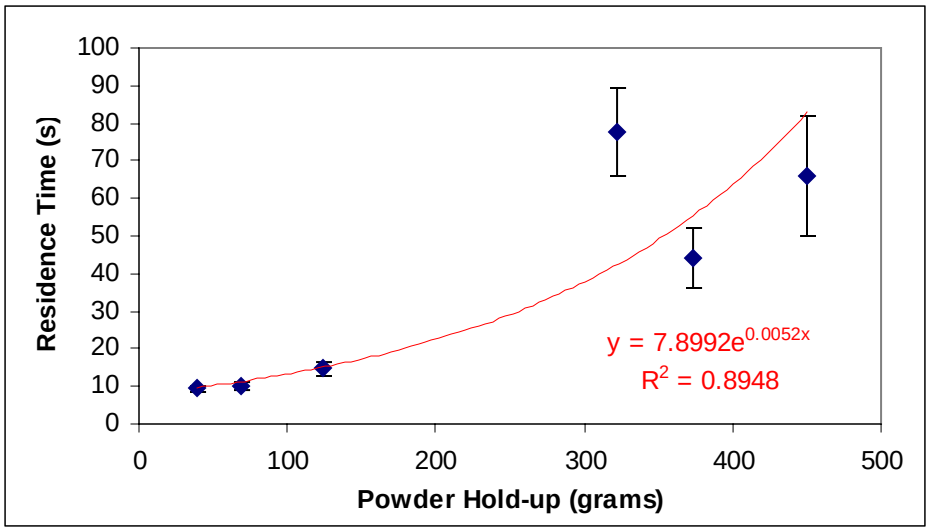

Figure 4.6: Residence time as a function of powder hold-up.

4.4.4 Effect of Cohesion

Interparticle attraction forces (both frictional and adhesive) are usually referred to as "cohesion". Cohesion is an important parameter affecting powder flow, and the effect of cohesion on the mixing rate is by no means simple. In this case study, edible lactose, was compared to the less cohesive Free Flowing Lactose. As shown in Figure 4.7 both materials illustrate similar decreasing residence time as a function of impeller speed. The more cohesive powder has greater residence times and a slightly higher slope. Notably, differences between the residence time profiles for the two materials is greater at lower speeds and negligible at high speeds. The agitator motion plays a vital role in the axial transport of the powder bed; at lower agitation speeds interparticle forces between the powders are likely to have a more dominant effect on the axial velocity than at higher rotation rates.

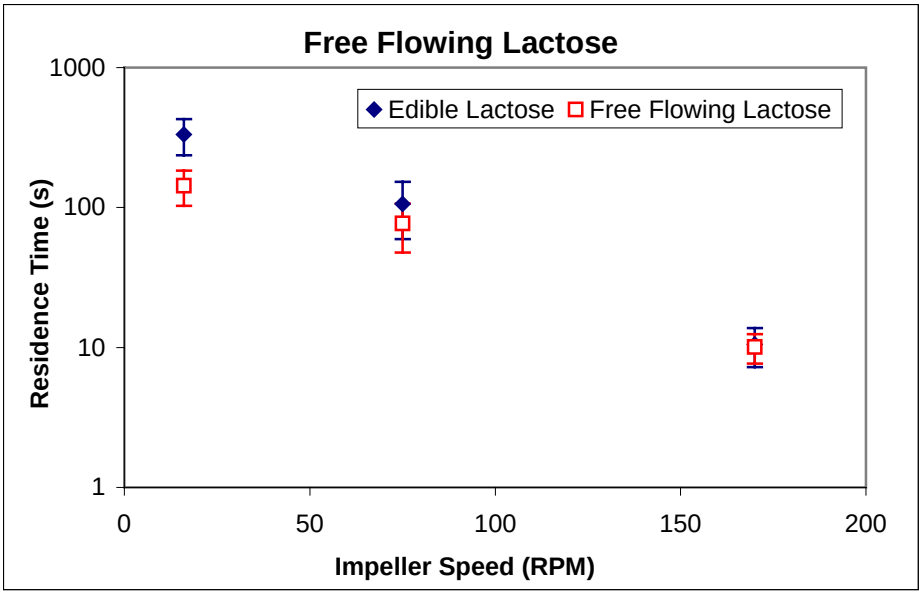

Figure 4.7: Logarithm of the average Residence Time as a function of impeller speed for Edible lactose and Free Flowing Lactose.

4.4.5 Spatial Residence Time

The axial length of the vessel examined here is .31 meters. However, as mentioned above, since a steep incline of 17° is used, the depth of the powder bed is likely to vary along the axis, and thus it is interesting to examine the residence time of the powder at different axial locations. To this end, the vessel is discretized into 5 subsections, as shown in Figure 4.8, each subsection has an axial length of .062 meters. The residence time corresponding to the i^{th} spatial area is denoted τ_i. For all the processing conditions examined here, each experiment is replicated 10 to 25 times, which results in total of 499 observations. The results shown in Figure 4.9 depict the average spatial residence time as a function of spatial position for the 10 process settings. From the figure, no direct relationship between the spatial residence time and axial interval is apparent. In order to determine if statistically the particles remained within specific areas of the vessel longer than others, statistical analysis on all the trajectories was conducted. The null hypothesis was that the residence time of each of the spatial areas isn't different,

hence: $\mu^2_{\tau_1} = \mu^2_{\tau_2} = \mu^2_{\tau_3} = \mu^2_{\tau_4} = \mu^2_{\tau_5}$. In order to dismiss this hypothesis, the p-value obtained from an ANOVA is typically required to be a small value, usually smaller than .05. Using SAS version 9.1, a one-way ANOVA summarized in Table 4.5 yields a p-value of .545, which given the large number of results used in this study, inicates that the particles spatial residence time is not substantially affected by its axial position (i.e., no larger "dead zones" appear to be present).

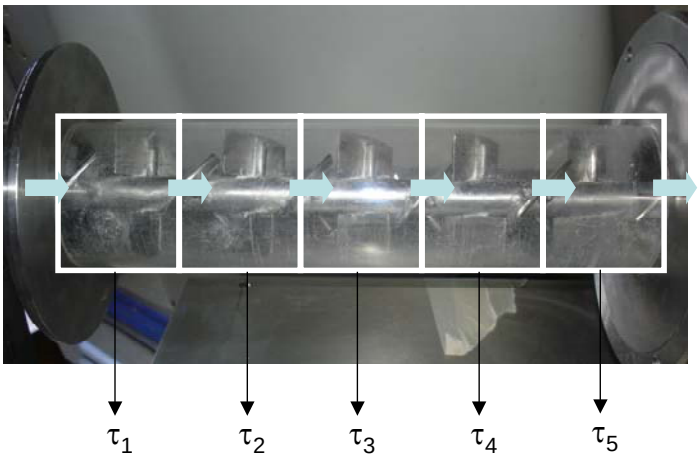

Figure 4.8: Detail of the continuous mixing vessel showing the five zones used to determine the possible dependence of residence time on axial location.

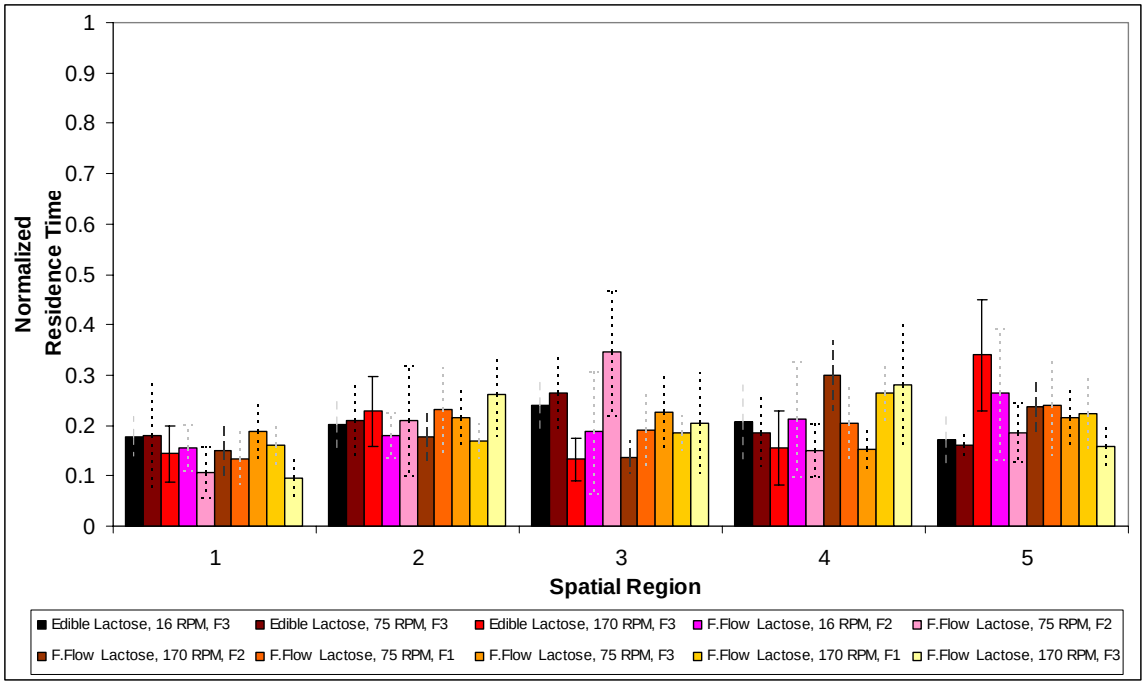

Figure 4.9: Average Residence Time as a function of 5 spatial regions within the vessel, where the 1st spatial region begins at the entrance (0-.062m), 2nd (.062-.124 m), 3rd (.124-.186 m), 4th (.186-.248 m), and 5th (.248-.31 m) at 10 different processing conditions (Material, RPM, Flowrate).

Table 4.5: Statistical Analysis on the hypothesis that the variance between the 5 axial residence time of 100 particle trajectories.

Source	DF	Sum of Squares	Mean Square	F	p
Spatial Area	4	1405	351	0.77	0.545
Error	494	225113	456		

4.4.6 Axial Displacement

The other parameter that evaluates particle mobility is the axial dispersion coefficient. Using the concepts of dispersion coefficient and Einstein's law, axial displacement was investigated by Laurent and Bridgwater (2002b) using the relationship:

$$D_{axial} = \lim_{\Delta t \to 0} \frac{\left\langle \Delta x^2 \right\rangle}{2\Delta t}$$

where Δx^2 is the mean square displacement. Laurent and Bridgwater (2002b) have extensively examined the axial displacement for closed convective systems composed of 1 and 6 blades for impellers rotation rates in the range of 25 to 45 rpm. They found that for the 1 blade scenario, axial dispersion coefficients ranged from 10 to 22 mm^2/s. For 6 blades the result was higher dispersion coefficients ranging from 10 to 45 mm^2/s. Moreover, in terms of powder hold-up, the coefficients increased for low hold-ups and than lessened from higher hold-ups.

The results communicated here confirm these trends. Initially the coefficient increased to 174 mm^2/s as the powder bed approached a 68.8 grams of holdup, and from there the coefficient decreased at higher hold up, as shown in Figure 4.10. This probably occurs because the volumetric fill level of material within the mixer affects the ability for the blade to propel the powder to neighboring areas, thus changing value of the axial transport coefficient.

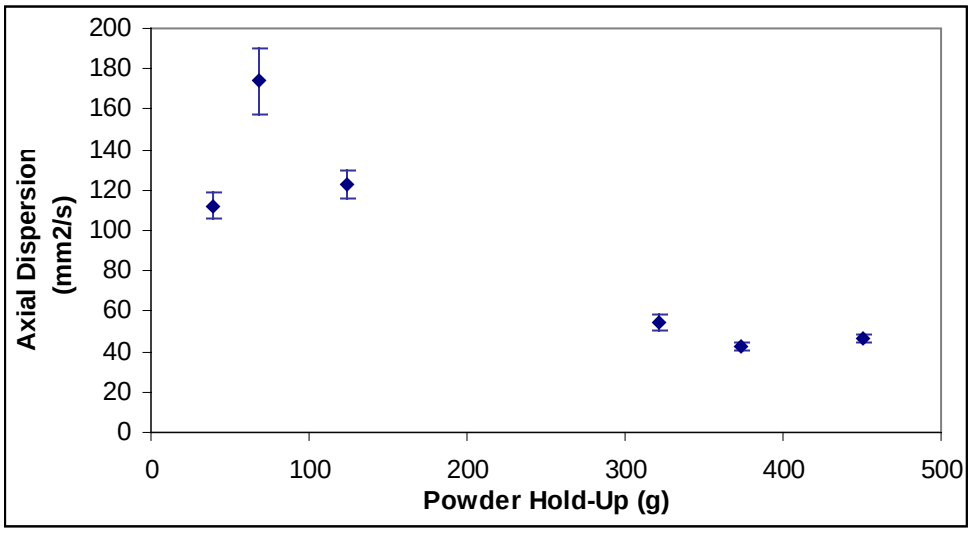

Figure 4.10: Axial dispersion coefficients as a function of powder hold-up.

Rotation rate also affects the rate of shear and the intensity of material dispersion. Laurent and Bridgwater (2002b) found that axial dispersion increased at higher rotation

rates for two different closed convective designs. The system they examined were equipped with one and six blades, whereas we examine a vessel with 14 convective blades that gyrate from 16 to 170 rpm. In agreement with the previous findings, we found that the axial dispersion coefficients increase at higher speeds (Figure 4.11). These findings were based on two different lactose grades. Very minor differences between the axial dispersions at the same rotation rate were found for the two materials. Furthermore, the dispersion coefficient we deduced from our study was greater than that found in previous literature using PEPT due to the additional blades in our mixing system. In order to determine whether the variability of the axial dispersion between the two different materials is significant, ANOVA is used to test the null hypothesis that the axial dispersion coefficient for edible lactose μ_{edible} and free flowing lactose μ_{free} at the three different rotation rates (shown in Figure 4.11) are equal, i.e. $\mu_{edible}=\mu_{free}$. Table 4.6 shows that the main effect of cohesion for 81 observations was fairly insignificant with a p-value of 0.71, whereas rotation rate clearly affected the axial dispersion. This suggests that the effects of interparticle forces on powder flow and mixing are not significant between these two materials under the conditions tested here.

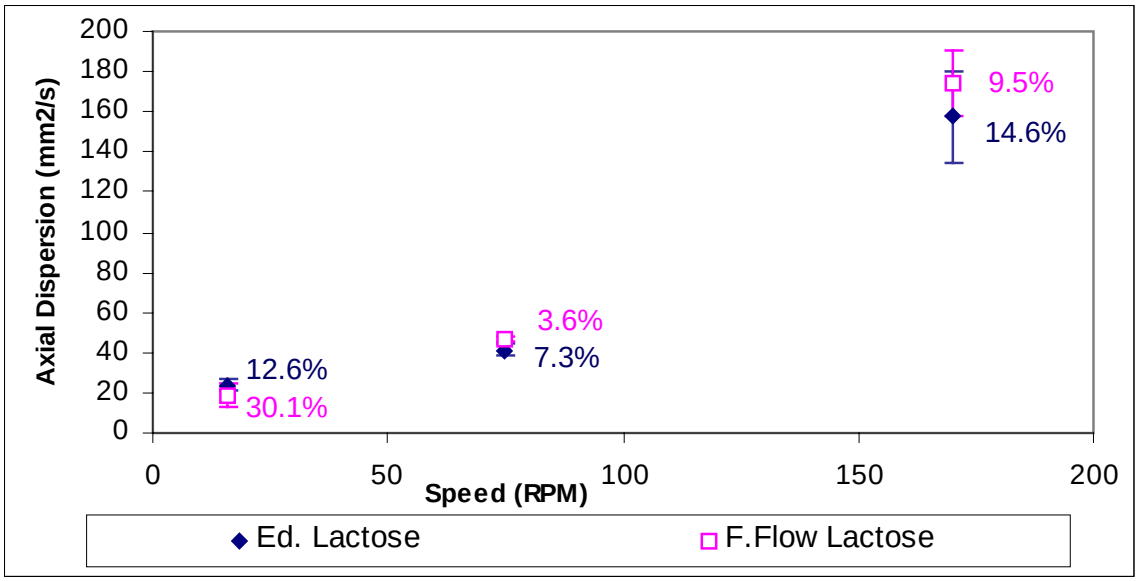

Figure 4.11: Axial Dispersion Coefficient as a function of impeller rotation rate (RPM).

Table 4.6: Statistical Analysis of cohesion on the Axial Dispersion Coefficient.

Source	DF	SS	MS	F	p
Cohesion	1	310.1325	310.1325	0.144982	0.704426
Rotation Rate	2	298163.3	149081.7	69.69313	0.000
Error	77	164711.9	2139.116		

In batch rotating systems, residence time distributions are used to retrieve axial dispersion coefficients from the axial-dispersion model. Sherritt and coworkers (2003) derived the dispersion coefficient under the assumption of large Péclet numbers (Pe>50). Large Péclet numbers are found in slow axial mixing vessels (such as rotating drums). The axial-dispersion coefficient, D_z, is then obtained from the mean tracer residence time, $\langle t \rangle$, residence time standard deviation, σ_t^2, and axial length, Z, as:

$$D_z = \frac{Z^2 \sigma_t^2}{2\langle t \rangle^3}$$

The data obtained from the experiments in this work is used to compute axial dispersion coefficient and residence time, as shown in Figure 4.12. Along with this data

is the comparison of the theoretical axial dispersion using the residence time to the negative third power. The function captures the experimental measurements fairly well at higher residence times. For both the theoretical and approximated axial dispersion coefficients, the lower residence time, the higher the axial dispersion coefficient. It is important to remember that this theoretical relationship between axial dispersion and mean residence time was found for low Péclet numbers.

One approach used to determine Péclet numbers for continuous mixing processes was found by Weinekötter and Reh (1995) under the following assumptions:

1) The powder is pushed through the mixer at a given axial velocity.
2) Dispersion is superimposed on the convective transport.
3) Dispersion is solely dependent on the external power input (agitator work).
4) Powders do not exhibit brownian motion.

Given the assumptions, the resulting axial mixing model is followed as:

$$\frac{\partial c}{\partial t} = -v \cdot \frac{\partial c}{\partial z} + D_z \cdot \frac{\partial^2 c}{\partial z^2}$$

where D_z is the axial dispersion coefficient, v is the axial velocity, and Z axial length. Applying boundary conditions, this equation is solved, resulting in the following expression for the Péclet number:

$$\frac{v \cdot Z}{D_z} = \text{Peclet number}$$

Given this definition for the Péclet number, the experiments examined in this work range from 8.09 to 137 with a mean average of 50.4. The Péclet number can be used to describe accurately the relation between the convective and diffusive motions (Lu and Hsiau; in press) and the mixing mechanism. For low residence times, the lower the

Péclet number, the greater the vessel performs in an ideal stirred vessel. On the other hand, larger Péclet numbers correspond to plug flow characteristics (Weinekötter and Reh, 1995). In the study, we find that lower residence time case studies, which occur at high rotation rates, result in flow characteristics closer to plug flow.

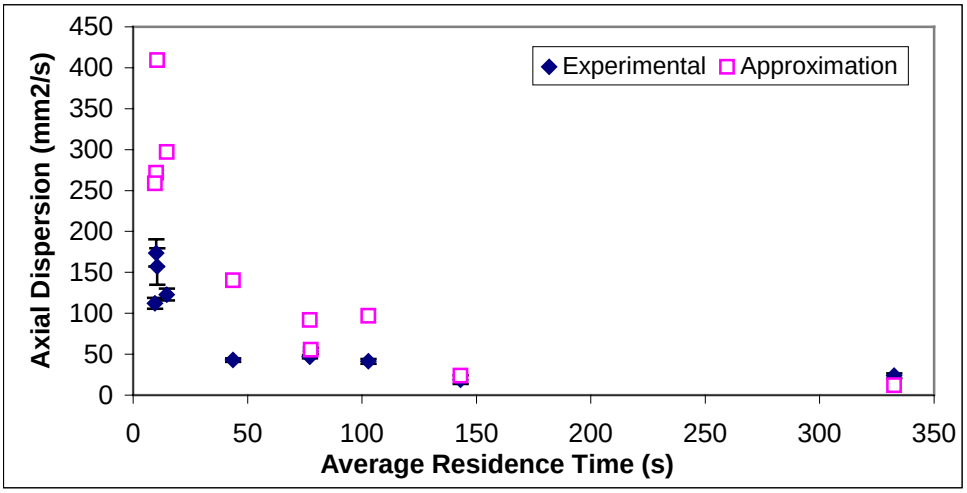

Figure 4.12: Axial Dispersion Coefficient as a function of Residence Time calculated from the PEPT data and estimated using Sherritt and Coworkers (2003) approximation.

4.4.7. Path Length

Einstein (1937) defined path length as the total distance covered by particles from the initial position (the entrance) to the final position. This is distinct from "step length" which considers intermittent bursts of movement between still periods as the particle moves along the path. The path length is important for two reasons: (1) it provides a basis for measurement and prediction of axial transport for a given fill level or powder hold-up; and (2) particle displacement is possibly impacted by electric charge particles may gain as they rub against other particles or vessels. Therefore, it may be an indicator of their tribocharge effect (Dammer *et al.*, 2004). In this work, an estimated value for the total distance a particle travels within the continuous mixer is calculated as it descends along the axial direction and propagates toward the mixers outflow. The different

particle paths obtained at the same processing positions are often different from one another because of the randomness of the particle movement due to the initial position and particle interactions. Here we determine the distance the particle traveled considering the 3 spatial coordinates. The initial particle position (x_0,y_0,z_0) is obtained and at each time step the new spatial position of the particle (x,y,z) is found, at each proceeding time step, Δt, the spatial change is obtained (Δx, Δy, Δz) and the total distance, ℓ_k, traveled between the time step is calculated as:

$$\ell_k = \sqrt{\Delta x_k \times \Delta x_k + \Delta y_k \times \Delta y_k + \Delta z_k \times \Delta z_k}$$

It is important to mention that the particles position may not be exact due to resolution issues in the PEPT camera and also because particle positions are captured at discrete time intervals; and a result, the path length calculated should be considered an estimate. In keeping with this statement, the path length traveled by the particle as it enters and leaves the vessel is *estimated* as the sum of all the distances traveled for all N times steps,

$$Path\ Length = \sum_{k=1}^{N} \ell_k$$

In this section we examined and compared the total path length between two flowrates and three rotation rates. We found that the particles covered a greater path length within the vessel at lower rotation rates. Clearly the conditions that result in the highest path lengths are correlated to the residence time as shown in Figure 4.13. At high impeller rotation rates, the residence time is lower, therefore a greater noise may exist in the measurements that might underpredict the particle path. In order to determine if this is due to a lower resolution at high speeds and not a time step effect at low residence times. The calculations shown in Figure 4.13 use a .0169s time step, we extend the calculations to two additional larger time steps .0336s and .0472s, in order to examine the

affect of time step on the particle path at low residence times. Our findings are shown in Figure 4.14, increasing the time step by a multiple of two results in a lower prediction of the path length estimated, however increasing residence time clearly yields higher path lengths.

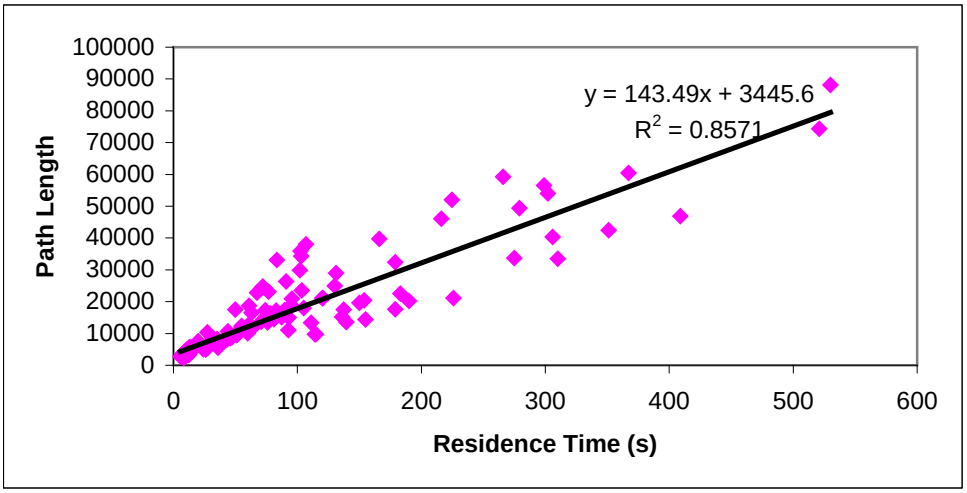

Figure 4.13: Total Particle Path Length as a function of Residence Time.

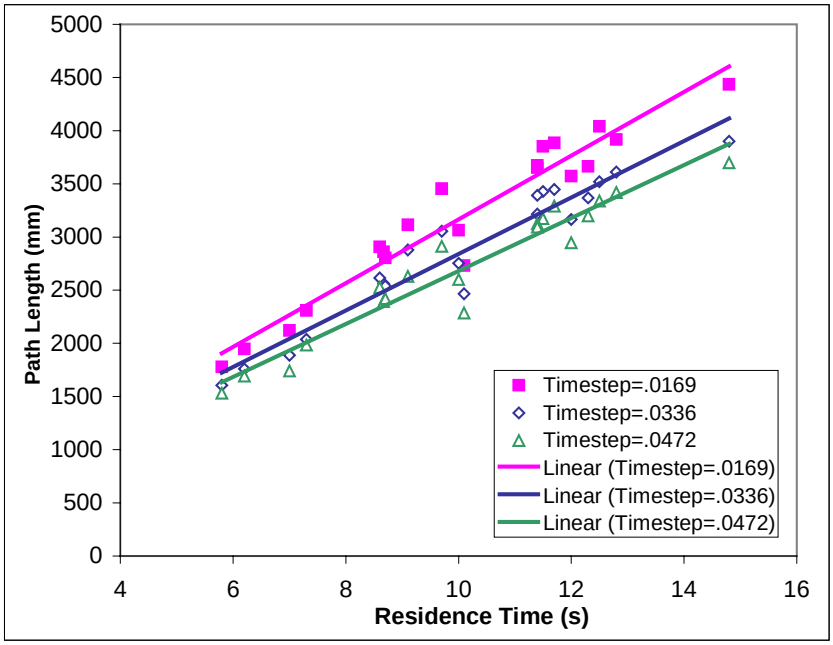

Figure 4.14 Total Particle Path Length as a function of Residence Time for high speed (170 RPM) impeller rotation rates.

Path length is also affected by powder hold-up. As shown in Table 4.7, path lengths increase for hold-ups up to 321.4 grams, followed by a decreasing path length as the hold-up increased further. In the previous section we examined two different lactoses that vary in cohesion grade. We found that for both grades of lactose the path length increased with rotation rate. The axial dispersion coefficients for the two different materials shown in Figure 4.11 are fairly similar and their difference is not statistically significant ($p=0.70$). On the other hand, the path length of these two materials was examined and a dramatic statistical difference ($p<.0001$) between both materials existed. Table 4.8 illustrates the path length at the different flowrates. At different throughputs and agitator speeds, particles moving in free flowing lactose experienced a longer path length than those in edible lactose. Statistically, as shown in Table 4.9, the total path length is affected by both cohesion and the speed. At 170 rpm, path lengths were very similar. Differences between the two cohesion levels, where each level was examined 14 times for a total of 28 observations, were no longer significant ($p= 0.6373$) shown in Table 4.10.

Table 4.7: Total Path Length at varying flowrates and rotation rates.

Material	Powder Holdup (g)	Path Length (mm)
F.Flo Lactose	39.2	4052.93±833.28
F.Flo Lactose	68.6	4131.54±751.92
F.Flo Lactose	123.4	4951.11±1902.19
F.Flo Lactose	321.4	25307.95±8789.02
F.Flo Lactose	373.4	12024.01±12049.87
F.Flo Lactose	450.2	14726.84±6107.98

Table 4.8: Total Path Length at varying rotation rates for both F. Flowing and Edible Lactose.

Material	Powder Holdup (g)	Path Length (mm)	Material
F.Flo Lactose	39.2	4052.93±833.28	F.Flo Lactose
F.Flo Lactose	68.6	4131.54±751.92	F.Flo Lactose
F.Flo Lactose	123.4	4951.11±1902.19	F.Flo Lactose
F.Flo Lactose	321.4	25307.95±8789.02	F.Flo Lactose
F.Flo Lactose	373.4	12024.01±12049.87	F.Flo Lactose
F.Flo Lactose	450.2	14726.84±6107.98	F.Flo Lactose

Table 4.9: Statistical Analysis on the effect of cohesion and rotation on the Total Path Length.

Source	DF	SS	MS	F	p
Cohesion	1	4.26E+09	4.26E+09	71.76818	1.51E-12
Rotation Rate	2	1.31E+10	6.56E+09	110.5186	4.36E-23
Cohesion*Rotation Rate	2	5.19E+09	2.59E+09	43.71334	2.60E-13
Error	75	4.45E+09	5.93E+07		

Table 4.10: Statistical Analysis on the effect of cohesion on the total path length at 170 RPM

Source	DF	SS	MS	F	p
Cohesion	1	1.79E+05	1.79E+05	0.227533	0.637
Error	26	2.04E+07	7.86E+05		

4.5 Summary and Conclusion

Apart from the experimental work examining the mixing performance, no previous work exists examining the trajectory of particles for continuous powder mixing processes. In this work, we examined the particles journey along the continuous blender and found that powder holdup plays a critical role on the residence time. Experimental work already existed measuring residence time within a continuous mixer. However, the local residence time along the vessel axis had not been explored. We found that particles move along the axial length at fairly the same pace everywhere, even when the vessel

was inclined upward 17°. Residence time showed an exponential trend with axial dispersion and a linear function with path length.

The effect of rotation rate on the residence time, axial dispersion, and path length was complex. The three agitator speeds examined were 16, 75, and 170 rpm. We found that greater speeds resulted in lower residence times, higher axial dispersions, and lower total path length. The effects of powder holdup was a bit more complicated, increasing the powder holdup predominantly increased the residence time. For higher powder holdups the coefficient initially increased, but then decreased. In terms of the particle path length, at high powder holdups particles traveled a longer distance within the mixer. Slightly higher axial dispersion was observed for the less cohesive material but this result was statistically not significant. However, the effect of cohesion on the particles path length was highly significant. The seeming inconsistency between these two trends remains to be clarified. The answer probably lies in the fact that higher cohesion resulted also in longer residence times and lower path lengths, which implies that although the material remains in the mixer longer, the material does not travel a longer distance, but travels at a slower rate. Clearly, the number of experiments that can be conducted is immense and lengthy. To further our investigation of granular mixing, a model can be an additional resource of information. The following chapter will explore the benefits of using a compartment model for powder mixing.

Chapter 5

Compartment Modeling

In this chapter, the main concepts of compartment modeling and how it is used to model a V-Blender, which is used as a case study, are described. Compartment modeling is used to elucidate the effects of initial loading on the mixing process, and determine the optimal sampling protocol including the sampling locations, the number of samples, the number of particles per sample, and sampling time. A summary of the results for the V-blender is presented.

5.1 Introduction

A number of approaches exist to model powder mixing processes, including Discrete Element Methods (DEM), Continuum Models, and Markov chains. However due to computational limitations, uncertainty in material properties and limitations in terms of process representation, these approaches are only applicable to simplified cases. For example, mixing simulations using DEM (Bertrand *et al.*, 2005; Ristow, 1996; Moakher *et al.*, 2000, Kaneko *et al.*, 2000) are common, yet the largest number of particles used within these simulations is 250,000 particles for 120 seconds (Lemieux *et al.*, 2008). Under these conditions, the CPU time on a Beowulf cluster (performed in parallel using up to 128, 3.6 GHz processors of a 1152-processor) was about 5 to 8 h per second of simulation. This computational expense limits the number of particles that can be modeled, the details of the system geometry (Cleary *et al.*, 1998), and the shape of the particles considered. Moreover, a model that takes longer than the process itself is poorly suited for process control purposes. Thus, the main purpose of this research is to

introduce an alternative modeling approach, which will require more input than particle dynamics methods, but is also much faster from a computational viewpoint and could be a feasible route for the development of models useful for real-time close-loop control of manufacturing processes.

Consistent with the nature of pharmaceutical manufacturing, which proceeds largely in batch mode, a majority of the mixing processes modeled have kept the particles confined within a vessel. However, in recent years, a keen interest in continuous processes has arisen. In such systems, time-dependent inflow and outflow of materials results in fluctuations in total mass and species concentration within the system at a given time and causes unsteady flow and mixing performance. Such systems have been modeled only in a handful of cases.

Unsteady state flows have been examined for hoppers using particle dynamics/Discrete Element Modeling (DEM) (Zhu *et al.*, 2006). The advantages of DEM approaches are that the models use parameters with clear physical meaning (friction, adhesion, restitution) although the relatively small number of large particles used by these models negates some of its physical appeal. Nonetheless, DEM models can be used to consider mechanistic effects, such as the effects of geometry or flow rate on stress and shear along the flow. Their disadvantages, as mentioned above, are the excessive computational requirements and the fact that they are largely limited to spherical particles.

The approach used here, compartment modeling, has been used to model fluid-based systems for several decades (Correa (1993); Shah and Fox (1999)), but has been seldom applied to particulate systems. The main advantage of compartment models,

which is the main motivation for our interest in them, is the low computational time required to simulate motion and mixing of millions of particles, which results in fast calculated results that can be used for process control (Portillo *et al.*, 2008). The essence of compartment modeling is to divide the mixer into multiple zones, and to simulate motion and mixing (and stagnation, and segregation) by prescribing fluxes of species between zones. Although stresses and strains on trajectories and wall collisions are not calculated explicitly, particles are still considered as discrete entities. Because these models do not attempt to capture the actual physics of motion, but only motion itself, they are not limited by particle size or geometry, provided that fluxes can be measured or calculated (much in the same way as population balances and other statistically-formulated models can make extensive predictions once aggregation and breakup kernels are formulated) (Ramkrishna *et al.*, 2002). Once flux parameters are selected, the simulation can be used to provide extensive information about the dynamics and the outcome of the process, for example, it can be used to predict mixing performance (in terms of a relative standard deviation of sample composition) along the axial length or at the discharge. Even more important, the model can be used to predict response dynamics following an atypical event such as a burst of a given ingredient at the entrance of the mixer, thus providing the starting point for the development of control laws.

5.2 Batch Mixing Methodology

Compartment modeling of solid mixers is applied by spatially discretizing the system into a number of subsections that are assumed to be perfectly mixed locally (in good agreement with experimental observations) and contain a stipulated number of particles. By also discretizing the time domain, the number of particles are required to

flow from each compartment to the neighboring ones at each time step defining the particle flux, F. The number of particles transferred account for the convective and dispersive mixing occurring throughout the vessel. Following the ideas of Fan *et al.* (1970), who described solid mixing as a random process, the particles selected to enter and leave each compartment are randomly selected. The change in the number of particles of species *j*, in compartment *i*, at time step *k*, is denoted as $\Delta\phi_{ijk}$. All of the particles in the entire mixer are represented by the sum of all the interconnected compartments (*w*). Thus, the change in each species *j* throughout all compartments at every time step must equal zero as dictated by equation (1):

$$\sum_{i=1}^{w} \Delta\phi_{ijk} = 0 \qquad (1)$$

Compartment modeling can in principle be applied to any mixing process as long as there is enough information regarding fluxes to identify different mixing regimes, define the number of compartments needed, and model the particle flux between neighboring regions. A V-blender is considered in this work as an illustrative case study (Figure 5.1a). The V-Blender rotates around the x-axis from the upright position to the downward position. The details of the process are given in Brone *et al*. (1998). Following the experimental observations of Brone *et al*. (1998), this blender can be modeled with five compartments as shown in Figure 5.1b. We identify each compartment as V_1, V_2, V_3, V_4, and V_5. The particle flux between compartments V_1 and V_2 is defined as F_1, and the flux between V_2 and V_3 is defined as F_2, as illustrated in Figure 5.1b.

(a) 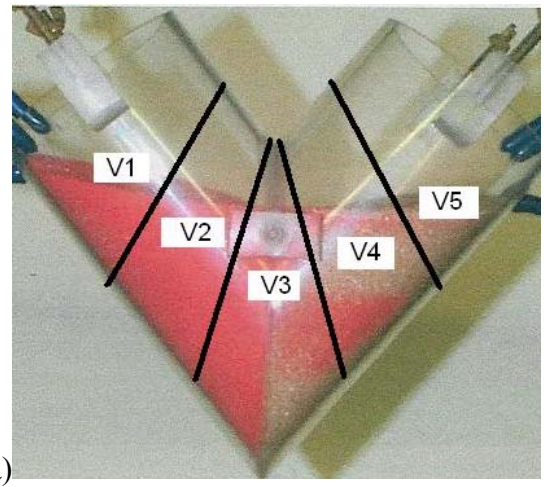

(b) 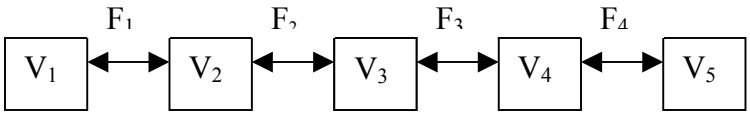

Figure 5.1: (a) A discretized V-blender (b) Compartment model of V-blender

5.3 Mixing Analyses Results

5.3.1 Vessel Composition (Initial load)

Several studies show that mixing performance can be improved by perturbing the symmetry of the mixer (Cahn *et al*., 1965; Chang *et al*., 1992; Chang *et al*., 1995; Brone *et al*., 1997). However, since this is not always a viable option for industrial scenarios, we examine the effects of initial loading. It is well known from experiments that initial loading can substantially affect the mixing process (Brone and Muzzio; 2000). Thus, the main focus of this section is to change the initial distribution of the ingredients in the vessel and examine the resulting variance profiles as a function of time. We compute the effects of initial concentration distribution on mixing time, defined as the time required to reach a homogenous state. The degree of homogenization, quantified by concentration variance, is used to characterize mixing.

The systems studied here consist of two groups of particles having different physical attributes such as chemical identity, size, and color. For the present analysis, a specific concentration is attributed to each particle group, such that the number of particles within each compartment determines the mixture concentration. Hence, in our study, one group of particles belongs to group 1 and another group of particles belong to group 2. At every time point, 100 samples from each of the five compartments are considered, each having 200 particles (the effects of sampling parameters will be discussed in the next section). In order to reflect blender symmetry, $F_1=F_4$ and $F_2=F_3$ (Figure 5.1b). Brone *et al*. (1997) showed that the main barrier to mixing in a V-blender is the axial flow of particles across the vertical plane of symmetry perpendicular to the V-blender. Thus, in order to better represent geometric characteristics of this vessel, we assume that $F_2<F_1$ and $F_3<F_4$; i.e., F_3 and F_2 correspond to the lowest particle flux, the compartment they affect is compartment V_3, which is considered the slowest mixing region (in comparison to all the other compartments). As a case study, the particle flux is set to 1000 particles per time step between compartments V_1-V_2 and V_4-V_5 (i.e. $F_1=F_4=1000$ particles per time step). The flux between V_2-V_3 and V_3-V_4 is $F_2=F_3=100$ particles per time step. The resulting mixing behavior is illustrated using the variance of the system, σ^2, calculated using equation (2).

$$\sigma^2 = \sum \frac{(x_i - \bar{x})^2}{n-1} \qquad (2)$$

where x_i is the concentration of sample i; $\bar{x}$ is the mean of sample concentrations; and n is the number of samples.

In order to investigate the effects of initial loading, we analyze two systems with the same composition, i.e., they both contain the same total number of particles for both

groups 1 and 2. As mentioned above, we are using 1 million particles in our study, and distribute evenly 200,000 particles throughout each compartment. Although the total number of particles within a vessel may be constant, the initial distribution of each type of particle may vary. For example, consider system A and system B, shown graphically in Figure 5.2a and 5.2b, respectively. The numbers within the compartment represent the composition percentage of particles pertaining to group 1. For example, system A has compartment V_1 with 50% group 1 and 50% group 2, that means 100,000 particles of group 1 and 100,000 particles of group 2 initially exist within this compartment. Compartment V_2 contains 100% of group 2, which signifies 200,000 particles of group 2 initially exist within this compartment. On the other hand, case B has 200,000 particles of group 2 within vessel V_1, and 100,000 particles of group 1 and 100,000 particles of group of 2 within vessel V_2. Although both cases have the same composition (200,000 particles of group 1 and 800,000 particles of group 2), the initial particle arrangement throughout the vessel varies. Additional distributions that have the same composition are used for system C and system D, shown graphically in Figures 5.2c, d. The subsequent mixing behavior of these systems is illustrated in Figure 5.3, which shows the variance of the composition of samples as a function of time.

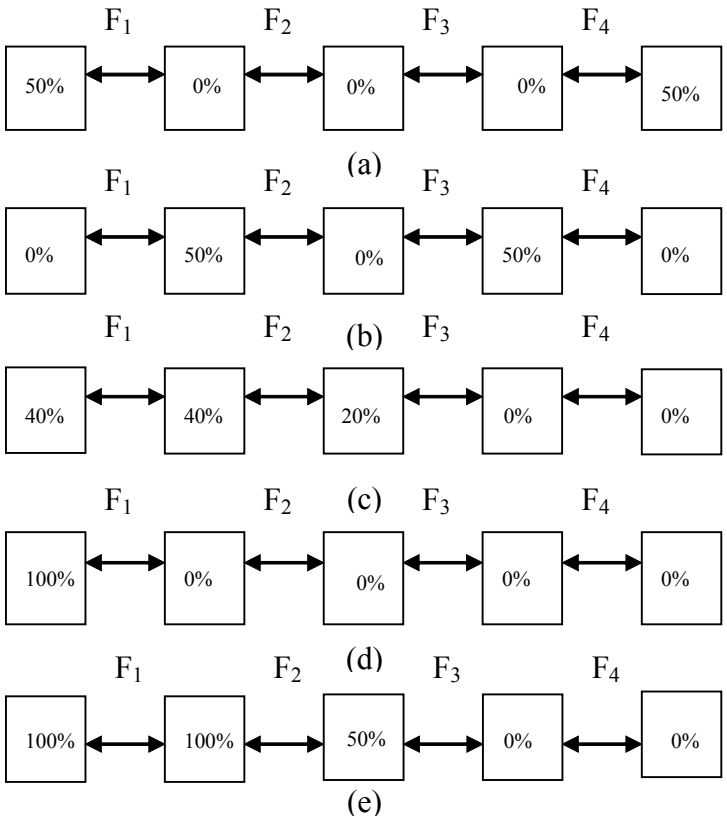

Figure 5.2: The initial load distribution profiles for the following five compartment models: (a) Case A (b) Case B (c) Case C (d) Case D (e) Case E. The percentages within the compartment represent the percentage composition of particles pertaining to group 1.

As shown in Figure 5.3, we significantly decrease the mixing time by varying the initial load distribution. The mixing time for system B is much lower than for system A. Thus, we conclude that system B exhibits superior mixing performance than system A. System B improves mixing because the initial load distribution of group 1, the material in the lowest concentration is closer to compartment V_3. Compartment V_3 is the slowest mixing area of the mixer, and since for system B the material distributes earlier throughout compartment V_3 than system A, and scheme B reaches equilibrium sooner.

In order to further investigate the effects of initial load distribution, two additional cases are studied, case C and case D, shown in Figure 5.2c, and 5.2d. Figure 5.3 shows that system C results in slower mixing compared to systems A and B. This is interesting

because case C has the most uniform initial distribution of particles pertaining to group 1, since it is initially dispersed throughout three compartments. However, the initial distribution is not dispersed throughout the compartments. This points to the fact that mixing time is strongly correlated to the initial load distribution. The highest mixing time of the examined cases is shown by case D, where particles pertaining to group 1 are loaded to only one area of the mixer. To further illustrate the effects of initial loading, a 95% confidence interval of variance is calculated for all cases and shown in Table 5.1. The results illustrate that case B has the narrowest variance confidence interval whereas case D has the widest variance confidence interval. As a result of changing the initial load distribution, the time required to reach homogeneity is reduced or increased as shown in Figure 5.3.

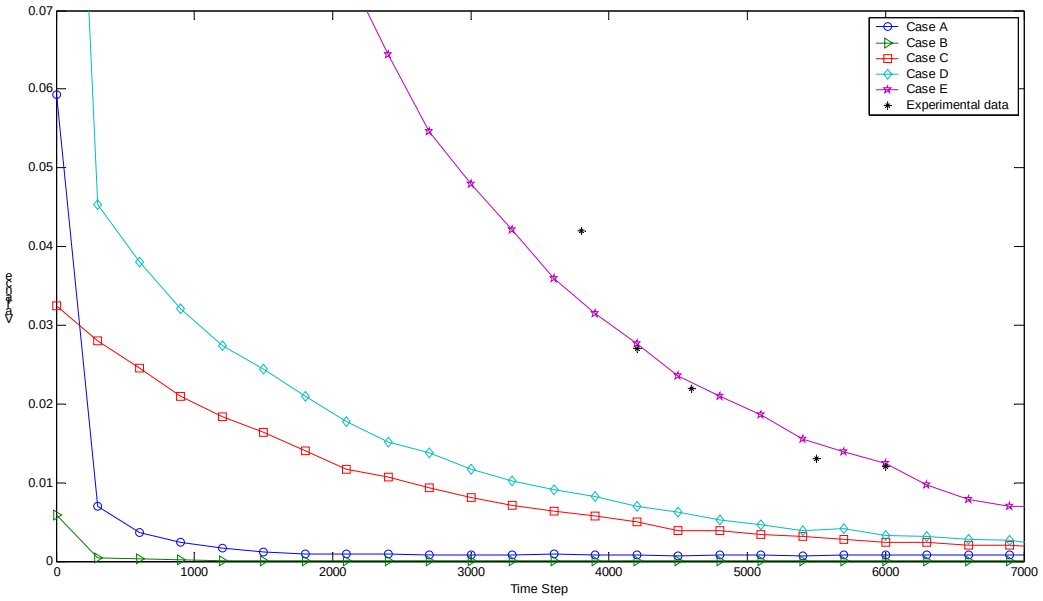

Figure 5.3: Unbiased variance as a function of time steps for five cases with different loading compositions as well as experimental data from Brone *et al*. (1997)

Table 5.1: The 95% of variance for the histogram of the variance frequencies for cases A-D for time steps [15,000, 20,000].

Case	Variance Confidence Interval	Δ
A	[8.98E-04, 6.99E-04]	1.99E-04
B	[1.09E-04, 4.76E-05]	6.16E-05
C	[9.12E-04, 7.08E-04]	2.03E-04
D	[9.16E-04, 7.11E-04]	2.05E-04

The mixing performance of a V-blender was studied by Brone *et al*. (1997) given an initial load distribution. The experiment consists of two groups of particles, the materials are loaded symmetrically that is one side to the vertical plane of symmetry perpendicular to the V-blender is loaded with particles of group 1 and the other side with particles of group 2. This system is simulated by case E (Figure 5.2e) and the results compared with the experimental results in Figure 5.3. We load 200,000 particles of group 1 in compartments V_1 and V_2 and 100,000 particles of group 1 in compartment V_3 whereas 200,000 particles of group 2 are loaded in compartments V_4 and V_5 and 100,000 particles of group 2 in compartment V_3. The experimental results plotted in Figure 5.3 from Brone *et al*. (1997) are obtained using one sample with 140 particles. The homogeneity of the vessel as a function of discrete time is plotted for the simulation and experimental studies. They both exhibit similar variance profiles. Variations arise due to the limited number of samples taken under experimental conditions as well as the inaccuracy that arises from sampling.

5.3.2 Sampling

The most common technique used to characterize a mixture is sampling. In order to properly characterize a mixing process, the sampling parameters (sampling locations, sample size, number of samples, and sampling time) must be carefully chosen to provide

accurate information. In this section, compartment modeling is used to elucidate the role of sampling parameters on the characterization of mixing performance.

5.3.2.1 Sampling Locations

An important consideration when sampling is the sampling location. As pointed out by Allen (1981), the two "golden rules" of powder sampling are that: (1) a powder is sampled only when in motion, and (2) a sample be collected uniformly from the entire process stream. Guidelines elucidate the importance of sampling uniformly throughout the mixer. However, most process analytical technology (PAT) approaches to-date sample the blender at a single location.

In this section, we examine the effects on variance of sampling at different locations within a mixing system. Initially, we examine three of the sampling schemes shown in Figure 5.4 (Schemes A, B, and C). Scheme A retrieves samples from only the middle compartment V_3, scheme B retrieves two compartments, one at each end (V_1 and V_5), and scheme C uniformly retrieves samples from each compartment (V_1 through V_5). Figure 5.5 shows that using a single sampling location (Scheme A, of Figure 5.4) in the center compartment severely underestimates the variance whereas two sampling locations (Scheme B, of Figure 5.4) overestimates the variance. In order to monitor the accuracy among the sampling schemes we develop an optimization model where the objective is to minimize the sum of the squared difference between the variance for the uniform sampling scheme (Scheme C, of Figure 5.4), σ_o, and the variance of the sampling scheme used, i, for n comparisons as shown in equation (3):

$$J=\sum_{i=1}^{n}\frac{(\sigma_o-\sigma_i)^2}{n} \qquad (3)$$

In this study, the uniform sampling scheme (Scheme C, of Figure 5.4) is used as the standard for the variance distribution. The variance difference between the standard and the sampling scheme chosen indicates the variance error. The smaller the variance error, the closer the sampling scheme represents the results of the uniform sampling scheme. The results show that case A has the largest variance error (Table 5.2) whereas case B has a much smaller objective function than case A, and as a result better approximates the variance distribution.

Scheme	Scheme Depiction
A	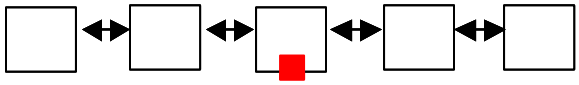
B	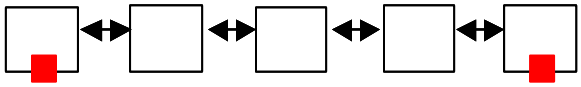
C	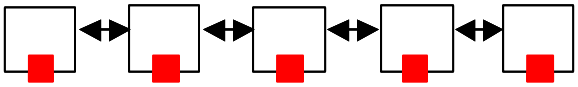
D	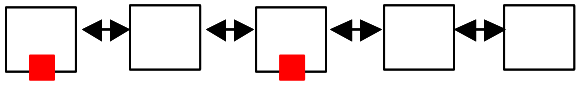

Figure 5.4: Four sampling location distribution possibilities (schemes A, B, C, D).

Table 5.2: The objective function results for sampling location schemes A, B, and D.

Scheme	J
A	6.2750
B	0.0349
D	0.6382

Since in most practical cases there exists a limit in the number of sampling locations that are used (i.e. 2 to 10), we again use a compartment model to determine the optimal sampling locations. Thus, given a constraint that only two sampling locations are

allowed, the question addressed in this section is where samples should be retrieved. Considering a limiting number of sampling locations (i.e. 2), two alternatives are further investigated as depicted in Figure 5.4 (Scheme B, and D). As shown in Figure 5.5, these two schemes result in widely different variance estimates. Scheme B shows a higher variance than scheme D before equilibrium is reached. However, based on the objective function results (Table 5.2), scheme B is closer to the uniform sampling results than scheme D. If the aim is to characterize the variance of the system as accurately as possible, the goal is to minimize J and scheme B should be favored. Thus as illustrated by these results, sampling location is important, since distributing the same number of sampling locations differently shows dramatically different results. Given that there exists a large number of sampling alternatives, compartment models offer an effective way of selecting the best sampling location for a specific system.

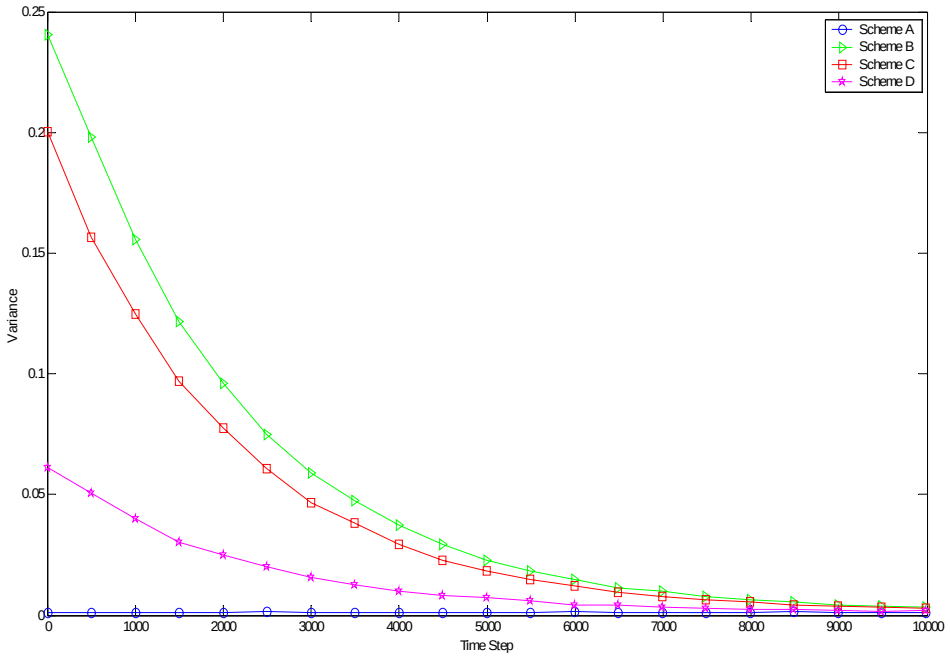

Figure 5.5: Variance as a function of time steps for the four sampling possibilities (schemes A, B, C and D).

5.3.2.2 Sample Size

In pharmaceutical applications, the size of a single tablet is usually the scale of scrutiny where it is critical to ensure that the active ingredient is well mixed (Muzzio *et al.*, 2004). Hence, an ideal number of particles in a sample should be equal to the number of particles in a tablet. However, this is not always possible and obtaining a microscopic sample can result in greater inaccuracy due to measurement errors, especially when using thief probes (Muzzio *et al.*, 2003) to perform the sampling. To understand the effects of sampling methodology, the actual relationship between sample size and variance is further examined in this section.

Consider the system in Figure 5.2e (case E), we assume three different sample sizes (200, 400 and 600 particles per sample). In all cases, 50 samples are used and selected randomly at each time step and an equal number of samples are retrieved from each compartment. Although variance behavior over time is similar in all three cases (closely overlapping variance profiles), larger samples result in narrower variance distributions (Figure 5.6 and Table 5.3). The results confirm that increasing the number of particles within each sample decreases the sample-to-sample concentration variability.

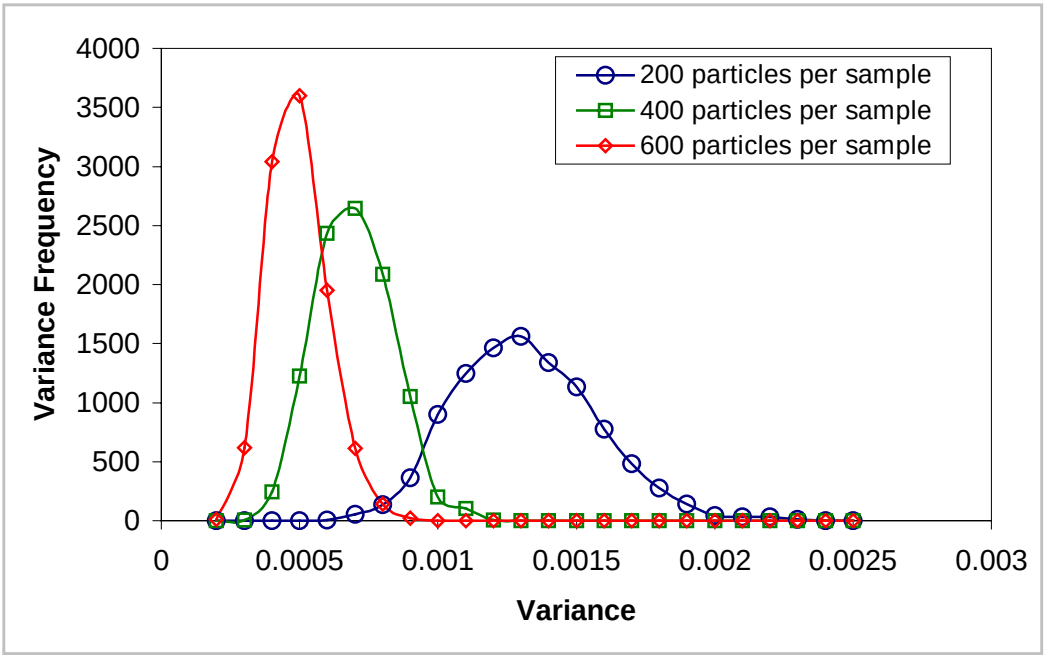

Figure 5.6: Normalized variance histogram for a) 200 particles/sample b) 400 particles/sample c) 600 particles/sample for the time interval [15,000 to 20,000].

In terms of computational feasibility, using compartment models leads to very efficient calculations as shown in Table 5.4. The CPU times for the three cases examined are on a SUNW SPARC Desktop (2) 900 MHz Processors 2GB and our compartment modeling code is written in FORTRAN. When we increase the number of particles per sample from 200 to 600, the simulation takes 600 CPU seconds longer to run due to increased number of iterations required to achieve convergence. Although increasing the sample size increases the CPU time due to additional calculations, the simulation time remains within a feasible range in comparison to existing mixing models.

Table 5.3: The 95% confidence interval of variance for the variance frequency histograms of sample sizes 200, 400, and 600 particles per sample for the time interval [15,000, 20,000].

Particles per Sample	Variance Confidence Interval	Δ Interval
200	[1.81E-03, 7.86E-04]	1.03E-03
400	[9.37E-04, 3.96E-04]	5.41E-04
600	[6.65E-04, 2.68E-04]	3.97E-04

Table 5.4: Computational results for 3 different sample sizes.

Number of Particles per Sample	CPU* (s)
200	8084
400	8093
600	8692

*SUN Blade 2000

Analytical methods, such as near infrared (NIR) spectrometry, use a small number of particles in each sample (Berntsson *et al., 2002*), hence raising concerns about small sample sizes. To further examine the effect of sample size, we explore cases involving extreme sample sizes.

Thus, the same system is analyzed with the following four sampling sets: 2 particles per sample, 4 particles per sample, 8 particles per sample, and 16 particles per sample. The number of samples taken is adjusted to keep a constant number of particles retrieved within one time step. Figure 5.7 shows a different variance profile for all the samples. As expected, sampling an identical system with more numerous but smaller samples results in a larger variance than if sampled with fewer but larger samples. As shown in Figure 5.7, once the system reaches the final mixed state, the final variance value is non-zero. The higher the final variance value, the greater the variance at a mixed state. Thus, although our system is identical, each sample set displays a different final variance value. This is especially important given that in order to satisfy the existing manufacturing criteria (CGMP's, October 2003), the Relative Standard Deviation (RSD) value should be less than 4.0% to be "readily passing" and less than 6.0% to be "marginally passing" (Many of the samples in Figure 5.7 will not satisfy even the marginally passing criteria.). In order to capture the variance as a function of sample size for a given system, we analyze the minimum variance attainable for several different

sample sizes of a given system. As shown in Figure 5.8, in agreement with the Central Limit Theorem, the minimum variance is inversely proportional to the sample size. Consequently as illustrated with the results in this section, the variance of the system can display a large range of values depending on the sample size. Hence, setting a measurement requirement for homogeneity (such as $\sigma \leq$ 4-6%) is ambiguous unless sampling parameters are defined. Thus, selection of the appropriate sample size is very important, especially for PAT methods that in practice sample very small amounts of material.

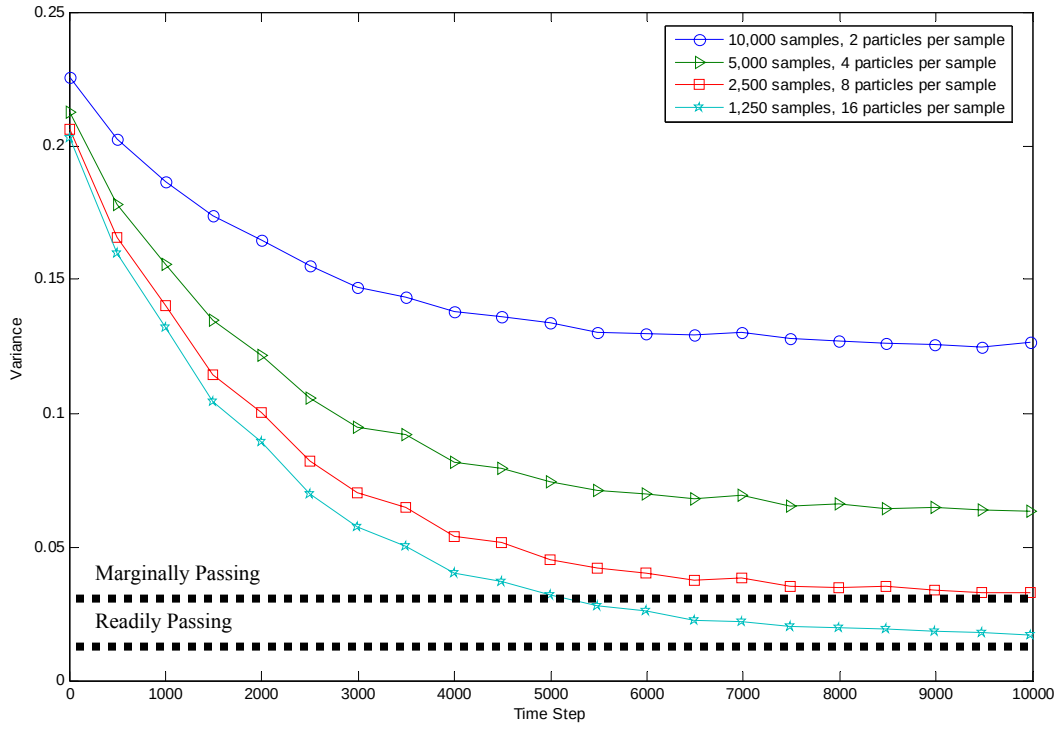

Figure 5.7: Unbiased variance as a function of time steps for four sample sizes for system E.

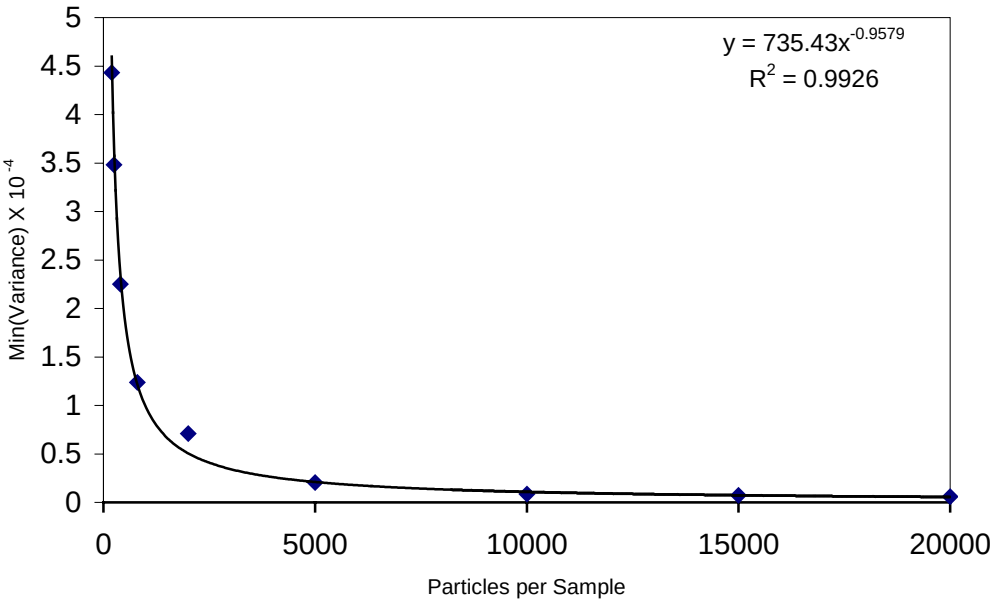

Figure 5.8: Minimal variance profiles as a function of particles per sample.

5.3.2.3 Number of Samples

In the previous section, a small number of samples were considered for all the calculations. In this section, we investigate the selection of the number of samples. For the same system, we vary the number of samples used to determine the variance. The aim is to minimize the number of samples required to characterize mixing in order to reduce the adverse impact of invasive sampling (Muzzio *et al., 1997*). To that end, we monitor the variance evolution for three identical systems, while varying the number of samples for each system. Each case is as follows: from case 1 we take 100 samples, from case 2 we take 200, and from case 3 we take 500 samples; each sample with 200 particles. No substantial difference in variance between these three systems is observed (closely overlapping variance profiles). However, the variance frequency reveals that increasing the number of samples leads to a narrower distribution (Figure 5.9 and Table 5.5) that visibly approaches a χ^2chi-square) distribution. It is also important to mention

that as the number of samples increase, the average variance decreases. Variance is indirectly related to the skewness of the χ^2-distribution. As shown in Figure 5.9, the skewness of the variance frequency increases as the number of samples increase.

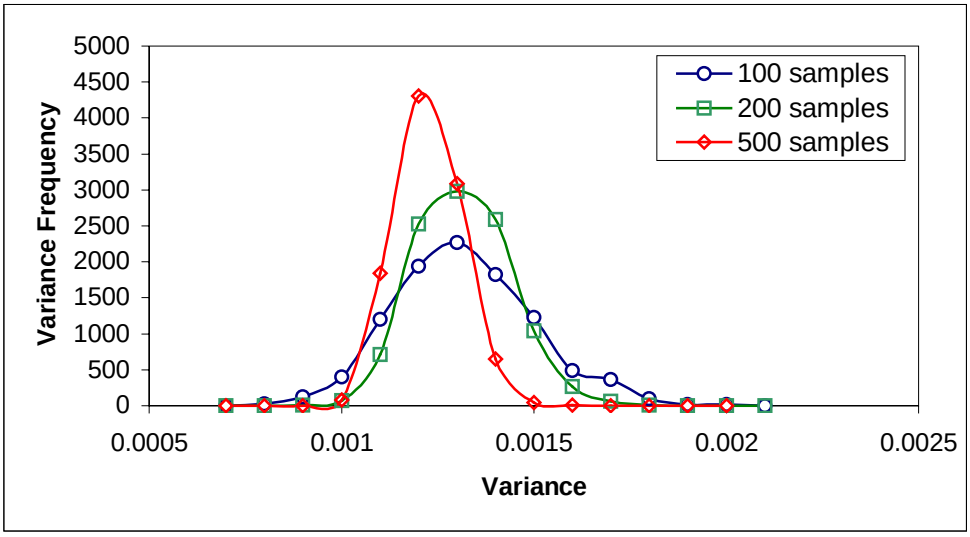

Figure 5.9: Normalized variance histogram for a) 100 samples b) 200 samples c) 500 samples.

Table 5.5: The 95% confidence interval for the variance frequency histograms for 100, 200, and 500 samples at the time interval [15,000,20,000] time steps.

No. of Samples	Variance Confidence Interval	Δ Interval
100	[1.67E-03, 9.35E-04]	7.31E-04
200	[1.56E-03, 1.04E-03]	5.22E-04
500	[1.47E-03, 1.13E-03]	3.49E-04

Table 5.6: Compartment modeling computational results for 100, 200, and 500 samples.

Number of Samples	CPU* (s)
100	8026
200	8636
500	9859

*SUN Blade 2000

Increasing the number of samples does require additional calculations, causing an increase in computational intensity. The additional samples prolong the simulation by

1,800 CPU seconds (see results in Table 5.6). This may be a feasible time period considering the time length of other mixing models.

Since the number of samples is often minimized, it is important to consider the effects of a small number of samples. Thus, the following cases are considered for a constant number of particles: 5 samples of 4,000 particles per sample, 10 samples of 2,000 particles per sample, 20 samples of 1,000 particles per sample, and 40 samples of 500 particles per sample. Although these cases showed similar variance behavior (closely overlapping variance profiles), the histograms evaluated for the time period between 15,000 and 20,000 time steps (Figure 5.10) show that a small number of samples are not sufficient to represent the χ^2-distribution. A small subset of it will have a different frequency distribution than the parent group. As the samples increase, the frequency distribution more closely resembles that of the large data set. χ^2 can be used to determine what sample size will provide a reasonable approximation of the larger set. Thus, a small number of samples may not sufficiently represent the homogeneity of the system as reported by Fan *et al.* (1970). A contour plot is used to illustrate the relationship between the variance the number of samples, and the number of particles per samples as shown in Figure 5.11. It can be noted from this plot that the smallest variance is obtained for the largest number of particles within the sample. Although increasing the number of samples also reduces the variance it is found that the number of particles per sample is the most effective factor.

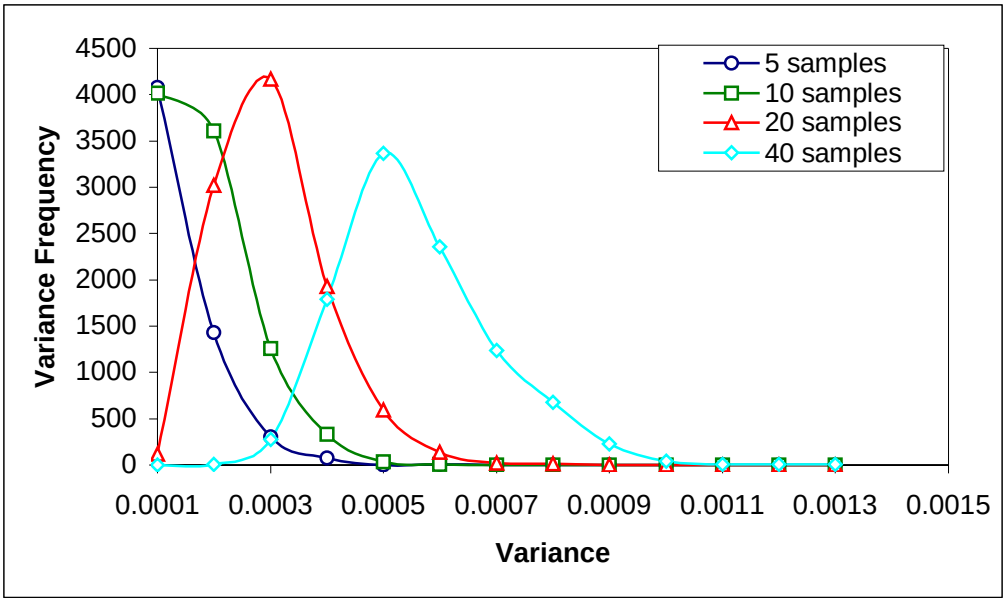

Figure 5.10: Normalized variance histogram obtained from: a) 5 samples b) 10 samples c) 20 samples d) 40 samples.

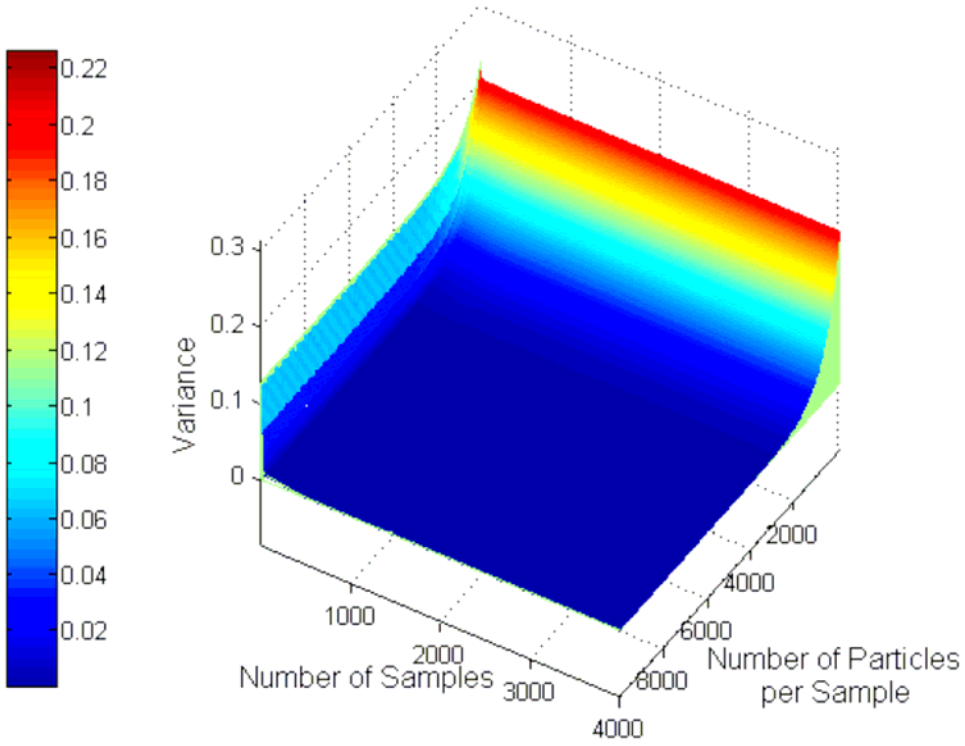

Figure 5.11: Surface contour graph for two sampling variables (Number of Samples, Number of particles per sample) as a function of variance.

The results illustrate some of the existing problems with product specifications. One problem is that setting a measurement requirement for homogeneity (such as $\sigma \leq$ 4-

6%) is ambiguous unless sampling parameters are defined. Secondly, the homogeneity of the mixture is not solely dependent on the mean variance, since the significance of the mean variance is dependent on the variance distribution as well as the confidence intervals. These confidence intervals are affected by the sampling set and although a homogenous mixture is present, an incorrect sampling basis will not distribute the variance as a larger sample set would.

5.2.2.4 Sampling Time

Determining when the mixture has reached homogeneity is obviously important. The focus of this section is to define when homogeneity is reached in order to determine when samples should be retrieved. To investigate the effects of this parameter, we analyze the variance distributions at several time intervals. As shown in the prior variance distributions, homogenous samples (uniform datasets) distribute variance as a chi-square distribution, given the appropriate sampling parameters. However, non-homogenous samples (non-uniform dataset) do not necessarily distribute the variance as a χ^2distribution; this can further be read on BookRags (2006). As shown in Figure 5.12, sampling at early time intervals results in variance distributions that deviate significantly from χ^2 distributions. This posses serious challenges to developing useful estimates of "goodness of fit" of measured values of σ^2.

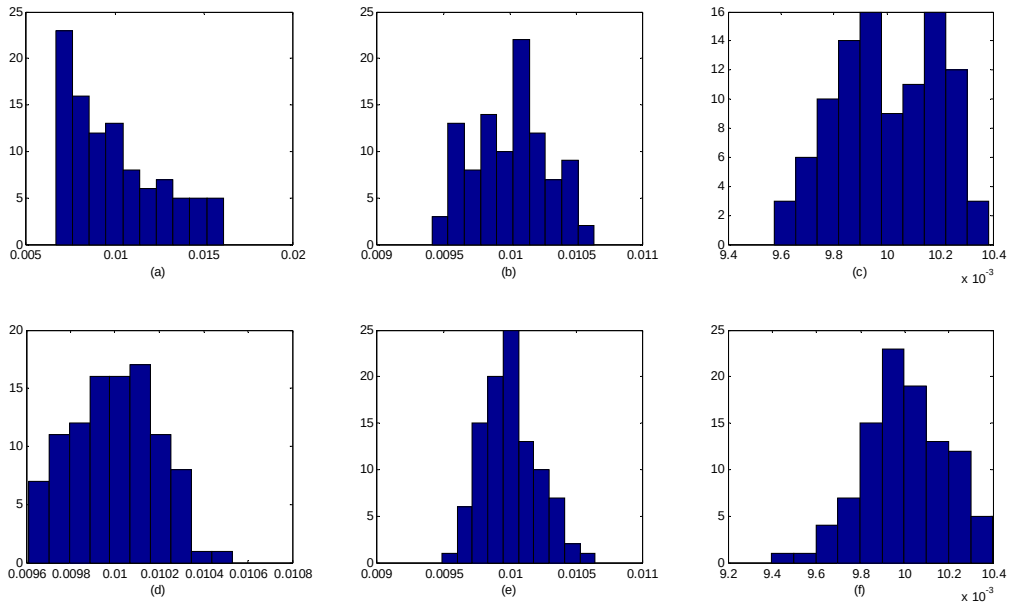

Figure 5.12: Variance histogram at the following time intervals: a) 1-100 b) 201-300 c) 401-500 d) 601-700 e) 801-900 f) 901-1000.

Quantitatively, we use the χ^2 test to characterize mixing over time as proposed by Gayle *et al*.(1958). The χ^2 test is evaluated as follows:

$$\chi^2 = \sum \frac{(N_O - N_E)^2}{N_E} \qquad (4)$$

where N_O, is the observed number of particles of a given physical attribute such as chemical identity, size, and color in a sample and N_E, is the expected number of particles in the mixture of the given physical attribute. When the mixture reaches a homogenous state, the χ^2 value reaches the lower limit. The lower limit is equal to the number of different components times the number of samples. In this case study, two components exist (particles pertaining to group 1 and 2) and 500 samples are taken within the mixture, so the lower limit is 1,000. Table 5.7 illustrates the χ^2 values at different time steps. The results show χ^2 reaches the lower limit before the sample time has reached 15,000.

Sampling early can be prevented by utilizing a compartment model that predicts when χ^2 has reached the lower limit.

Table 5.7: Chi-square results at varying time steps.

Sample Time	No. of Particles labeled with 1 at each Compartment					χ^2
	1	2	3	4	5	
5000	130348	128956	100060	71271	69365	35230
10000	108896	108406	100245	91624	90829	3041
15000	102367	102870	100150	97391	97222	284
20000	101031	101099	99784	98878	99208	42
25000	100362	100024	100062	99597	99955	3.0
30000	100141	100165	100105	99810	99779	1.4

5.4 Conclusions

In this work a powder mixing process is simulated based on compartment modeling. The main advantage of the proposed approach is that the computational time is significantly reduced, allowing the simulation of a large number of particles. A V-blender is considered as a case study blender and simulated using the proposed compartment model. In terms of variance, the effects of the sample location, number of samples, particles within the sample, and sampling time are examined. It was shown that initial loading could substantially increase the required mixing time to reach a homogenous state. With respect to sampling, it was first determined that a small number of particles overestimate the variance of the system. Second, a large number of samples decrease the variance histogram width at equilibrium. Third, sampling locations can dramatically offset variance distributions. Finally, sampling early will not exhibit the variance histogram as a χ^2 distribution. Utilizing compartment models we characterize the mixing behavior of several mixing processes under several different sampling conditions. The integration of these models to existing powder mixing processes can

reduce any misrepresentation of variance profiles as well as improve mixing performance. Given the advantages of compartment modeling illustrated in this chapter for a batch mixer, the following chapter applies compartment modeling to continuous powder mixing.

Chapter 6

Compartment Modeling for Continuous Processing

The compartment modeling described in the previous chapter, followed by the experimental setup used to examine the powder flow, is presented for continuous mixers in this chapter. The method used to determine the fluxes from experimental data is explained. The modeling parameters, the effects of sampling, and validation of processing conditions are also examined.

6.1 Introduction

As mentioned in the previous chapter, compartment models require substantial input (from experiments, or from particle dynamics calculations) to provide realistic predictions. Unfortunately, at the present time, little experimental work exists on continuous mixing, particularly for pharmaceutical applications. Kehlenbeck and Sommer (2003) examined $CaCO_3$ - Maize Starch mixture. In our previous work (2008), an Acetaminophen (APAP) formulation was examined, and it was shown that mixing performance was strongly affected by blender operating parameters such as angle of incline and impeller speed. Some work exists indicating a well-controlled continuous mixing process can enhance productivity significantly (Muerza *et al.*, 2002; Marikh *et al.*, 2005). However, in order to develop an effective control law the first requirement is the development of efficient predictive models that can be used for process optimization and control. Moreover, the use of accurate models can reduce the need for sampling, which is difficult in continuous operation, always inconvenient, and an additional source of uncertainty often leading to Type I errors.

6.2 Mixing Model

As mentioned in the introduction, several limitations hinder the application of existing modeling approaches (Stewart *et al.*, 2001; Laurent, 2006) for real time optimization and control. To overcome this problem we propose a method that predicts product homogeneity using the basic ideas of compartment modeling found in chapter 5. The main idea behind compartment modeling is that it discretizes the space of the mixing vessel into locally homogeneous compartments. Particles move from compartment to compartment to account for both convection and dispersion. In this work, a three-dimensional compartment modeling approach is utilized. As shown in Figures 6.1 and 6.2 the mixer is discretized in both the axial and radial dimensions. The axial compartments are denoted by the index i whereas the radial dimension is represented by index j, identifying each compartment as S_{ij}. The total number of radial compartments (at a given axial position) is represented as N_r and the number of axial discretizations as N_a. The total number of particles in the vessel (N_t) is the sum of particles in all of the compartments; each compartment contains N_{ij} particles so $N_t = \sum_{i=1}^{Nr}\sum_{j=1}^{Na} N_{ij}$. The intensity of fluxes within the mixer depends on the number of compartments and the way that the compartments are connected. For example in a binary system, two different types of particles are represented (A_{ij} and B_{ij}) and $N_{ij} = A_{ij} + B_{ij}$. The effects of other particle properties (size, morphology etc) are captured by their fluxes.

Two important comments need to be made at this point. The first major comment concerns the estimation of fluxes. As mentioned above, this is critical input for the model. In principle, flux information can be obtained in several ways:

- From comparisons with samples taken along the axis of the mixer
- From comparisons with samples taken at the discharge
- From Residence Time Distribution
- From PEPT or PIV measurements
- From DEM models run for as short period of time

The goal is to introduce the approach, validate it, and demonstrate its use for evaluating sources of error associated to sampling, and only the first two sources of information are considered in this section.

Another important point is that we assume all radial compartments to be equally filled. In reality, the mixer fill level is half-empty; however, during operation, particles moved quickly along the radial direction and although the mixer theoretically may have a low fill level, the material is largely uniformly distributed in the radial direction. For the mixer examined here, radial heterogeneity is not a concern, and transport in the radial direction is largely a minor concern. Radial compartments are retained as part of the model, only to lay the foundation for more complex situations where mixing in the radial direction could be an important issue.

For the specific geometry of the continuous mixing system examined in this work, uniform fluxes between radial compartments are used since the convective blades rotate radially. The axial fluxes are uniform along the horizontal length of the mixer since an equally distributed number of blades are located along the axis (as shown in Figure 6.1). Independent of the mixer inclination, due to mass conservation, powder flow will not vary along the axial position. A weir is used to maintain a specified fill-level.

Once the number of particles that are interchanged between compartments is determined, the actual particles exchanged are randomly chosen among all particles within the compartment.

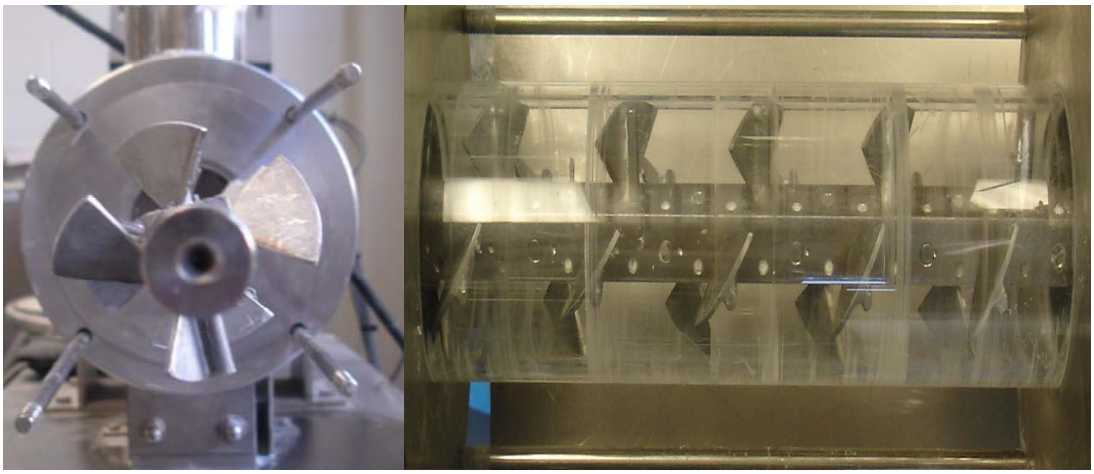

Figure 6.1: Radial and Axial view of horizontal cylindrical mixing vessel investigated.

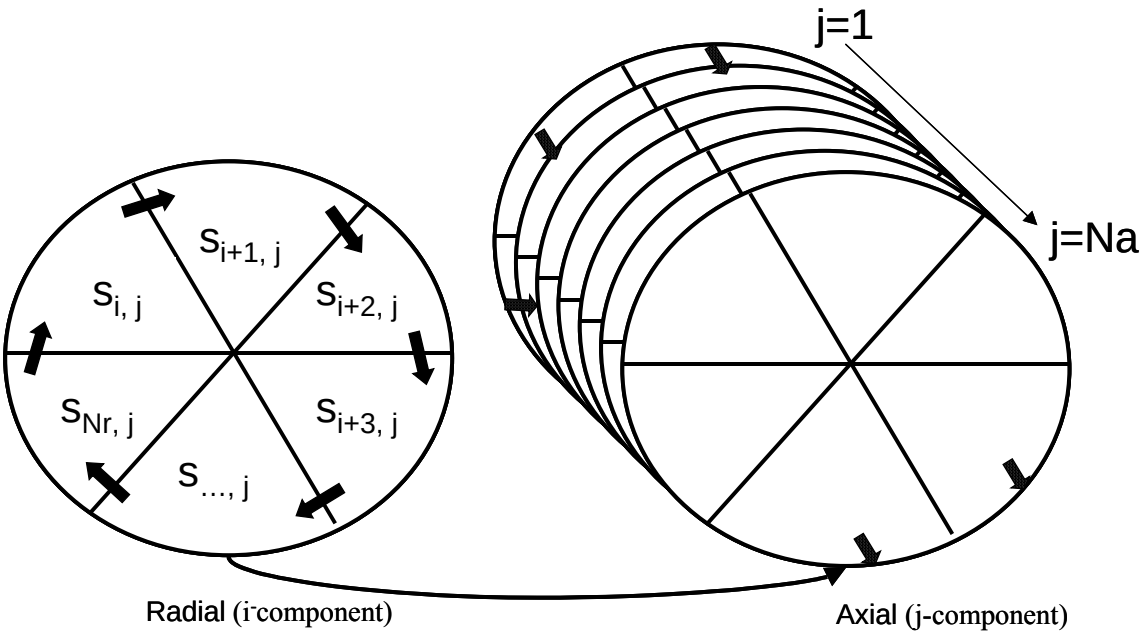

Figure 6.2: Schematic of a compartment diagram used to model the cylinder-mixing vessel.

6.3 Experimental Setup

The continuous mixer modeled here is manufactured by Buck Systems in Birmingham, England. The mixer is 0.31 meters long and the radius is 0.025 meters. The mixer's rotation rate ranges from 17 RPM to 340 RPM. An adjustable number of triangular flat blades are placed within the horizontal mixer. The feeding system used in these experiments is composed of two vibratory mechanisms (Eriez, Erie, PA). The variability in the flowrate depends on powder properties such as particle size, surface roughness, electrostatic charge, and other properties that affect cohesion (Bhattachar *et al.*, 2004). The processing parameters used within the feeder to change flow rate are vibration speed and spring thickness. The feeding flow rate is also dependent on the powders bulk density (since the powder will not be compressed significantly by the gentle vibration used by the feeders). The average bulk density of Lactose 125 and Acetaminophen/Lactose 125 blends are shown in Table 6.1. The error in the estimation of the density is measured as standard deviation of ten samples.

Table 6.1: Density of Powder Formulations

Active %	Density (g/ml)
Lactose 125M	0.785±0.009
Lactose 125M and 8% 30 μm milled APAP	0.939±0.009
Lactose 125M and 9% 30 μm milled APAP	0.882±0.013
Lactose 125M and 10% 30 μm milled APAP	0.928±0.013
Lactose 125M and 12% 30 μm milled APAP	0.919±0.018
Lactose 125M and 15% 30 μm milled APAP	0.92±0.014
Lactose 125M and 16% 30 μm milled APAP	0.934±0.025

The average flow rate and its variability are calculated by weighing the mass of powder discharged in one second, once the procedure has been performed multiple times. The deviation from the mean flow rate will affect the overall amount of each ingredient fed to the system. In the flow studies conducted for this research, we found higher variability in the flowrate of the pre-blend composed of Acetaminophen and Lactose 125

compared to pure Lactose 125. This is probably due to electrostatic agglomeration of Acetaminophen in the vibratory feeder, as well as the increased cohesion of the blend containing Acetaminophen (Mehrotra *et al.*, 2007). The Lactose feed mass flow rate was determined three times, and outflow variability was found to be $12.54\pm1.80 gs^{-1}$, $13.65\pm2.70\ gs^{-1}$, $10.29\pm2.90\ gs^{-1}$, with an overall average of $12.16\pm2.46 gs^{-1}$. The pre-blend component flowrate was also determined three times, and outflow was found to be $6.56\pm1.08\ gs^{-1}$, $7.42\pm1.44\ gs^{-1}$, $5.65\pm0.96\ gs^{-1}$ with an overall average of $6.55\pm1.16\ gs^{-1}$.

Experimental measurements of the fluxes between compartments is a complicated task. For batch mixers, fluxes can be estimated using specialized experimental procedures such as solidification (Wightman *et al.*, 1996) and image analysis of a discretized mixer (Massol-Chaudeur *et al.*, 2002). However these approaches, which require sacrificing the mixing vessel are difficult to implement for continuous mixing experiments. Therefore, we decided to resort to sampling, which, while cumbersome, is easily carried out.

The mixing vessel was constructed with openings on the top that allow for axial sampling as shown in Figure 6.3. In order to measure mixture homogeneity as a function of axial length, samples were retrieved and analyzed using Near Infrared Spectroscopy (NIR). The NIR System used to analyze the experimental data presented in this research is the Nicolet Antaris, Near-IR Analyzer from Thermo Electron Corp. The calibration curve for the Acetaminophen and Lactose 125 blend is illustrated in Figure 6.4, the linear square fit for these data was $R^2=0.9932$.

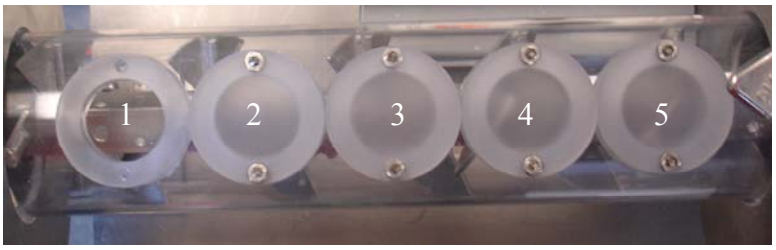

Figure 6.3: Axial sampling ports of the horizontal cylindrical vessel.

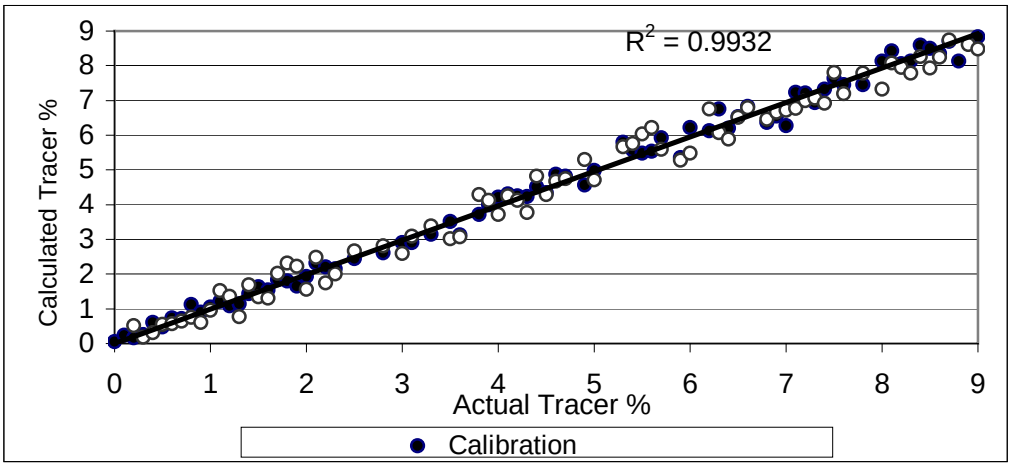

Figure 6.4: Near Infrared (NIR) spectroscopy calibration curve determined using Partial-least squares method using 2nd order derivative equation of the absorbance versus wavelength spectra of the calibration samples.

One of the difficulties of online sampling is that a stationary sample must be scanned multiple times in order to obtain an accurate reading. As illustrated in Figure 6.5, which shows the results of NIR spectroscopy as a function of the number of scans for three samples, respectively containing 0.6%, 3.5%, and 5% Acetaminophen. Based on these three specific sample concentrations, the best number of scans based on the minimum error is 38, pointing to the importance of a large number of scans in order to get accurate results. Given the current nature of NIR spectroscopy, in a continuous mixer, the powder moves too fast to allow a large number of scans directly online. Thus, we resort to invasive methods. While they have the disadvantage that powder is physically removed from the system, possibly disturbing the blend and affecting its composition distribution, they allow for multiple means of sample analysis, mitigating

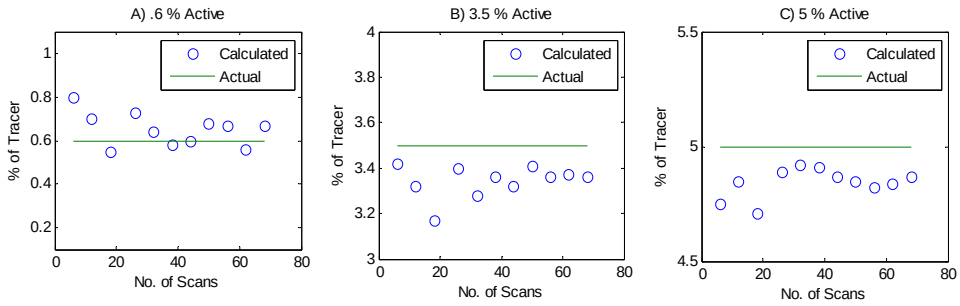

Figure 6.5: Scans of three samples A) 0.6% B) 3.5% and C) 5% of tracer concentration analyzed with 6 to 68 scans.

6.4 Homogeneity Measurements

The homogeneity of a powder mixture is measured by calculating the variability of the samples retrieved. For batch mixing vessels the samples are typically retrieved throughout the powder bed (Muzzio *et al.*, 2003) whereas for continuous mixing the powder can be analyzed both at the outlet (Portillo *et al.*, 2008) and along the axis (as presented in this work). For binary mixtures measuring one of the components is sufficient to determine the distribution within each sample. However, for a multi-component mixture composed of r species, r-1 measurements per sample are required to determine the component distribution. This is important in pharmaceutical applications because both the amounts of active and excipients must be consistent in order to achieve uniformity of dosage and dissolution (Chowhan and Chi, 1986). While customarily only the active ingredient is analyzed, in NIR spectroscopy, variability of excipients also needs to be measured in order to avoid errors in the method.

Consider a set of n samples retrieved from a binary mixture where the amount of a minor component (the tracer) within the k^{th} sample is represented by X_k. The average

tracer concentration of all the n samples is defined as $\overline{X}$. The homogeneity of the mixture is represented by the Relative Standard Deviation (RSD) of all the n samples tracer concentration.

$X_k=\{c_1,\ldots c_{m-1},c_m\}$

$$\overline{X}=\frac{X_1+.....X_n}{n}$$

$$RSD=\frac{1}{\overline{X}}\sqrt{\sum_{k=1}^{n}\frac{(X_k-\overline{X})^2}{n-1}}$$

Each sample X_k, is composed of "m" number of particles, where the "l^{th}" particle is represented by c_l. The greater the number of particles the larger the sample size. In addition, the greater the number of samples, the higher the number of X_n^{th} terms. Within each compartment, a number of samples are retrieved; the RSD of the i^{th} radial compartment and j^{th} axial compartment is denoted as RSD_{ij}. The variability within all the radial compartments at a fixed axial position "j" is denoted as RSD_j. This measurement is calculated by determining the relative standard deviation between all samples retrieved within all radial compartments at a fixed axial position j. S_{ijk} represents the tracer concentration of the k^{th} sample from the ith radial and jth axial compartment. The total number of samples taken within the compartment is n. The average of the n samples retrieved within all N_r radial compartments at a fixed axial (j^{th}) position is represented by $\overline{X_j}$.

$$\overline{X_j}=\frac{1}{N_r}\sum_{i=1}^{N_r}\frac{1}{n}\sum_{k=1}^{n}X_{ijk}$$

$$RSD_j = \frac{\sqrt{\frac{1}{N_r \times n}\sum_{i=1}^{N_r}\sum_{k=1}^{n}(X_{ijk} - \overline{X}_j)^2}}{\overline{\overline{X}}_j}$$

Lower RSD values mean less variability between samples, which implies better mixing. In order to obtain the RSD within the axial section, the RSD within all the radial sectors that lie within the axial compartment are measured. Samples are retrieved from each of the radial slices and the RSD of all the samples within that axial portion are used to determine sample homogeneity.

6.5 Powder Fluxes

One of the most important parameters in setting up the compartment model is the determination of the flux, which is a function of the number of particles exchanged between compartments and number of compartments. The fluxes between compartments are fine-tuned in order to account for the varying powder flowrates as well as stagnant mixing regions. The higher the rate, the larger the number of particles exchanged between compartments. The number of particles exchanged between two compartments $(S_{ij} \rightarrow S_{i'j'})$ is denoted by $\lambda_{ij \rightarrow i'j'}$, and represents a randomly selected number of particles that are transferred from compartment S_{ij} to compartment $S_{i'j'}$. It should be noted that this flow is between two compartments and compartments exist in a three-dimensional space, thus capturing a bi-directional flow. The flux, $Flux_{ij \rightarrow i'j'}$ is defined as the ratio of number of particles transferred to a neighbor compartment $(S_{i'j'})$ with respect to the total number of particles within the compartment. The total number of particles within each compartment may remain constant ($\Delta N_{ij}=0$) or may change ($\Delta N_{ij} \neq 0$).

The compositional distribution of particles within a compartment may also remain constant. This would require that at time point k and a subsequent time point k+1 the ratios between each species (for a binary system *A* and *B*) also remain constant, i.e., $\Delta_{k\to k+1}\frac{A_{ij}}{N_{ij}}=0, \Delta_{k\to k+1}\frac{B_{ij}}{N_{ij}}=0$. This is statistically very improbable (Ross, 2002); a more probable scenario is one where the distribution changes and the component distribution changes $\Delta_{k\to k+1}\frac{A_{ij}}{N_{ij}}\neq 0, \Delta_{k\to k+1}\frac{B_{ij}}{N_{ij}}\neq 0$. In these examples, the total number of particles within each compartment remains constant but the component ratio within each compartment changes.

6.6 Effect of Compartment Modeling Parameters

The modeling parameters examined in this section consists of the fluxes between the compartments, the number of radial and axial compartments, and the number of particles per compartment. These parameters affect both the quality of the results and the computational time. Other parameters examined that are difficult to characterize experimentally but known to affect homogeneity estimates are the number of samples retrieved and the sample size. These parameters are examined in section 6.7.

6.6.1 Compartment Fluxes

In order to use the proposed compartment approach discussed in section 6.3 the fluxes between the compartments must be determined as follows: Samples are retrieved at the designated axial locations shown in Figure 6.3 and the slope of the sample variability along the axial length of the mixer is calculated. Due to the symmetry of the convective motion and short axial distance ($\Delta\ell_k$), the change in variability between the designated locations is assumed to be linear. Since the axial length ($\Delta\ell_k$) is represented

by N_{Ak} compartments, the change in content uniformity along these compartments is represented as $m \cdot \frac{\Delta \ell_k}{N_{Ak}}$. This describes a scale effect where N_{Ak} compartments are used to model the $\Delta \ell_k$ axial length of the vessel.

Although the change in concentration that occurs along the axis is monitored, the content uniformity of the samples retrieved at a fixed axial position measure the radial variability. In the model, the vessel diameter is discretized into (N_R) radial slices and the particles fluxes are between $N_R - 1$ compartments. Mixing occurs by the convective motion of the blades rotating 360° at a constant rate. As a result, the rate of the number of particles exchanged within the radial compartments is uniformly expressed among the radial compartments as $\psi = \frac{m \cdot \frac{\Delta \ell}{N_A}}{N_R - 1}$. The flux depends on the number of particles exchanged between compartments relative to the total number of particles. Thus the radial $\text{Flux}_{ij \to i'j'}$ represents the fraction of the total number of particles exchanged from one compartments (ij) to another ($i'j'$) to the total number of particles in compartment ij.

In the model developed here, the rate of mixing depends on the number of the particles exchanged between the compartments. Increasing the number of particles exchanged between compartments results in higher fluxes and a faster mixing rate, which ultimately means that the mixed state is reached faster. The particles selected to transition to other compartments are random. The fluxes are defined as the ratio between the number of particles interchanged within two compartments (S_{ij}, $S_{i'j'}$) relative to the total number of particles within each compartment, $\text{Flux}_{ij \to i'j'} = \frac{\lambda_{ij \to i'j'}}{N_{ij}}$. The non-dimensional

flux can range between 0 and 1, depending on the level of exchange from no mixing where no particles are exchanged to a high degree of mixing where all particles are exchanged. A total mixing rate, $MR_{total} = \sum_{i'=1}^{N_R}\sum_{j'=1}^{N_A}\sum_{i=1}^{N_R}\sum_{j=1}^{N_A} Flux_{ij\rightarrow i'j'}$, can be defined considering the effect of the total number of particles within the vessel and the rate of interchanging them as a function of all the compartments in the vessel. As Figure 6.6 illustrates, increasing the flux results in lower RSD curves which in effect means faster mixing.

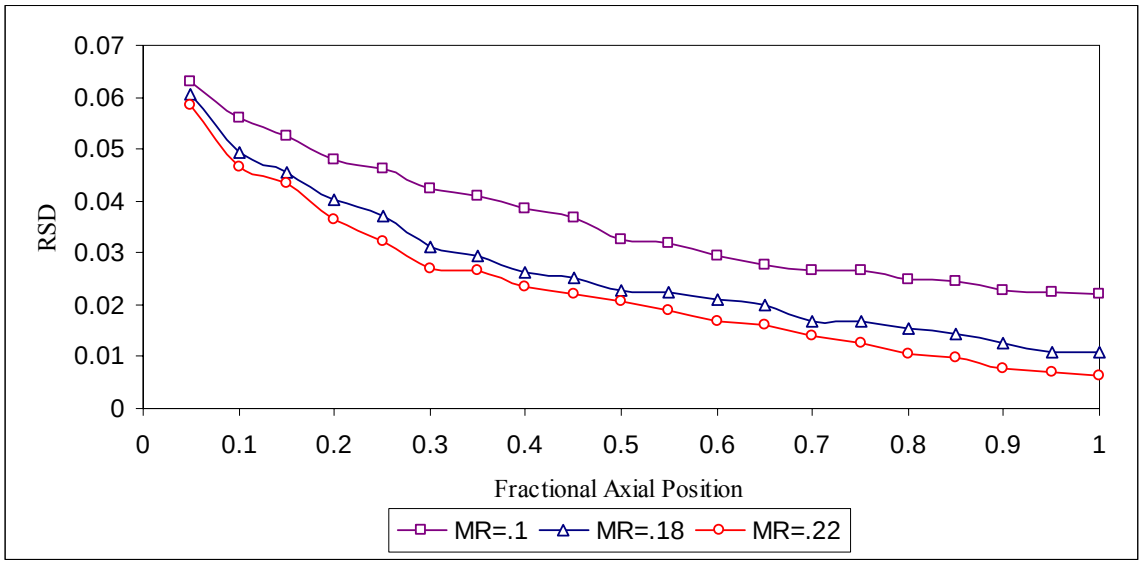

Figure 6.6: Effect of flux (0.1, 0.18 and 0.22) between compartments, all the other modeling parameters are kept constant.

It is important to mention that in chapter we illustrated that increasing the rotation rate within the mixer did not improve the overall mixing performance. This occurs because at higher rotation rates, the particles also tend to spend less time in the mixer, they are dispersed for a shorter period of time within the vessel and as a result the dispersion is reduced leading to a lower total mixing rate for higher rotation rates.

6.6.2 Number of Radial Compartments

The number of radial compartments has an effect on the estimate of radial variability of the flowing powder, in particular at or near the inflow region. The greater the number of radial compartments, the higher the precision with which the radial component of the compositional variance can be determined. Moreover, the larger the number of compartments, the greater the number of fluxes between the compartments that must be defined. Statistically, the lower the number of compartments the lower the initial variability since higher uniformity exists between a smaller number of larger compartments (averaging effect).

Consider a binary formulation, where some of the compartments are loaded with one component and all other compartments are loaded with the other component. Figure 6.7 illustrates the effect of loading the exact percentage of tracer in each example but varying the number of radial compartments. For example, in the case of 5 radial compartments, one is loaded with the tracer and the other 4 with non-tracer; in the case of 10 radial compartments, two are loaded with tracer and the other 8 with non-tracer. The flux is adjusted to account for the change in the number of fluxes as well as for the variation in the flux magnitude. This keeps the percentage of the tracer constant, in order to keep the total number of particles dispersed between compartments constant. For example, if a finite number of particles denoted as P_{total} exist, and they are divided among a number of radial compartments, N_{radial}. The flux is expected to change along with the number of radial compartments. Thus, the greater the number of radial compartments N_{radial}, the lower the flux between the compartments given the greater the number of

fluxes between compartments. At a fixed axial position the radial mixing rate can be found using the following equation:

$$\mathrm{Flux}_{ij_{new}\rightarrow i'j'_{new}} = \frac{\sum_{i'=1}^{N_R}\sum_{i=1}^{N_R}\mathrm{Flux}_{ij\rightarrow i'j}\times N_{ij}}{N_{ij}\times N_{R_{new}}} \quad \forall i$$

In this case study the Relative Standard Deviation (RSD) between the radial compartments represents the radial degree of homogeneity of the mixture, where the number of samples is the number of compartments and the sample size is the number of particles per compartment. The Central Limit Theorem states that for independent samples, sample variance is inversely proportional to sample size. In agreement to the theorem, the case study with the lowest number of radial compartments contained the largest number of particles per radial compartments and resulted in the lowest variability. This in fact introduces a grid effect in the estimate of homogeneity. To avoid this grid dependence problem, the sample size should be the same, i.e., should contain the same number of particles, independent of the total number of compartments or the number of particles per radial compartment.

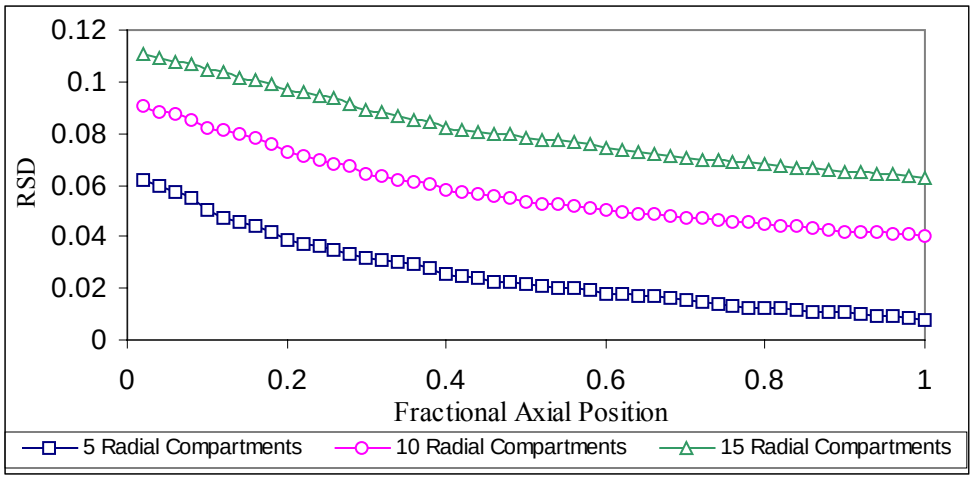

Figure 6.7: Effects of changing the number of radial partitions, while the number of axial partitions, total mixing rate, and the total number of particles are kept constant.

6.6.3 Axial Compartments

In this section the effect of the number of axial compartments is examined while the number of radial compartments, the total dispersion, and the total number of particles are kept constant. Ten, twenty, and thirty axial compartments are used to track the relative standard deviation along the axial trajectory. At the horizontal mixer setting, the axial flux is the dominant axial rate of transport (ie. there is no back flow) and there is basically a uniform residence time. In order to compare the results using a larger number of axial compartments, the flux between the compartments was reduced to maintain the same overall axial mixing rate. When adjusting the number of axial compartments, the total number of compartments changes, which affects the total mixing rate. In order to keep the total mixing rate constant, $MR_{total}=C_2$, when the number of axial compartments, N_A, changes the fluxes must be adjusted to keep the sum of all the fluxes constant:

$$C_2 = \sum_{i'=1}^{N_R}\sum_{j'=1}^{N_A}\sum_{i=1}^{N_R}\sum_{j=1}^{N_A} Flux_{ij\rightarrow i'j'} = \sum_{i'=1}^{N_R}\sum_{j'=1}^{N_{A_{new}}}\sum_{i=1}^{N_R}\sum_{j=1}^{N_{A_{new}}} Flux_{ij\rightarrow i'j'}$$

Counter-intuitively, the reduction in the fluxes when the number of axial compartments changed from 10, 20, and 30 result in a reduction of the CPU time required even though a greater number of compartments were used. All simulations were conducted using a Sun Sparc 900 MHz Processor 2GB. In summary, decreasing the number of axial compartments will decrease the accuracy of the models content uniformity predictions as visually illustrated in Figure 6.8.

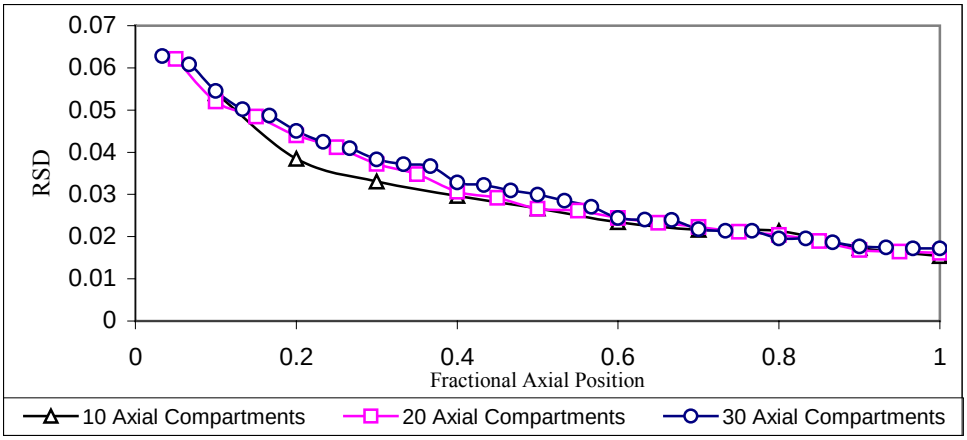

Figure 6.8: Effects of changing the number of axial partitions from 10 to 30, keeping the radial partitions and total number of particles constant.

6.6.4 Effect of Number of Particles

Most of the existing simulation approaches suffer from limitations in the number of particles they can handle; for example simulating 4000 to 30000 particles in high-shear mixers that range in diameter from 8 mm to 200 mm (Bertrand *et al.*, 2005; Cleary *et al.*, 2002) is far from the experimental conditions. In reality, particle size of some common excipients such as lactose can be 30 to 50 μm, and for MgSt and SiO_2 it can be as small as 1-5 μm (Bridson *et al.*, 2007). Calcium carbonates particles are found in the range of 5-214 μm (Johansen and Schaefer, 2001). Therefore the actual number of particles involved is several orders of magnitude larger than that considered in particle dynamics simulations. The question that still remains however is what is the minimum number of particles required in the simulation to represent the physics realistically. This is an open question that depends, at least in part, on flow properties such as cohesion. In some rotating drum case studies, decreasing the number of particles and increasing the particle size will still result in the same dilation effect or powder flow properties (Faqih *et al.*, 2006). However, in mixing it is important to use a large enough number of particles to minimize effects of sampling parameters on the estimate on mixing performance.

In the modeling approach explored in this work we need to specify (a) the number of particles within each compartment, (b) the number of particles in the entire vessel, which reflects the sum of particles in each compartment, and (c) the fluxes between compartments. Figure 6.9 illustrates the effect of changing the number of particles in each compartment by a factor of 10x while keeping the number of compartments constant. The overall effect of increasing the number of particles is not substantial in terms of the RSD curve trend and slope. However, the CPU time required for the larger number of particles was increased from 51 CPU seconds to 8005 CPU seconds, a factor of 157. The difference between both RSD curves was measured by obtaining a polynomial for each of the RSD curves, as a function of the fractional axial position, x. The polynomials fit the RSD curves with a R^2 greater than 0.99. The area between both curves was calculated and resulted in relative standard deviation of 3.83%.

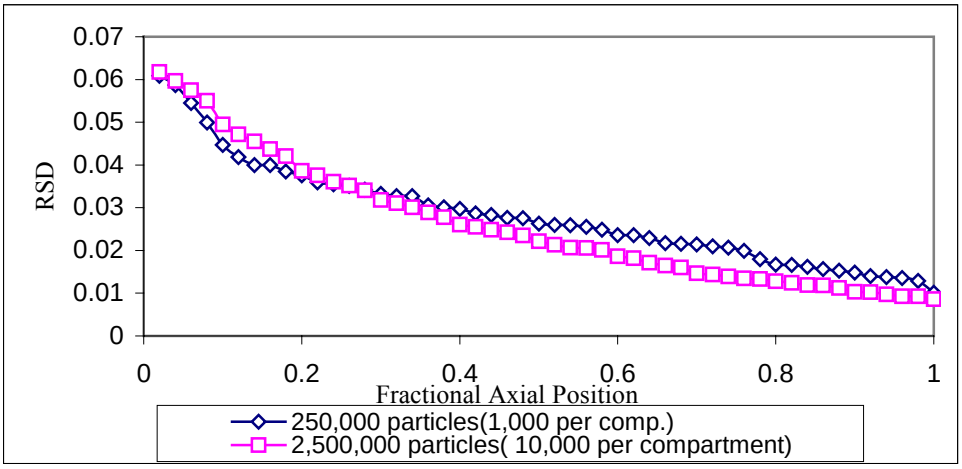

Figure 6.9: Effect of the number of particles per compartment on RSD profile considering 250 compartments in both cases.

6.7 Experimental Sampling Results

Sampling is very important in order to determine the quality of the pharmaceutical product. FDA has established a "Guidance for Industry" (2003) that assesses powder

uniformity and correlates in-process dosage units with powder mixing for batch mixers (V-blenders, tote-blenders, etc.). However, as of now the FDA has yet to establish any guidelines on sampling the continuous mixing process and many of the existing sampling issues mentioned in this work have not yet been addressed by regulatory language (or, in fact, discussed in the literature to any significant degree). Thus, it is deemed important here to begin to examine the sampling parametric space for continuous mixing.

One sampling question that arises is whether to increase the number of samples taken throughout the vessel or the sample size. One difficulty that exists is a small number of powder samples results in greater variability (lower statistical power) of the homogeneity index. However, the effect of the sample size and the number of samples can be accurately predicted only for random mixtures (i.e., mixtures that are statistically homogeneous), to which the CLT applies. While the random mixture model is a useful limiting case, real systems, and, in particular, systems that show mixing problems deviate substantially from the random model. For such systems the main sources of heterogeneity (agglomeration, segregation, stagnation) all cause non-Normality in composition distributions. For such systems, which are precisely the systems that sampling is (or should be) designed to "catch", the effect of sampling parameters cannot be easily predicted, and must be laboriously determined.

Fortunately, compartment modeling is an excellent tool for simulating sampling of non-homogeneous systems, nicely adding an arrow to our QbD quiver. Thus, the focus of this section is to illustrate how compartment modeling predicts the behavior of the powder in the mixer as a function of sample size as well as compare the experimental data derived from retrieving samples from the continuous blender and analyzing them

using NIR, thereby illustrating the problems associated with obtaining an accurate sampling prediction for continuous processing as well as examining the effect of changing the size and number of samples.

6.7.1 Sample Size

Sample size is defined as the amount of powder within one sample. The limitations that exist using a large sample size are that dead or segregated zones smaller than the sample space can remain hidden. Decreasing sample size can result in higher measurement errors from the true blend homogeneity. However it is important to keep in mind, that the scale of scrutiny is based on the sample size of the target delivery system.

Experimentally these effects can be noticed using advanced sampling techniques, particularly solidification of the powder bed (Brone *et al.*, 1998) or vessel partitions (Massol-Chaudeur *et al.*, 2002). However, these experiments are invasive and somewhat impractical; for example, using thief probes drags powders along the sampling path, thus altering the powder distribution prior to sampling. As a result, it becomes more important to optimize sampling in order to maximize accuracy of characterization, while minimizing disturbance of the powder blend. Online non-invasive sampling would be ideal but method validation is challenging, because the sample is not captured and cannot be analyzed by a corroborating method, and they require both fast data acquisition and an accurate and fast algorithm to filter the noise spectra in a short sampling time window. To the best of our knowledge, up to this point Near-Infrared Spectroscopy has not been successfully integrated online for continuous powder mixing processes.

In this work the effect of changing the sample size on the axial measurements is examined using compartment modeling and experiments. The sampling analysis includes

the effect of the sample size as well as the number of samples. To determine the effect of sample size, we examine 250 compartments containing a total of 10,000 particles. Samples were taken from the radial compartments and used to calculate the RSD of the tracer concentration at a fixed axial position. The total number of samples taken is kept the same but the number of particles in each sample is varied from 50 to 1000.

Figure 6.10 illustrates the different curves for each of the sampling sizes in comparison to the RSD obtained from examining all the particles within the compartments. Clearly, the variability for the small size (50 particles) is high. In fact, the average variability between the sample measurements and actual measurements for all the measured data points is 59% for 50 particles, followed by 17.1% for 500 particles and 12.5 % for 1000 particles. Increasing the number of particles further results in smaller fluctuation from the curve characterizing all the particles in the compartments. Computationally increasing the number of particles in the sample results in a very small increase in computational time e.g. for the 50 particles it takes about 51 CPU s, for the 500 particles 56 CPUs, and for the 1000 particles 61 CPU s.

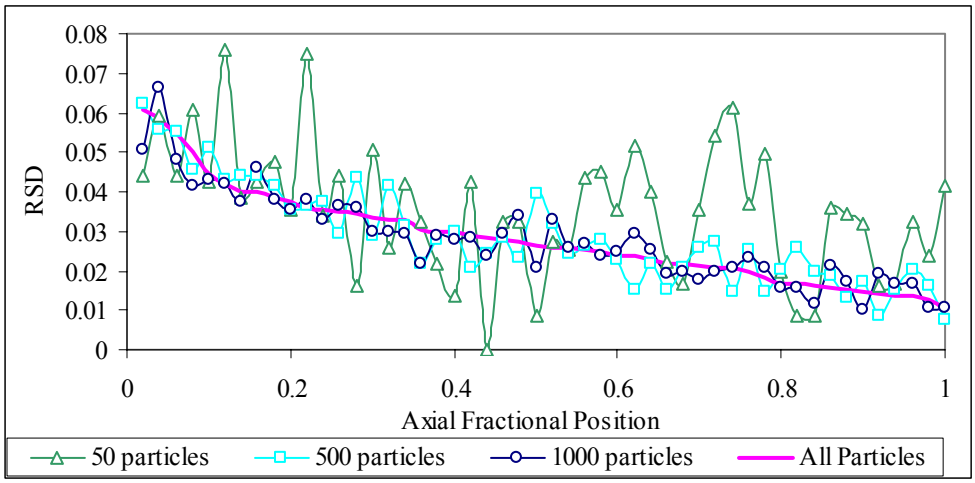

Figure 6.10: Effect of the number of particles per sample, keeping the number of samples constant on the homogeneity measurement.

The effect on the content uniformity measurements by increasing the sample size was examined experimentally for continuous mixing experiments where the percentage of APAP varied in the inflow. The samples were analyzed using NIR under two confocal windows with a 10.8mm and a 30.8mm diameter. The effect of the larger window is a larger sample size. The results shown in Table 6.2 illustrate that increasing the sample size for 6 different continuous mixing experiments resulted in a lower sample-to-sample variability. The experiments illustrate that increasing the samples almost always reduced the variability between the samples. Since these effects are a factor in content uniformity measurements, using compartment modeling the effect of sample size can be quantitatively captured to show how RSD values and sample noise are affected within a short computational time.

Table 6.2: Effect of the sample size using two focal diameters under NIR absorbance.

Experiment No.	RSD		Experiment No.	RSD	
	Focal Diameter			Focal Diameter	
	10.8 mm	30.8 mm		10.8 mm	30.8 mm
1	0.150	0.086	4	0.229	0.199
2	0.156	0.176	5	0.183	0.092
3	0.220	0.171	6	0.195	0.087

6.7.2 Number of Samples

In this sub-section we examine the effects of the number of samples. Increasing the number of samples expands the sampling space studied, moreover, reduces the probability of overlooking stagnant regions. It also increases the statistical power of the sample population estimates. The disadvantage is that invasive sampling requires removing more samples from the system thereby altering the powder distribution. Thus, the sampling objective is to determine the optimal number of samples. This requires a compromise between experimental limitations and reassurance that no unmixed zones are

overlooked within the entire vessel, and that the variability in population estimates are sufficiently low to give a high quality assessment of blend properties.

Experimentally, the number of samples retrieved within the axial length of the mixer processed under identical conditions was studied. The mixing system was rotated at an impeller speed of 50 RPM and inclined in the horizontal position (the experimental procedure was described in detail in the experimental approach section). The results shown in Figures 6.11 clearly indicate that by varying the number of ~1.6 gram samples retrieved at each spatial area from 3 to 5 samples, experimentally and computationally, the variability in the measured degree of content uniformity decreased. Using 3 or 5 samples, compositional values showed oscillating behavior, but the mean values at each axial location were not dramatically different. However, for 3 samples the error bars for the three experiments conducted at the given process conditions were higher than for the 5 samples.

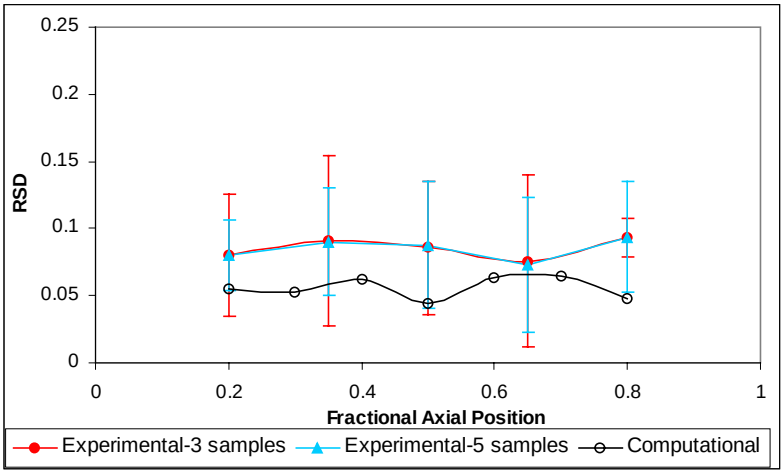

Figure 6.11: Compartment model and experimental results RSD measurements for 3 and 5 samples (model-100 particles per sample; experimental 30 mm diameter) taken throughout the axial length.

The model showed lower RSD values than the experiments. In general, this is to be expected, since experiments are subjected to additional variability due to analytical

error, while simulations are not. One question that therefore arises is what is the optimum number of samples and how accurately the model can capture the decreasing RSD profile measured in experiments. The RSD behavior for a larger number of samples is shown in Figure 6.12, where the number of samples is varied while keeping fixed the number of particles per sample (100). The percentage error change due to the number of samples from 37.3% for 25 samples, 39.5% for 50 samples, and 28.2% for 200 samples, shows that by increasing the number of samples the variability between the samples will not decrease as it did when the sample size increased (i.e, grid independence is achieved). This leads to the conclusion that fluctuations are mainly due to the sample size and not the number of samples. We should also mention that the computational time was trivially increased, 51.8 CPUs for 25 samples, 52.3 CPUs for 50 samples, and 55.5 CPUs for 200 samples.

For batch mixing, an important aspect of sampling is to identify dead zones and segregation. Thus, increasing the number of samples is not sufficient, but is also necessary to evenly distributing sampling locations in order to prevent overlooking any area within the vessel. However, for continuous mixing, a variation in active distribution along the axial length is not necessary due to dead zones but due to the mass flowrate variability introduced by the feeding mechanism, which can be transported along the axis by “plug flow”. Thus, it is important to understand that taking more samples within larger axial areas should not be expected to result in a monotonically “improved” measured mixing performance even if mixing is improving. However larger samples will have a greater probability of better characterizing the behavior that is actually taking place.

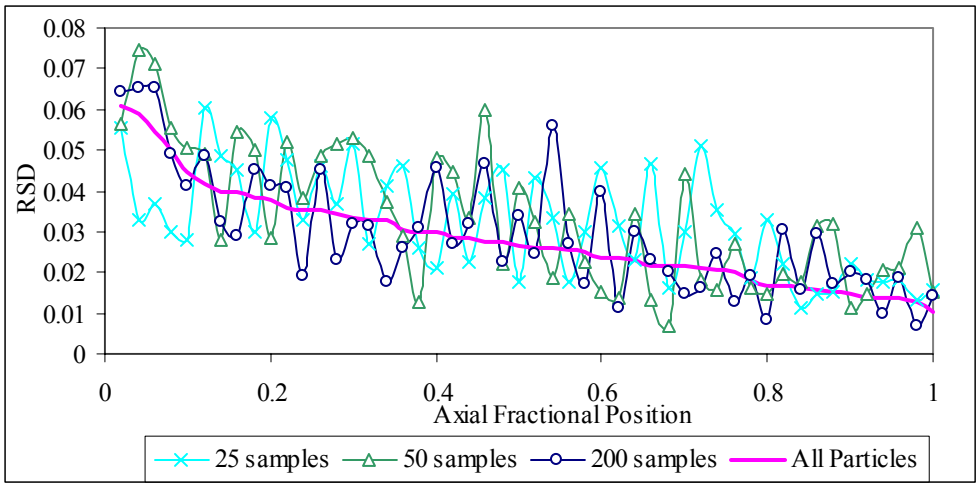

Figure 6.12: Effect of increasing the number of samples keeping the number of particles within each sample constant.

6.8 Experimental Validation

In this work, powder samples were extracted axially from the horizontal mixer as illustrated in Figure 6.3. For the present study, the purpose of this data was to allow us to validate and fine-tune the compartment modeling results. The experimental data is obtained by getting five samples from each of the spatial areas illustrated in Figure 6.3. Due to the hold-up limitations that arise as a result of processing inclination, rotation rate, and vessel design, five samples were retrieved per location.

The computational data is obtained using radial and axial compartments and retrieving 5 samples of 100 particles each. The experimental samples were ~1.6 grams, however it is important to mention that the NIR system will only examine a small fraction of this powder that reflects the incident light. The impeller speed was 50 rpm for this experiment. Computationally the mixing rate utilized was chosen to match the outflow variability. However, as shown in the sampling section, the smaller the number of samples retrieved, the higher the noise frequency. The results using 5 samples are illustrated in Figure 6.13 and compared to the computational results. The computational

model is within the error values of the experimental data but does not illustrate the oscillations found in the experimental results, which may be due to sampling or to NIR analysis. This highlights another advantage of the compartment methodology, which is that it can offer a way to quantify the powder dispersion within the mixing vessel although the actual physicals are not explicitly described (or completely understood).

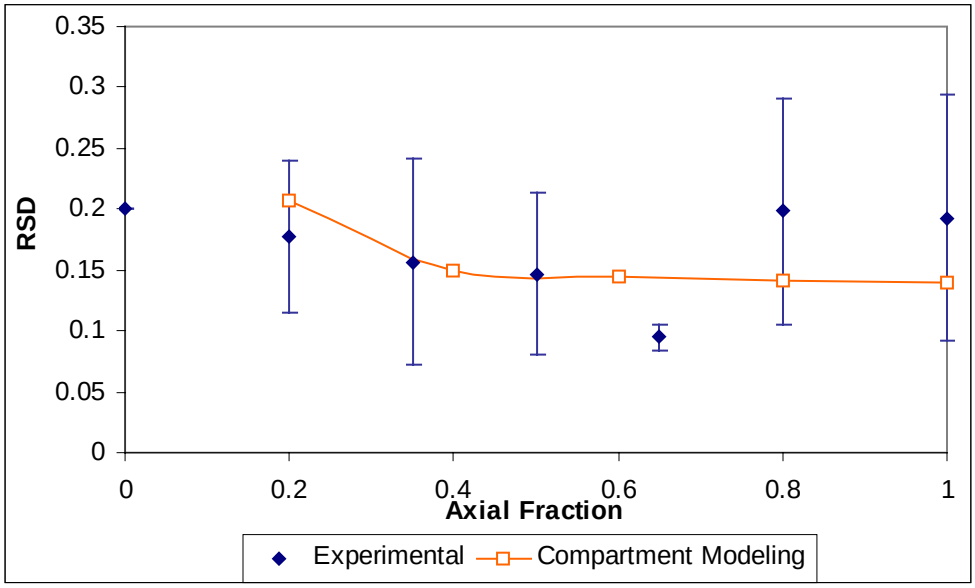

Figure 6.13: Relative standard deviation as a function of axial length within the mixer.

6.8.1 Effects of Processing Angle

In chapter 2 we illustrated the impact of processing angle on the relative standard deviation of the outflow content uniformity. What we showed was that increasing the processing angle to the upward position resulted in a longer residence time, which led to better mixing. Up to this point, the experimental work presented here (specifically the results in Figures 6.11 and 6.13), was based on a horizontal processing angle. Here we examine the effect of using an upward processing inclination of +17°, and the processing impeller speed was 50 RPM. The experimental study consisted of determining the

relative standard deviation between the samples retrieved from five spatial areas. Six samples were retrieved for each spatial area.

The experimental results and computational output utilizing compartment modeling are both shown in Figure 6.14. At the upward inclination, the powder remains in the vessel the longest amount of time, which results in lower sample-to-sample variability early along the mixer. The residence time pattern was exhibited in chapter 2 were the results showed that at a constant speed the residence time was highest at the upward and lowest at the downward inclination. The pattern correlates well with the findings in chapter illustrating that content uniformity is best (lowest RSD) in the upward inclination where the residence time is longer. The lower RSD is observed throughout the axial length for the upward position as shown in Figure 6.14. In addition, RSD values within the axial length are also fairly stable with low experimental error bars.

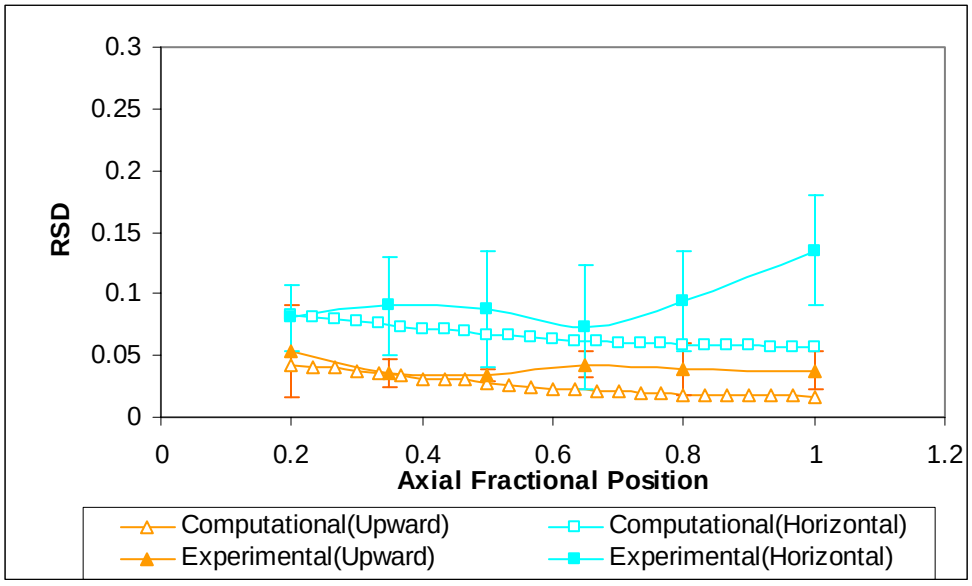

Figure 6.14: Experimental results obtained from changing the processing angle and Compartment modeling results at the upward processing angle.

6.8.2 Effects of Product Formulation

A large array of publications exist dealing with the different physical properties such as particle size (Gilbertson and Eames, 2003), particle morphology, powder density, and surface structure, all of which affect powder flow (Alexander *et al*., 2006), mixing (Chaudhuri *et al.*, 2006), and diagnostics (Beddow *et al.*, 1980). Unfortunately, lacking "mixing rules" for material properties, systematic characterization of the properties of all relevant powders that could be used in a continuous mixing process by the pharmaceutical, metallurgical, and environmental industries, to name but a few, is an immense task. In this work we content ourselves with examining the effect of changing the APAP concentration in the blend, and showing that the compartment modeling approach can be refined to capture these effects.

Experiments were conducted at various APAP concentrations using two sample sizes in the NIR analysis of the experimental data. The larger sample size has 30 mm and the smaller a 10 mm confocal diameter. The results showed that increasing APAP concentration decreased the sample-to-sample variance in the outflow, as illustrated in Figure 6.15. In addition, the larger the sample size window the lower the measured standard deviation values. One possibility is that for higher APAP concentrations, a greater number of tracer particles exist in each sample, thus reducing the variability in the individual sample concentration. Using compartment modeling the variability was noticed to be a function of sampling size as shown in Figure 6.15. The computational results illustrate that the outflow behavior is a function of sampling size. As shown in the computational results, the RSD trend that corresponds to the experimental data is the profile with the smallest number of particles, i.e. the smallest sample size. This indicates

that the experimental data showing higher content uniformity for smaller APAP percentages maybe due to a small sampling window.

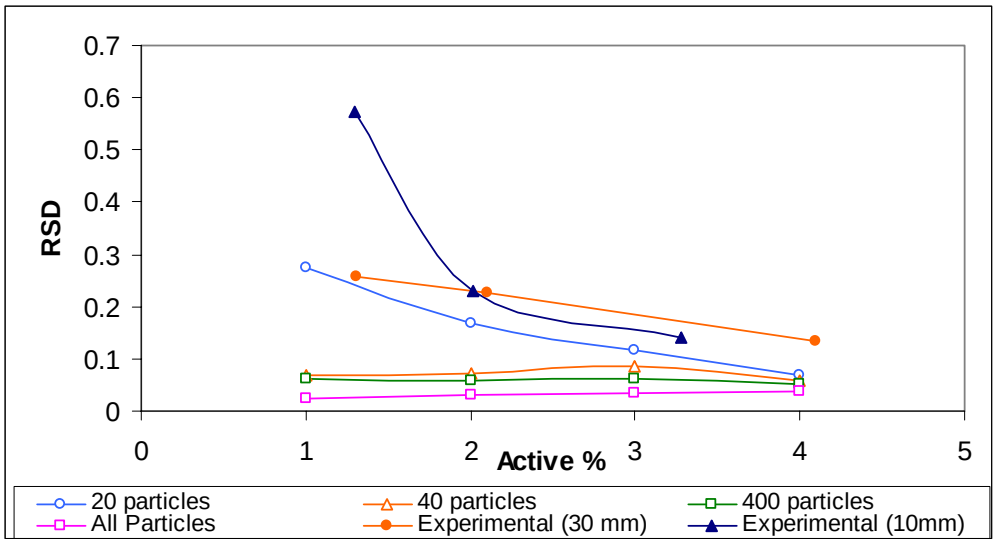

Figure 6.15: Experimental and Computational RSD results obtained from varying the percentage of Acetaminophen. The computational results are shown as a function of 4 different sample sizes 20 particles, 40 particles, 400 particles, and all the particles (concentration of the entire output).

The effects of inflow APAP fluctuations are also examined in this section. Continuous mixing performance is sometimes assessed by computing the Variance Reduction Ratio (VRR), which accounts for the inflow fluctuations that arise due to the feeding mechanism. Utilizing vibratory feeders we have demonstrated that feeding variations are present and limit the flowrate capacity.

As a result, predicting the effect on the outflow of a given inflow variability has sparked interest in the pharmaceutical community. The variability within the active mass is modeled with a pseudo-random flow rate calculated from the active experimental variability. Using the methodology proposed in this work, the effect of the input variability on the outflow was calculated and is illustrated in Figure 6.16. The top curve represents the mass fraction of active ingredient at a test point and the bottom curve is the

corresponding outflow. The variance of the fluctuating inflow in Figure 6.16 is 1.82E-04. After mixing the resulting RSD profile has a variance of 3.02E-05 with a resulting VRR, defined as the inflow variance over the outflow variance, of 16. The VRR is high which implies good mixing as discussed by Williams and Rahman (1971a) and Beaudry (1948).

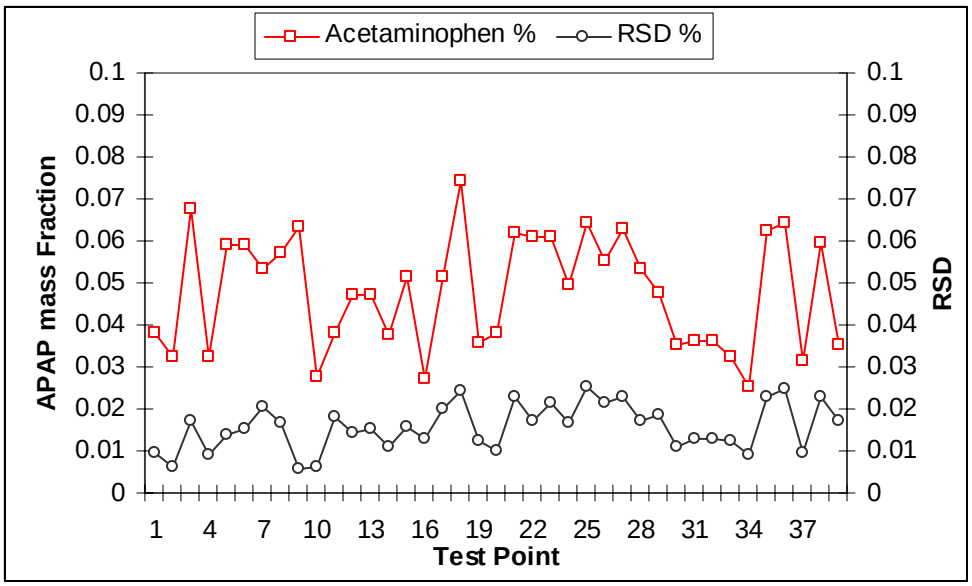

Figure 6.16: Compartment model results showing the effect of variability in the active mass fraction of the inflow and the RSD of the outflow homogeneity of the powder.

6.9 Summary and Discussion

The focus of this work is to introduce a modeling method, based on compartment modeling, that provides a fast and convenient alternative to particle dynamics methods, and that is suitable for understanding the effects of sampling parameters, and, potentially, for control purposes toward process characterization. Given the current interest in continuous powder blending, the case study selected in this work focuses on the axial mixing behavior within a continuous mixer as a function of processing parameters.

Experiments and computations are used to capture the mixing behavior of powders within a continuous mixer. Experiments were carried out within the continuous

blender using a Lactose/APAP formulation. The experiments were conducted to examine the effect of sampling in the outflow and within the vessel, illustrating that sampling effects on the measured mixing performance. The content uniformity as a function of processing angle on the mixing behavior was examined within the vessel, and illustrated that the upward angle results in better mixing performance compared to the horizontal inclination. The effect of APAP concentration was also examined, and showed that content uniformity within the outflow was better when a higher percentage of APAP was used. However, as shown with compartment modeling this may be due to experimental limitations that limit the sample size.

The work outlined the suitability and flexibility of compartment modeling to capture the dynamics of continuous powder blending. The advantages of this approach are (a) the sampling flexibility, which plays an important role in properly analyzing powder blends, particularly crucial for pharmaceutical applications; (b) the short computational time; (c) the ability to predict the axial and outflow variability given inflow fluctuations which can be used for on-line control and optimization. The modeling parameters examined include the number of axial and radial compartments, the number of particles, and particle fluxes between compartments. Results show that the compartment modeling approach is both feasible and quite convenient. Effects of sample size and number of samples were clearly captured by the model. Fluxes could be adjusted easily to account for differences in mixing performance resulting from changes in processing parameters such as the angle of inclination of the mixer. Effects of formulation (API content) and feed variability could be effectively captured.

Arguably, while having been extensively used for fluid processes, the approach presented here is in its infancy when it comes to powder processes. Much work remains to be done for the method to reach full blossom. To wit, multiple sources of information about fluxes need to be tested and incorporated into a general framework. Given the advantages and limitations of compartment modeling other modeling sources may be beneficial as a result the next chapter will connect a DEM simulation and a compartment model to improve the computationally efficiency of DEM for powder mixing.

Chapter 7

Hybrid Compartment-DEM Modeling Approach

In this chapter a new methodology, the main ideas of compartment modeling and discrete element method approaches are outlined. The new hybrid approach presented is used to examine a number of case studies for the horizontal mixer. A discussion of the results is presented, where the effect of the number of compartments and time step will show to affect computational savings and accuracy.

7.1 Introduction

Powder mixing processes are typically difficult to characterize since powders cannot be classified as either solids or liquids (Jaeger and Nagel, 1992). The unusual flow behavior of powders is of particular importance since segregation and agglomeration reduce the powder uniformity of powder blends used in a large number of applications. In order to model powder flow and improve the characterization of powder processes, several models have been proposed. Wightman and coworkers (1998); Ottino and Khakhar (2000) distinguished the following groups of mixing models: Monte Carlo simulations, particle dynamic simulations, heuristic models, and models based on kinetic theory. Although these models have proven successful in describing the mixing behavior in many case studies, there are a number of remaining challenges that are briefly summarized here. In Monte Carlo simulations it is difficult to correlate real mixing time to simulation time. In the case of particle dynamic simulations, the computational requirement for realistic mixing systems is extensive, thus the computational power required limits the beneficial usage. The main limitation of the heuristic models is that

they are based on ideal conditions whereas the models based on kinetic theory are capable of simulating only binary and tertiary mixtures. Another method well suited to model deforming solid materials is smoothed particle hydrodynamics (SPH) (Cleary and Prakash, 2004). This method was originally developed for fluid mechanics, but has been applied to solid mechanic problems where there is fracturing, shattering, and possible phase change. It has, however, not been used to model solid mixing except where particle fractures occur.

In chapters 5 and 6, we demonstrated the use of compartment modeling as a tool to efficiently model and characterize powder mixing. Although compartment modeling is a very powerful analysis tool for mixing characterization, it does not predict the details of particle behavior such as particle location and particle trajectory, which can be determined using a particle dynamic simulation such as discrete element method (DEM).

Discrete element method (DEM) is a simulation methodology that predicts the trajectories of individual particles by solving Newton's equations of motion (Pandey *et al.*, 2005). A number of studies have been performed using DEM, including modeling tumbling mixers (Cleary *et al.*, 1998; Wightman *et al.*, 1998; Zhou *et al.*, 2004)), and convective mixers (Bertrand *et al.*, 2005; Yang *et al.*, 2003; Sinnott and Cleary, 2003). An excellent review of the recent advances in the field of powder mixing and DEM can be found in Bertrand *et al.* (2005). However, as shown by Bertrand *et al.* (2005) the computational cost is significant since the equation of motion for each particle must be solved at each time step which limits the applicability of DEM models. In order to overcome this limitation the particle morphology is approximated or the number of particles are reduced (Moreno-Atanasio *et al.*, 2005; Li *et al.*, 2005). However, in many

cases only a small area of the mixer has to be modeled using a detailed DEM simulation. This has been shown by Zhou and coworkers (2004) that illustrated that for sufficient fill levels, the physical actions of the impeller no longer affect the contents of the vessel within certain sections. The method proposed in this work takes advantage of this fact and combines the computational simplicity of compartment modeling with the detailed particle simulation of a mixing process achieved by DEM. Along the same lines, McCarthy and Ottino (1998) proposed an approach based on the integration of geometric insight with particle dynamics to form a hybrid technique for a tumbler operating in the avalanching regime.

In the proposed approach, the areas that need better characterization in order to model the mixing process are solved with DEM whereas` the rest of the system is captured with a compartment model. For example, in the case of a horizontal stirred mixer, the impeller area is captured using DEM and the surrounding area is simulated using compartment modeling. The compartment and DEM simulations are run in parallel, interchanging particles for the desired mixing time. The proposed framework results in a detailed description of the mixer with a substantial reduction of computational time compared with DEM simulation.

7.2 Discrete Element Method (DEM)

Discrete element method (DEM) was developed by Cundall and Strack (1979) and refined by Walton and Braun (1986). The method is based on a finite number of discrete, semi-rigid spherical shaped particles interacting deterministically by means of contact or non-contact forces. All the particles within the system have a known exact spatial position. The system is spatially discretized into a number of 3-dimensional grids

and each particle is contained within at least one grid. If a force is exerted on the particle, the particle will most likely collide with other particles that exist within its grid or neighboring grids. The force model between two particles considers that the collision or interaction between two particles occurs either in a single point or a finite area (Zhu and Yu, 2006). Walton and Braun's (1986) partially latching spring model is utilized for elastic particle collisions. Once the collision takes place, the force on the particle is calculated using Newton's equations of motion and the particle trajectory is determined.

DEM models have been extended to account for the cases where a moving impeller is present in a mixing system. One strategy is based on discretization of the boundary surfaces by means of a finite-element mesh that can be determined using a mesh generator known as multi-wall method established by Kremmer and Favier (2001). Another approach is developed by Cleary *et al.* (1998) that use a series of particles to represent a boundary domain. For the case of a rotating drum with a blade, the blade consists of an assemblage of particles with physical properties that mimic the interactions that the particles have with the impeller. Due to the increasing number of interactions and particles, the simulations become computationally cumbersome. As shown by Bertrand *et al.* (2005), the computational complexity increases exponentially with the number of particles in the vessel, which limits the applicability of DEM (Table 7.1). Another alternative to reducing the computational time of a DEM simulation is parallelizing the model algorithms. Parallel programming takes advantage of parallel computing systems by separating tasks, allocating and synchronizing tasks to different processors. As shown in Table 7.1 increasing the number of processors linearly decreased the computational time.

Table 7.1: CPU time/impeller revolution with DEM from Bertrand *et al.* (2005)

Number of Particles	Serial Computer	32 procs (speedup=16)	64 procs (speedup=32)
10^3	3 h	10 min	5 min
10^4	1.25 days	2 h	1 h
10^6	4 months	1 week	3.5 days

7.3 Compartment Modeling and DEM Comparison

A comparison between compartment and DEM modeling is performed in this section to illustrate the advantages and limitations of each method. A discrete element model was used by Wightman and coworkers (1998) to describe a horizontal cylindrical vessel undergoing rotational motion. The study consisted of modeling the motion of identical particles, red and blue. The vessel was initially loaded with side-by-side loading, one half of the cylinder filled with red particles and the other half with blue particles. The granular mixing vessel was subjected to pure rotation, meaning the cylinder rotates along the horizontal axis. Wightman and coworkers (1998) compared the results of the DEM simulation with experimental data (Wightman *et al.*, 1996) obtained from solidifying the powder mixture at a moment in time. Once solidification occurred, slices of the mixture were taken and analyzed under image analysis. The fraction of red particles throughout the vessel showed good agreement with the experimental study and DEM simulation. To compare with this study a 16-compartment-model, is used to simulate the horizontal cylindrical vessel (Figure 7.1). The fraction of red particles is determined as a function of axial length at four different time points. The graph in Figure 7.2 shows that the compartment model can very well capture the particle compositional behavior as a function of axial length.

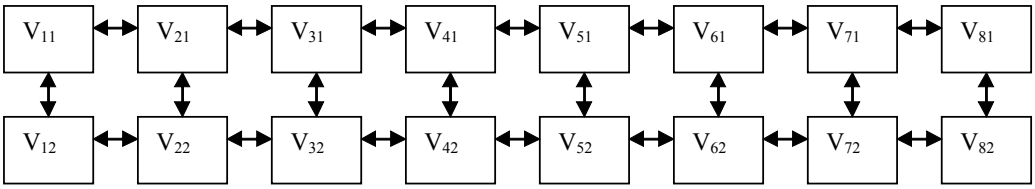

Figure 7.1: Compartment Model representing a horizontal tumbling blender

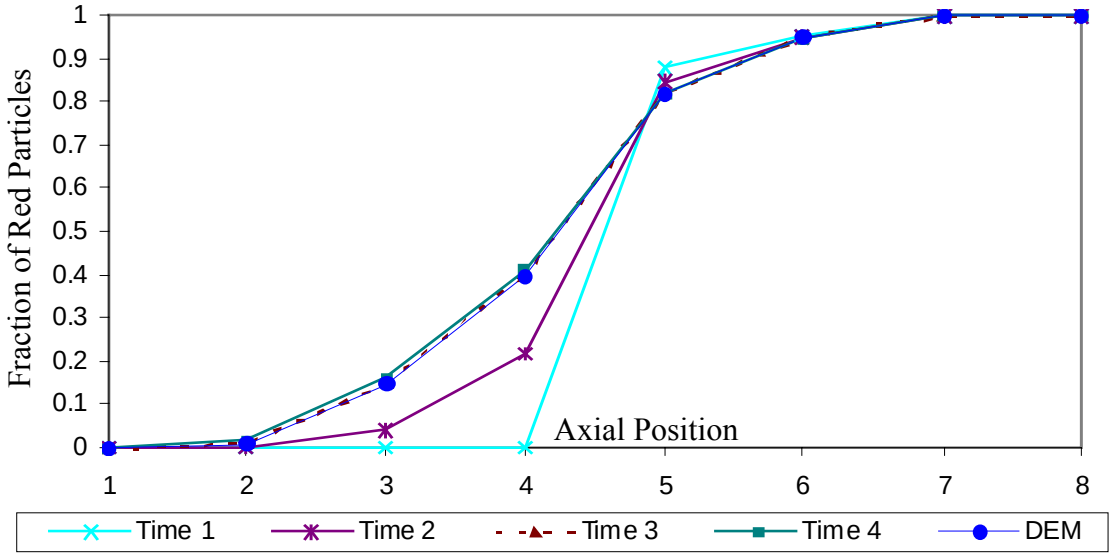

Figure 7.2 Compartment model results for the red particle fraction at time points 1 through 4 in comparison with a DEM simulation at one time point for a horizontal tumbling cylinder.

The main advantage of compartment modeling is its computational speed. For this case, the compartment simulation required 2,084 CPU sec on a Sun Sparc 900 MHz Processor 2GB whereas the DEM simulation performed by Wightman and coworkers (1998) required about 48 h of CPU time for every second of real time simulated on a Sun Sparc 20.6 Workstation thus, revealing huge computational savings. However, it should be pointed out that the DEM simulation results in the detailed characterization of particle behavior including particle position and trajectory which is not obtained using compartment modeling.

7.4 Hybrid Compartment-DEM modeling Approach

As described in the previous section, DEM calculates the spatial trajectory of every particle under the effects of convective, shear, dispersive, and gravitational forces. The main drawback however is that DEM simulations can be computationally very expensive especially when complex geometries are considered. Thus, the main objective of this work is to reduce the computational expense of powder mixing simulations by partitioning the mixing system into regions of higher complexity to be modeled by DEM and regions of lower complexity to be simulated using compartment modeling.

Proposed Framework

The steps of the proposed approach, which are shown in the flowchart depicted in Figure 7.3 are as follows:

Step 1: First, the mixing system is partitioned into different mixing regions depending on the level of complexity. Complexity is defined as the degree of variability within particle circulations that exists within that mixing region. Regions of high complexity are modeled using DEM (or any other detailed simulation approach) and lower complexity regions are simulated using compartment modeling (or any other statistical model). In the next section, two approaches are presented for partitioning the mixing system.

Step 2: In this step, the parameters needed to perform the numerical simulations are determined. For the areas described by DEM, the number of particles, particle diameter, and vessel geometry corresponding to each chemical or physical group within the vessel must be specified. For the compartment model, the number of compartments, the number of different particles within each compartment, and the particle fluxes must be defined. The particle flux is defined as the number of particles exchanged, between compartments

per time step. The particle flux is calculated based on the difference between the number of particles (N) that are within the region (*i)* at time (*t*+Δ*t)* and the number of particles at the same region at time (*t*) divided by the elapsed time (Δ*t*): $\frac{N(i,t+\Delta t)-N(i,t)}{\Delta t}$.

Step 3: Once the system parameters are defined in the previous step, the DEM and compartment simulations are run in parallel. The trajectory of particles leaving one mixing regime and entering another are captured as particle exchanges between the compartment and DEM simulations. Thus, at selected time points, a designated number of particles located at the interface between DEM and compartment modeling are randomly exchanged. The approach used to model the particle exchanges is described in the Exchanging Particles between Model section.

Step 4: The simulations continue to run until the check point time is reached, t_{check}. At this point, we check the hybrid results to those obtained from well-established methods (described in the Quantifying Model Accuracy and Validation section). If the difference is within an acceptable tolerance level, which is pre-postulated by the user, the simulation continues to run and stops when the desired real-time has been modeled, t_{stop}, otherwise parameters are adjusted and the simulations are repeated.

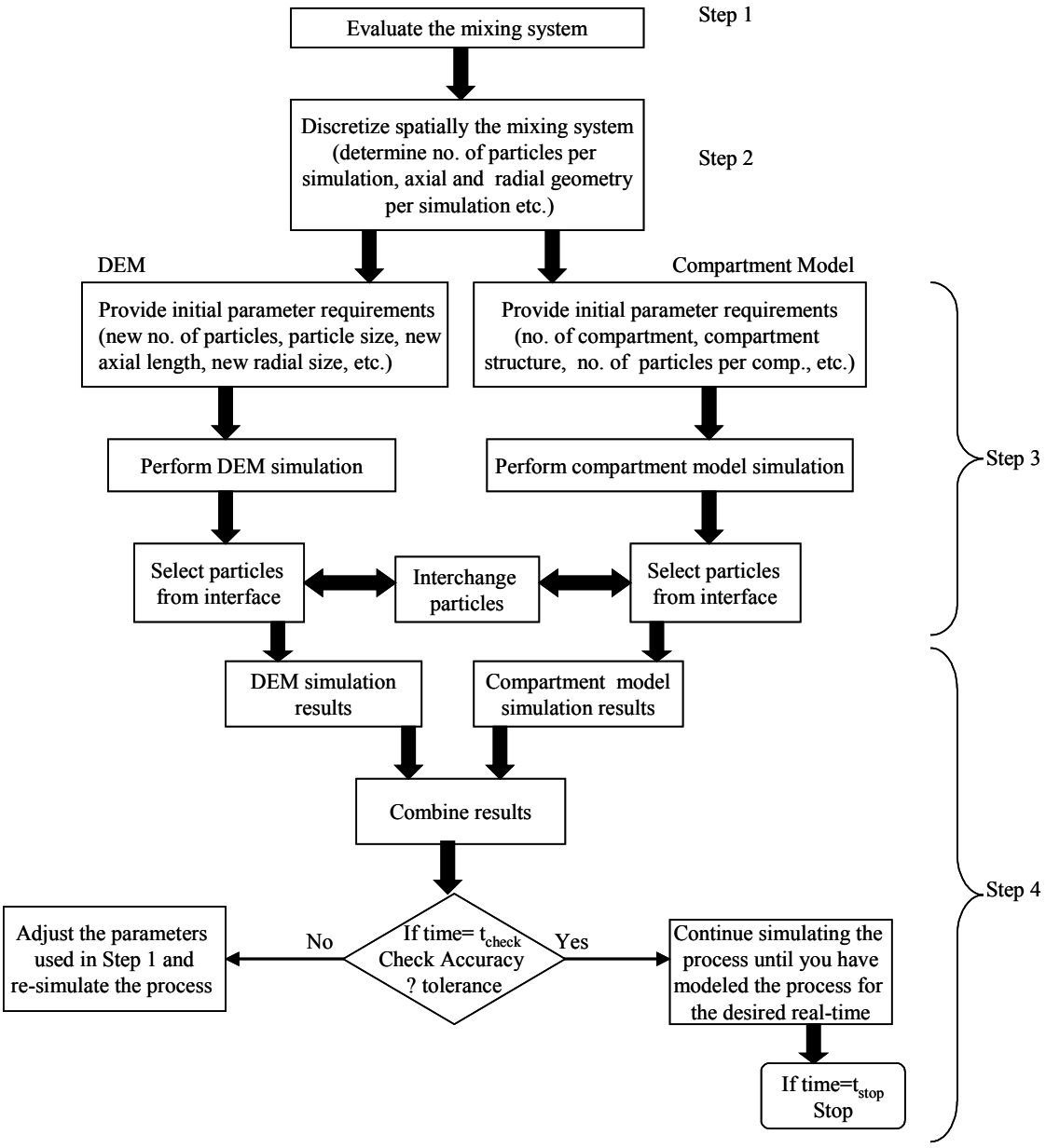

Figure 7.3: Proposed New Hybrid Algorithm

7.5 Mixing Process Partition

As mentioned in the previous section, the first step in the proposed hybrid approach is to determine the degree of complexity in each section in order to treat each section with the appropriate modeling tool. In this section, two methods are described that can be used to partition the mixing system. The first approach is based on heuristics

and geometric arguments, whereas the second approach is centered on estimation of particle velocities.

7.6 Partition Method I

The first method involves the spatial discretization of the mixer given prior knowledge of the different mixing regimes. Once the vessel is divided into regions, the particle flux defined as the slope of the number of particles at different time intervals (j) is denoted as m_j. This is determined for each section computationally or experimentally. Since the particle fluxes at each region vary as a function of time, the particle fluxes are evaluated at different time intervals. The standard deviation is evaluated based on the difference between the average particle fluxes with one region at different time points. If the particle fluxes exhibit high variability in terms of the standard deviations (σ), a detailed model is used to account for the mixing behavior in that region. On the other hand, if the particle fluxes show a small degree of variability at different time intervals, then a less expensive model such as a compartment model can be used to simulate this region.

7.6.1 Partition Method I - Illustrative Example

An illustrating example is used here to demonstrate the previously described approach. The system studied is a horizontal cylinder with an impeller with the parameters shown in Table 7.2. The vessel is loaded with two types of particles distinguished by their color (red or blue). The horizontal cylinder within an impeller attached to a rod, shown in Figure 7.4a, is divided into five regions all with the same diameter, d, and axial length, L/5, as shown in Figure 7.4b. Once the vessel is divided into the pre-selected number of regions, the particle flux (i.e., the number of particles

exchanged within each region, j, at each time step) is determined. The fluxes denoted as m1, m2, and m3, for three different time intervals and all the regions, are displayed in Table 7.3. Regions 1 and 2 exhibit higher variability. This is expected since these regions are closer to the moving blade. Thus, using the first approach regions 1 and 2 will be modeled using a discrete element method while regions, 3, 4, and 5, will be simulated using a compartment model.

Table 7.2: Simulation Parameters for the DEM simulations of a horizontal cylinder with a blade.

Number of Red Particles	700
Diameter of Red Particle	.01 m
Number of Blue Particles	700
Diameter of Blue Particle	.01 m
Radial Length of Vessel	.1 m
Axial Length of Vessel	.5 m
Length of Impeller Rod	.45 m
Diameter of Impeller	.1 m
Impeller thickness	.05 m

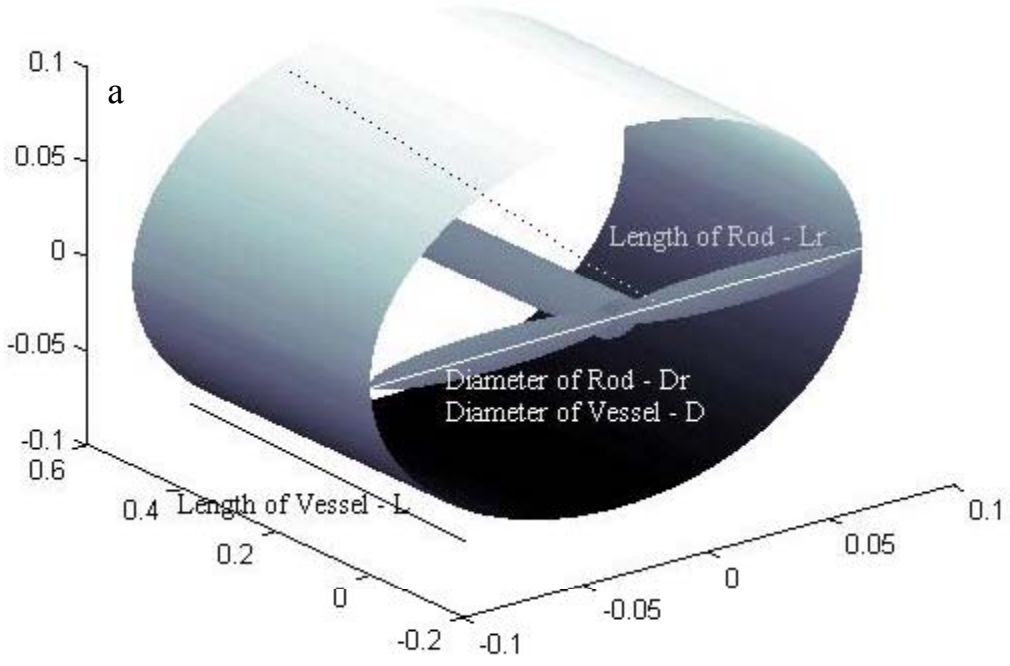

Figure 7.4: (a) A schematic of the mixer modeled in the case studies.

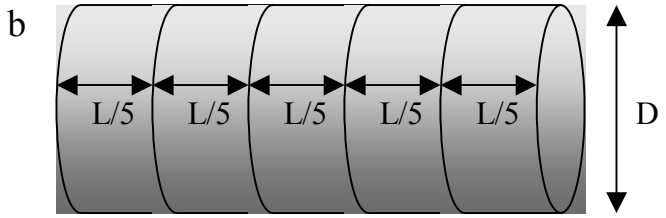

Figure 7.4: (b) A mixer partitioned into 5 regions with the same radial distance.

Table 7.3: The particle fluxes for both red and blue particles in five regions within the horizontal cylinder.

Particle	Blue				Red			
Region	$\|m_1\|$	$\|m_2\|$	$\|m_3\|$	σ	$\|m_1\|$	$\|m_2\|$	$\|m_3\|$	σ
1	27.08	11.69	12.84	8.6	2.34	14.01	20.97	12.0
2	2.48	6.82	7.50	5.6	0.13	2.36	10.10	9.9
3	1.58	2.40	4.90	1.7	0.76	6.41	4.95	5.7
4	3.78	4.92	9.54	3.1	3.26	3.48	10.10	3.9
5	1.83	0.70	2.74	1.0	3.22	2.58	6.16	1.9

7.7 Partition Method II

The second approach partitions the mixer into separate regions depending on the particle velocities in comparison to the first approach that uses the variability in particle fluxes. For conditions where no experimental measurements exist, the velocity profiles can be determined using a computer simulation. In this case, in order to limit the computational requirements, the simulation time is reduced to the necessary time needed to characterize the system. To determine whether reducing the modeling time affects vessel partitioning, the particle velocities at succeeding time intervals are evaluated. For the system described in the previous section, the particle velocities as a function of axial length at different time intervals are obtained from a DEM simulation and displayed in Figure 7.5. The figure illustrates that as time increases, the particle velocities exhibit the same behavior with respect to axial length. The average velocity variance as a function of local axial area is shown in Figure 7.6 which also illustrates that as time increases the

variance does not pose significant changes, confirming that running the DEM simulations for a small period of time is sufficient to identify the areas of high complexity.

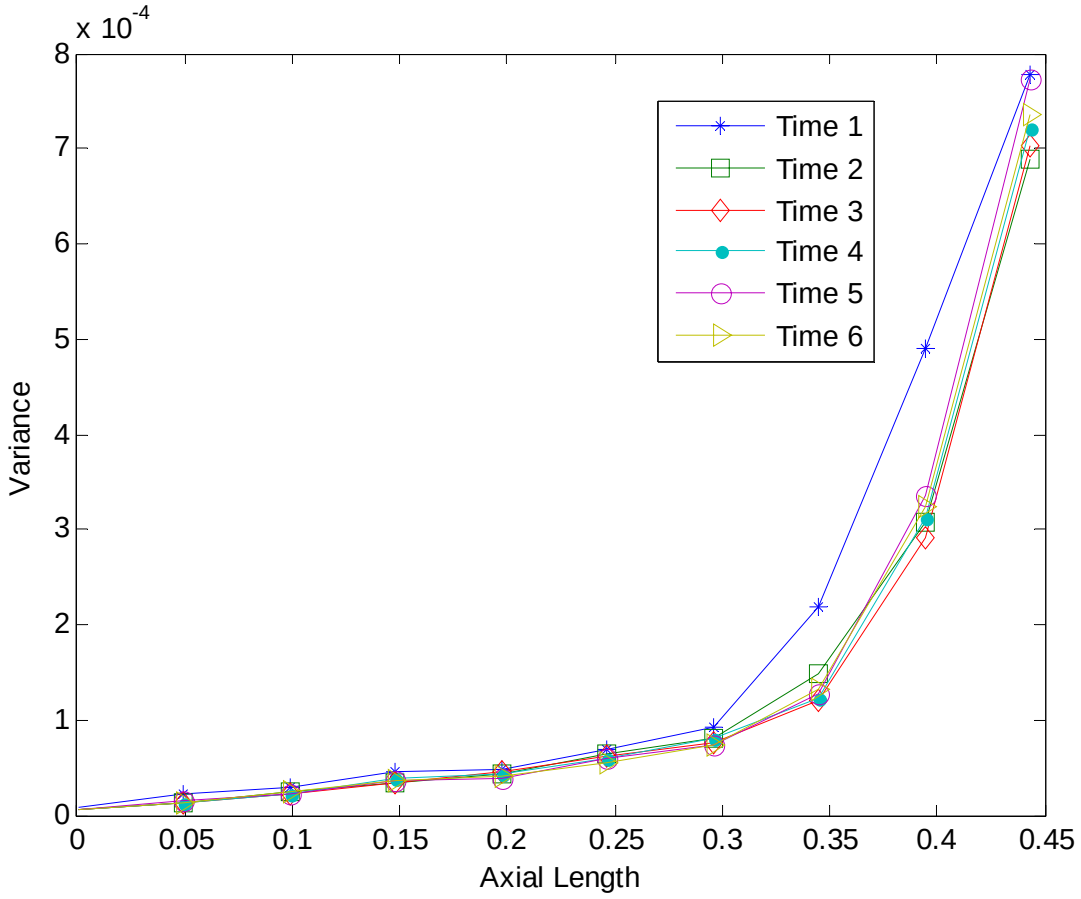

Figure 7.5: Velocity component profile at increasing time intervals (a) (.5s-.75s), (b) (.75s-1s), (c) (1s-1.25s), (d) (1.25s-1.5s), (e) (1.5s-1.75s), and (f) (1.75s-2s).

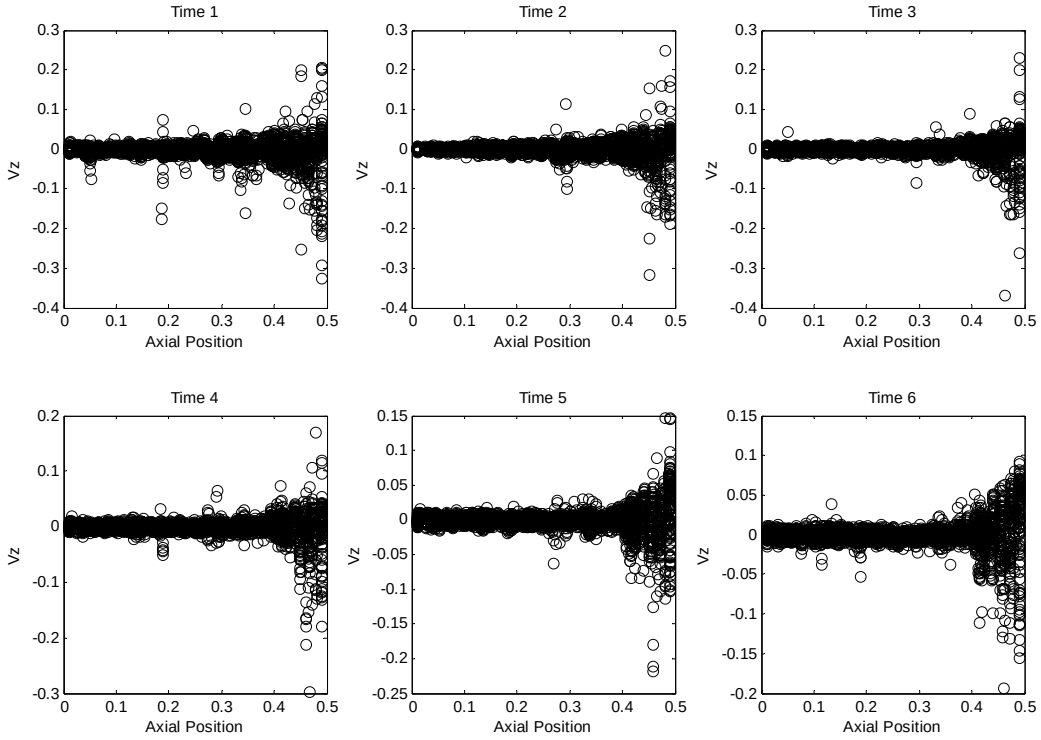

Figure 7.6: Velocity variability as a function of axial position for the following time intervals: Time 1 (.5s-.75s), Time 2 (.75s-1s), Time 3 (1s-1.25s), Time 4 (1.25s-1.5s), Time 5 (1.5s-1.75s), and Time 6 (1.75s-2s).

7.7.1 Partition Method II - Illustrative Example

This section focuses on illustrating the partitioning method that utilizes particle velocities obtained from a DEM simulation with the geometric specifications shown in Table 7.2. Using these parameters, the particles' radial velocity is obtained and plotted in Figure 7.7 with respect to axial length. As the figure shows the mixer can be partitioned into two areas, a region with an axial position greater than .25 m which is modeled with a detailed DEM simulation, whereas the rest of the vessel is simulated using compartment modeling. Thus, the mixer was discretized into ten regions, considering that the mixer length is .5 m and the particle distribution at every .05 m needs to be monitored. Thus five regions will be simulated using the DEM and the remaining five will be simulated using compartment modeling. Comparing the two partition methodologies, we observe

that the second method resulted in a larger percent of the total volume modeled using DEM, 50% compared to 40% with the first method. This is mainly because the second partition method utilizes a more accurate description of the particle behavior based on particle velocities compared to the first method, which is based on system knowledge.

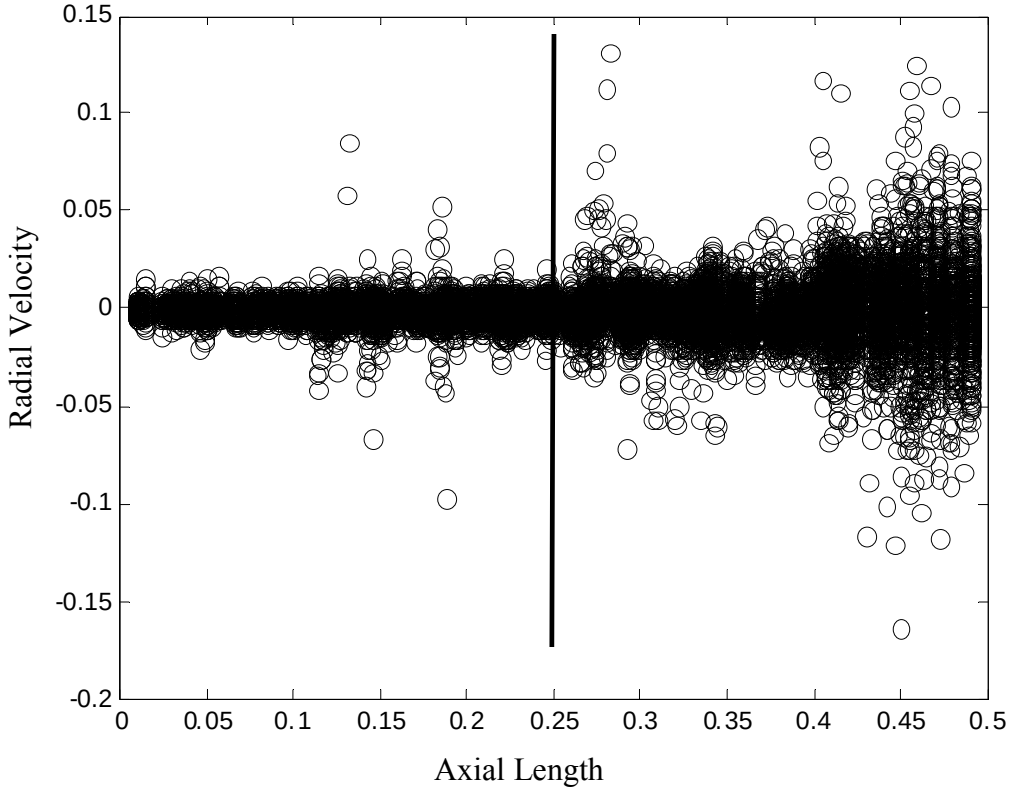

Figure 7.7: The radial velocity of particles with respect to their axial position within the cylinder. The solid line represents the point where we differentiate between two simulations.

7.8 Exchanging Particles between Models

Particles are exchanged between the different model simulations in order to account for the realistic trajectory of particles moving throughout the mixer. The particles are randomly selected from the regions closer to the neighboring simulation boundaries. However, a problem arises when exchanging particles between a DEM simulation and statistical model because the positions, velocities, and forces of the

particles entering the DEM simulation are unknown. Defining these values is important since a detailed simulation like DEM requires the particles' present conditions in order to calculate the particle's future trajectory. To address this problem, we tag each of the particles entering the DEM simulation with the exact position, velocity, and force of a randomly chosen particle exiting the DEM simulation. For example, if particle l leaves the DEM simulation whereas particle k enters, particle k will replace the position occupied by particle l as shown in Figure 7.8. It is important to point out that the physical identity of the particle does not change because the idea behind exchanging the particles is to account for the variation in composition.

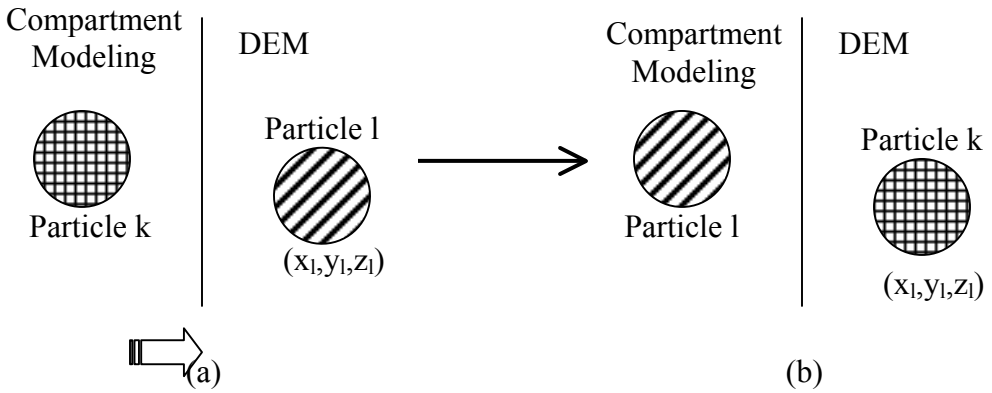

Figure 7.8: Simulation interface exchanging particles between compartments (a) before an exchange (b) after an exchange.

7.9 Quantifying Model Accuracy and Validation

For many industrial products, processes need to be strictly characterized throughout the processing stages in order to guarantee product quality. Typically the homogeneity of a powder mixture is measured via sampling within the actual process or model. The variability within the samples must comply with guidelines that require that the variance does not exceed a certain limit. There are several factors that contribute to the variability of the mixture that are not a result of mixture in-homogeneities but other

inaccuracies such as the sampling parameters, and the uncertainty due to the method used to retrieve samples. In order to minimize the error introduced due to modeling approximations, the variance is measured and bounded by a pre-specified tolerance as follows.

In order to determine how well the hybrid approach captures the overall flow in the mixing vessel we compare our results with a detailed particle dynamic model such as DEM. The accuracy of the hybrid approach is quantified by calculating the difference between the compositional profiles determined in each iteration of the hybrid approach to ones obtained either from experimental data obtained using NIR or PEPT as described in the Compartment Modeling section, or through another computer simulation as a DEM model. The results are used to validate the proposed hybrid approach; ideally the hybrid approach distributes the particles as closely to the realistic distribution in the mixing system examined. In a given spatial domain (i), the number of particles of component (j) found using the hybrid approach is defined as H_{ij} and the expected number of particles is denoted as E_{ij}, using an experimental analysis or computer simulation. Thus the percentage error is defined as: $e_{ij} = \frac{(E_{ij}-H_{ij})}{E_{ij}} \times 100$. Alternatively the sum of squares of deviations of different measurements $\sigma_j^2 = \frac{1}{\eta}\sum_{i=1}^{\eta}(E_{ij}-H_{ij})^2$ can be used to evaluate the accuracy of the proposed model where η are the total number of regions.

A smaller time point is used to prognosticate the behavior of the system denoted as $\mathbf{t}_{check}$. The longer the time period modeled, the greater the computational requirement. As shown in the Partition Method II section the behavior does not change as time progresses leading us to believe varying the check time point will not necessarily

improve the validation of the results. The metrics used to quantify the differences between the composition profiles obtained from the simulation and the results obtained either from experimental evidence or from simplified simulations are discussed in the previous section. At t_{check}, if the hybrid model obtains similar outcome to that of the substantiate results, the simulation continues until completion. Otherwise, the number of particles interchanged between simulations, the number of particles within each simulation, and the area modeled with the detailed simulation approach are adjusted and the simulation is repeated using the new parameters.

7.10 Case Study

In this section the hybrid approach is applied to model a horizontal agitated mixer, which is the same as the one depicted in Figure 7.4a. A similar horizontal mixing system was simulated by Müller and Rumph (1967), they demonstrated that the inclination of the blades promotes axial convection, likely by improving the flow of the material in the space above the blades. Moreover, Laurent and Bridgwater (2002d) showed by using PEPT with two different tracers that the mixing of a horizontal mixer has two zones in the trans-axial plane, one immediately above the agitator shaft and the other beneath it.

The geometric specifications of the horizontal mixer studied in this section are shown in Table 7.4. The vessel was loaded with two types of particles distinguished by their color (red or blue). The mixer was discretized into ten regions in order to track the particle distribution axially at every .05 m. The vessel is partitioned using the method discussed in the Partition Method I section. As a result, the variability that existed within the particle fluxes, showed that four regions should be modeled using DEM (Figure 7.9a, non-shaded area) and the remaining six (Figure 7.9a, shaded) can be simulated using

compartment modeling as shown in Figure 7.9b. The results were analyzed using the metrics discussed in the Quantifying Model Accuracy and Validation section by comparing the compositional distribution of the different types of particles with the results of a simulation, which is based entirely on DEM.

Table 7.4: Simulation Parameters

Number of Red Particles	5000
Diameter of Red Particle	.055 m
Number of Blue Particles	5000
Diameter of Blue Particle	.055 m
Radial Length of Vessel	.1 m
Axial Length of Vessel	.5 m
Length of Impeller Rod	.45 m
Diameter of Impeller	.1 m
Impeller thickness	.1 m

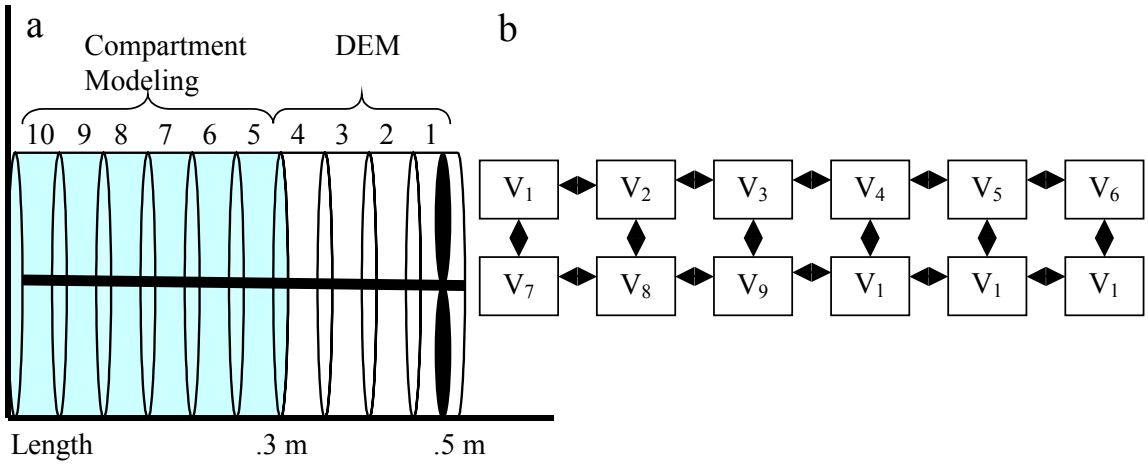

Figure 7.9: (a) Horizontal cylinder partitioned into regions tagged with a numerical representation shown on the top of the vessel (b) Compartment model using the partitioning strategy described in Section 7.6

The compositional distribution of the blue particles as a function of time for 3 regions (2,3, and 4) is shown in Figures 7.10a, and as a function of time for 2 regions (9 and 10) 10b. It is important to point out that the compositional distribution behavior determined using a DEM simulation is accurately captured by the hybrid approach. The percentage errors for both the red and blue particles in all ten regions are shown in Table

7.5. The average error for all regions and components is 7.96%. Notably, DEM simulations randomly distribute particles throughout the vessel, and as the particles collide at different positions on the impeller, the particles are deflected to neighboring regions. Thus, it is expected that region 2, the region closest to the impeller, exhibits the largest error in comparison to other regions.

Table 7.5: Average percentage errors using the first partitioning strategy described.

Region	*Red Particles Avg. % Error*	*Blue Particles Avg. % Error*
1	1.60	3.47
2	26.69	20.45
3	2.42	10.89
4	7.39	2.11
5	12.87	9.60
6	11.39	9.38
7	10.60	11.24
8	1.18	9.90
9	1.32	2.95
10	0.29	3.49

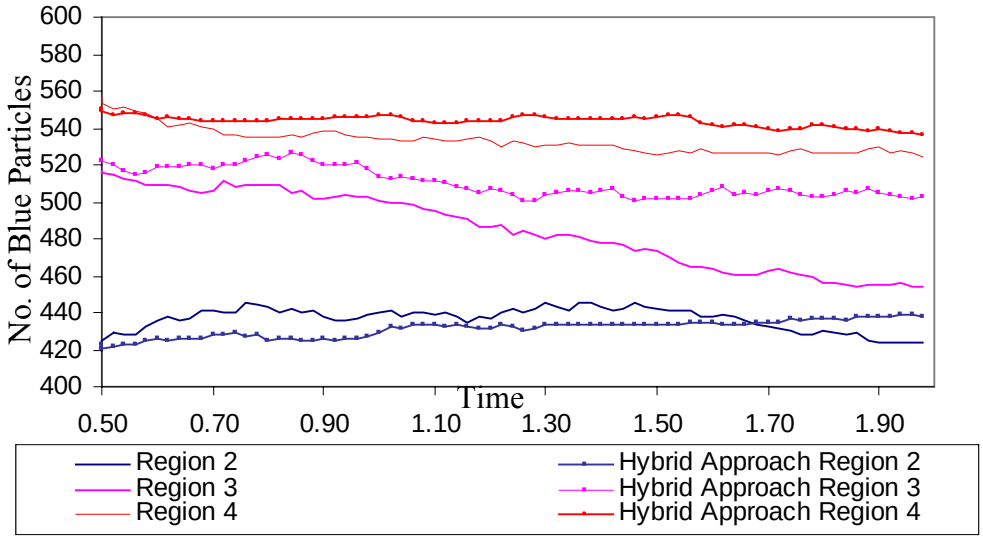

Figure 7.10: Results from the case study using the partitioning strategy described in Section 7.6. The compositional distribution of a region detained from using an entirely based DEM simulation and the hybrid approach.

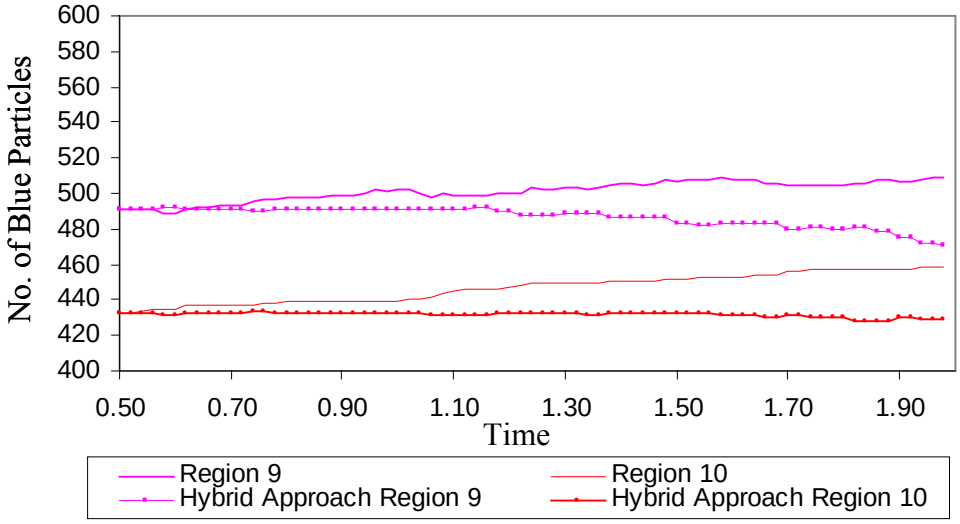

Figure 7.10: Results from the case study using the partitioning strategy described in Section 7.6. The compositional distribution of a region detained from using an entirely based DEM simulation and the hybrid approach.

The hybrid approach required 2603 CPU sec to run, whereas a simulation entirely based on DEM took 16625 CPU sec using a Sun Sparc 900 MHz Processor 2GB. Although there is an approximation error introduced in the system description utilizing the hybrid approach compared with the DEM simulation, the computational requirement is significantly reduced which allows the simulation of more realistic mixing systems.

The second partition strategy as described in the 7.2.2 Partition Method II section uses particle velocities in order to partition the mixing system. The particle velocities shown in Figure 7.11 are determined with a DEM simulation modeled for a short time period as discussed in the Partition Method II section. The velocity profile illustrates that the greatest particle velocity variability occurs for the particles that have an axial length greater than .4 m. As a result, the particles with an axial length greater than .4 m are solved with DEM and a 16-compartment model is used for the remaining area. Using the second partitioning strategy the system is simulated in 2540 sec of CPU time, in comparison to an entirely based DEM simulation that took 23820 sec of computational

time. The additional computational time arises because this partition method predicts that a larger volume of the mixer be modeled with DEM. The vessel was partitioned into ten regions in order to partition the mixing system as described in the Partition Method II section. Table 7.6 lists the percentage error for each region. The average percentage error for all regions is 5.46%, which is considered marginal given the inherent errors that exist within DEM modeling. DEM models assume several assumptions such as: spherical particle morphology, large particle dimensions, and vessels filled with small particle quantities, given all these postulations the existing DEM model results in errors that make the hybrid approach's 5.46% error seem marginal. The hybrid approach clearly reduces the computational time, but it is important to consider the trade-offs between model accuracy and computational efficiency. Using the first partition method the hybrid approach required 2603 CPU sec (computational savings were 84 % compared to DEM simulation) and the error of the solution is 7.96%, whereas the second partition method required a little more time 2540 sec for CPU time (87% computational savings) since an additional volume of the mixer is modeled with DEM but the error is reduced to 5.46%.

Table 7.6: Percentages error results using the second partitioning strategy described.

Region	***Blue Particles Avg. % Error***	***Red Particles Avg. % Error***
1	3.99	7.35
2	5.17	3.95
3	15.79	10.60
4	2.29	5.13
5	11.83	3.26
6	8.15	5.31
7	9.45	3.38
8	1.60	1.09
9	1.46	2.02
10	3.86	3.43

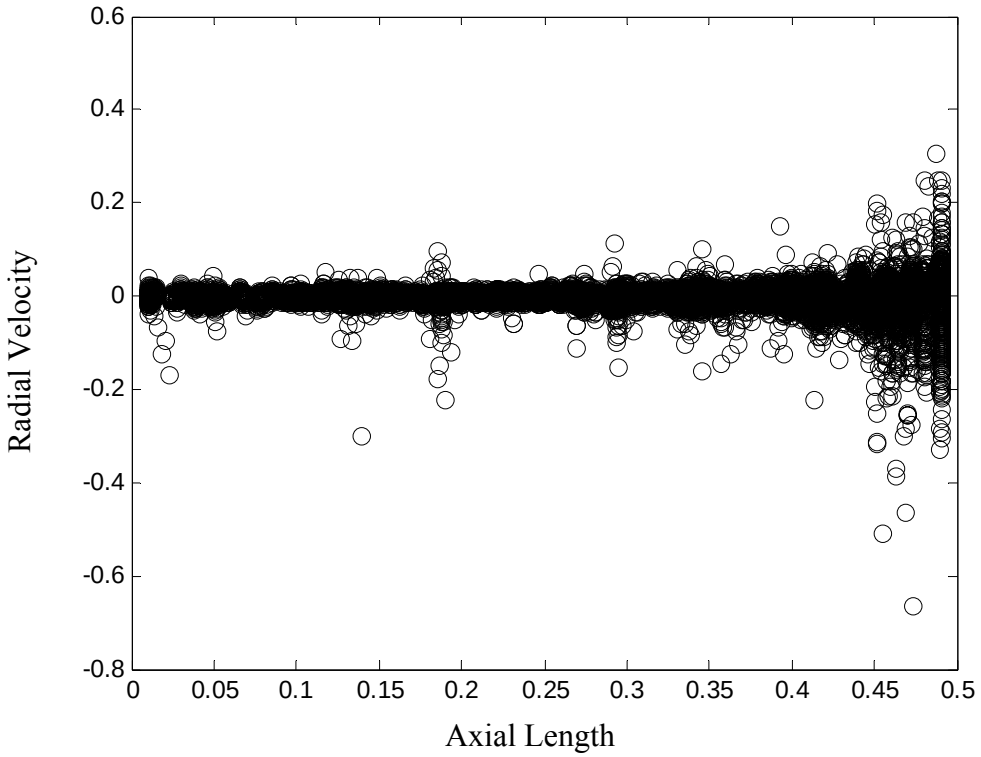

Figure 7.11: Radial velocities as a function of axial length using the partitioning strategy described in Section 7.7.

7.11 Effects of Space and Time Partitions

In this section we examine the effects of time steps and number of partitions on the performance and computational time of the hybrid approach. The cases examined use a similar vessel to the one mentioned in the previous sections which is horizontal cylinder (.5 m) with a horizontal blade (.05 m thick) held up by a rod (.01 in diameter and .5 in length) which is located at one end of the vessel as shown in Figure 7.4a. The results shown in Tables 7.7 and 7.8 consider 40% of the vessel using a DEM simulation and 60% using compartment modeling.

Table 7.7: Computational and Accuracy effect as a function of Time Steps.

Time Step, ∇t (s)	*DEM Cputime (min)*	*Hybrid Approach Cputime(min)*	*% of Computational Reduction*	*Average % of Error*
.01	638	289	55	5
.02	277	148	47	6.3
.03	183	108	41	8.04

As shown in Table 7.7, increasing the time steps does reduce the computational requirements, however, within particle dynamic simulations the barrier that exists is that larger time steps result in imprecise particle trajectory predictions. Which is a result of inaccurate calculations of the forces acting on the particles that leads to smaller accuracy. Also, as shown in Table 7.7, as the time step decreases the computational time required to run the DEM simulation increases due to the additional number of calculations, although the computational cost decreases for the hybrid approach is not as large since only 40% of the system is simulated using DEM. The computational cost increase in a DEM simulation is due to the fact that DEM simulations calculate particle positions and velocities as a first-order differential system, under the assumptions that the forces remain constant at each time step, particle positions are then calculated at each time step. Due to the constant force assumption during integration, the time step is kept small in order to achieve reasonable precision and conserve numerical stability (Wightman *et al.*, 1998).

As mentioned in the previous paragraph, since 60% of the mixer is modeled using the compartment modeling, another important parameter of the system simulation is the number of compartments considered. As the number of partitions increases the spatial area of each compartment decreases, which means that, there is a better tracking of the particle behavior within each region. However, additional particle fluxes are required

between each compartment. The computational efforts caused by increasing the number of compartments given that a constant number of particles exist is negligible in comparison to computational requirements of the spatial section modeled with DEM, as shown in Table 7.8. Increasing the number of compartments improved the accuracy of the method at the expense of a slight computational increase.

Table 7.8: Computational and Accuracy effect as a function of Partitions.

# of Partitions	***DEM Cputime(min)***	***Hybrid Approach Cputime(min)***	***% of Computational Reduction***	***Average % of Error***
10	277	104	63	6
12	277	127	56	3
16	277	125	55	1.1

7.12 Discussion and Future Work

Although DEM modeling is well developed, the computational efficiency of DEM makes the applicability of this approach rather limiting. As described in the Discrete Element Method section, Bertrand and coworkers (2005) showed that as the number of particles in the system increase, the computational intensity of a DEM simulation becomes prohibitive. Moreover, modeling the mixing effects of a large number of particles under the influence of a moving boundary increases exponentially the computational burden since convective, dispersive, and shear mechanisms should be considered. In response, DEM models are solved by embellishing the particle morphology (Moreno-Atanasio *et al.*, 2005; Li *et al.*, 2005) and reducing the number of particles in the system in order to trim down calculations (Cleary *et al.*, 1998; Cleary *et al.*, 1998), inarguably trading one type of model error for another.

In order to overcome computational complexity without sacrificing the accuracy of the calculations, a new approach is presented in this work to model powder mixing.

The main idea behind the proposed approach is to identify areas that can be solved using a statistical model and the areas that require a detailed particle dynamic model. As a result the computational time is reduced by an order of magnitude while capturing the mixing behavior of the system. However, it is also important to note the limitations in the applicability of our model. For example, Alexander and Muzzio (2001) showed that in a horizontal mixer the particle velocities are dependent on their axial position. As a result, decreasing the axial length of the vessel examined under DEM will result in dramatically different velocity values. Thus, if the exact velocity value for each particle is required, a detailed DEM should be used for the entire vessel. However, it should be noticed that based on a recent comparison to experimental measurements performed by Kuo *et al*. (2004) it has been illustrated that even DEM simulations can over-predict the particle velocities. Particle velocity calculations are affected using large time steps. As a result reducing the computational complexity, implores the possibility of trimming down the time steps. As a result, the hybrid approach can be utilized to reduce some of the computational complexity of the discrete element mixing models in order to improve the determination of particle velocities.

To our knowledge, no work has been published utilizing such a hybrid framework, but rather the common approach is to reduce the number of particles considerably. The work presented here illustrates that the computational savings are very significant and no restrictions exist that hinder adapting this approach to other convective or tumbling mixers. As a result the algorithm developed shows enormous potential to improve performance of powder mixing models. The next and final chapter summarizes the work presented in this thesis as well as some suggestions for future work.

Chapter 8

Summary Of Thesis Work and Suggestions For Future Work

In this chapter, the work presented in the thesis is summarized followed by some suggestions for future experimental work. Some preliminary results are presented utilizing a new approach to derive particle fluxes required at the compartment model from residence time distributions. Suggestions about extension of this work are also presented.

8.1 Summary Of Thesis Work

The work presented in this thesis focuses on the characterization of continuous mixing processes and the development of computational methods in order to efficiently used for modeling powder mixing. Continuous mixing is affected by a number of parameters. These parameters affect the content uniformity as well as the residence time and therefore the strain effects on the powders leaving the mixer.

In chapter 2, we found that processing angle affected the content uniformity and residence time for two different continuous mixers. Mixing angle and rotation rate affected residence time and increasing the residence time improved the mixing performance. The number of blades and blade angle affected the axial transport. In addition, increasing the axial transport resulted in lower residence times; this decreased the time inflow fluctuations could be diminished.

In chapter 3, statistical analysis was used to show that mixing angle and cohesion both affected the mixing performance. On the other hand, the effect of rotation rate was scale dependent. This was further shown in the 4-way ANOVA, where the variability between the mixers was considered to be significant.

Using Danckwerts RTD method we were able to obtain residence time distributions that showed that increasing speed resulted in lower residence times. In collaboration with the University of Birmingham, we used Positron Emission Particle Tracking (chapter 4). We examined the time a radioactive particle traveled within a continuous mixer. We confirmed that increasing the speed decreased the residence time. In addition, spatial residence time was examined inside the mixer. We were able to find that although a particle traveled at an upward inclination, variations in the fill level along the axial length did not statistically affect the particles temporal mobility. We were also able to obtain the particles mobility, in terms of total particle distance and axial dispersion coefficient. The findings showed that at a lower rotation rate, the particle traveled a much longer total particle distance.

Discrete element methods can also used to map particles' spatial trajectory, however, the method is computationally very intensive and limits the number of particles that can be modeled within the vessel. To overcome this limitation, in this work we examine a more computationally feasible methodology based on the ideas of compartment modeling. Chapters 5 and 6 present this approach to model powder mixing processes for batch and continuous systems. The method showed to be useful in elucidating how important sampling parameters affect homogeneity measurements. Sampling location, sample size, and the number of samples are some of the parameters that showed effects on computed results.

In chapter 7, we examined a new modeling approach that connects the DEM and Compartment Modeling and tested using a horizontal cylinder with two convective blades. The methods used to discretize the mixers areas are discussed. The results of the

case study show good agreement between a complete DEM model and the hybrid methodology discussed. The big advantage of this hybrid method is that the computational time was decreased by almost 50 percent. The important parameters that affected the computational time were the number of spatial regimes, the time steps, and the sizes of the areas modeled.

8.2 Suggestions For Future Work

Granular batch mixing has been examined for several decades. However, continuous mixing has just started to be examined. In this thesis, the focus was to examine different parameters including rotation rate, mixing angle, and cohesion affected the final content uniformity. In order to further expand the knowledge of the effect of cohesion, additional excipients and actives should be examined. Particularly grades of Avicel, Lactose, and MgSt, shown to agglomerate and segregate.

In addition to content uniformity and residence time measurements, several other powder properties such as density, agglomeration, attrition, and electrostatics should be measured. Measurements should be taken within the mixer as well as at the discharge, considering powder properties may change during operation handling and discharge. The understanding of these powder properties can lead to findings used to further improve mixer design and define optimal operating conditions.

Process synthesis is another important issue in pharmaceutical manufacturing, which may include recycling powder streams and unit process integration. For example considering the presence of agglomerates within APAP, the active was milled to prevent feeding agglomerates. However, during powder handing, the intensity of shear within the mixer may induce the formation of agglomeration within the process itself. In this case it

would beneficial to connect a mill at the outflow of the mixer to examine if content uniformity is improved.

Validation of the content of these samples is also important. In this study, the analysis was based on Near Infrared Spectroscopy. However, this analytical method has been shown to be significantly affected by the number of scans as well as the sample size and in some cases, the extent of sample segregation. In order to further validate the effectiveness of Near Infrared Spectroscopy additional work should focus on other analysis alternatives such as High Pressure Liquid Chromatography (HPLC) or Raman. Gathering additional alternatives, is essential in situations were Near Infrared Spectroscopy cannot accurately detect the presence of a chemical component, such as Citric Acid. Once an accurate method has been established, the next step is to ensure the accuracy of the method for online usage. Development of an efficient online method can be used as feedback information for control applications. Control methods such as Model Predictive Control, can adjust the processing parameters to ensure product quality.

The implementation of control methods such as Model Predictive Control, leads to future computational work suggestions. We have established that compartment modeling can capture mixing behavior and consider the effect of sampling in its predictions. However, in order to effectively use compartment modeling, the fluxes between compartments are very important.

Obtaining particle fluxes from residence time distributions is beneficial because of the ability to incorporate many of the physical properties that affect the transport phenomena. As mentioned in chapters 5 and 6, compartment models require substantial input (from experiments, or from particle dynamics calculations) to provide realistic

predictions. Unfortunately, at the present time, little experimental work exists on continuous mixing, particularly for pharmaceutical applications. Previously Claudel and coworkers (2003) have used residence time distributions to obtain fluxes. Obtaining particle mobility from residence time is not a new concept, considering Sherritt and coworkers (2003) approximation that uses the mean and standard deviation of the residence time to obtain the axial dispersion coefficient.

As explained in chapters 5 and 6, a compartment model can have several different structures. Furthermore, increasing the number of compartments also results in an increase in the number of particle fluxes between compartments. Here, an analytical approach to compartment specification is considered, where each compartment is considered to be a well-mixed vessel in order to illustrate the limitations of obtaining fluxes solely based on residence time distributions. Consider a 4-compartment system, where material is only fed at a flowrate of F_{in}, in the first compartment with an outflow flowrate from the 4th compartment at F_{out} as shown in Figure 8.1.

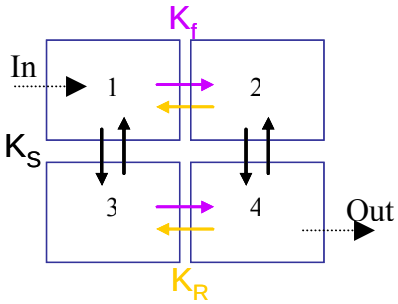

Figure 8.1: A Four-Compartment Model Schematic

The concentration within each compartment can be represented as a series of differential equations, as shown below:

$$\frac{\partial c_1}{\partial t} = F_{in} - (k_f + k_s)c_1 + k_R c_2 + k_s c_3$$
$$\frac{\partial c_2}{\partial t} = k_f c_1 - (k_R + k_s)c_2 + k_s c_4$$
$$\frac{\partial c_3}{\partial t} = k_s c_1 - (k_f + k_s)c_3 + k_R c_4$$
$$\frac{\partial c_4}{\partial t} = k_s c_2 + k_f c_3 - (k_s + k_R)c_4 - F_{out}$$

where c_i, represents the concentration within compartment i, where i=1,2,3,4. In this work we assume that the volume within each compartment is constant, in order to prevent including additional constraints on the fluxes to maintain a finite compartment volume.

The fluxes can be found using a direct search method on a specific range for each of the fluxes. For example k_f, k_r, and k_s exists in the space (t_0:Δt:t_f), where t_0 is the initial time point, Δt is the time interval, and t_f is the final time point. From there we find the fluxes that best fit the experimental residence time distributions. These fluxes are the ones with the lowest deviation between the data and the compartment model for all the n points, as follows:

$$\text{Error} = \frac{\sum_{t=1}^{n} \sqrt{(y_{model}(t) - y_{experiment}(t))^2}}{n}$$

The lowest error for the selected parameter range gives rise to the optimal fluxes, k_{fo}, k_{ro}, and k_{so}.

As discussed in chapter 2, the residence time distribution is the probability distribution function that describes the time that the powder elements spend within the process, which in this case is a continuous powder mixer. The effect of changing the

mixing inclination on the residence time is shown in Figure 8.2. The upward angle results in a broader residence time distribution whereas as the angle is shifted from the horizontal to downward the distribution width decreases.

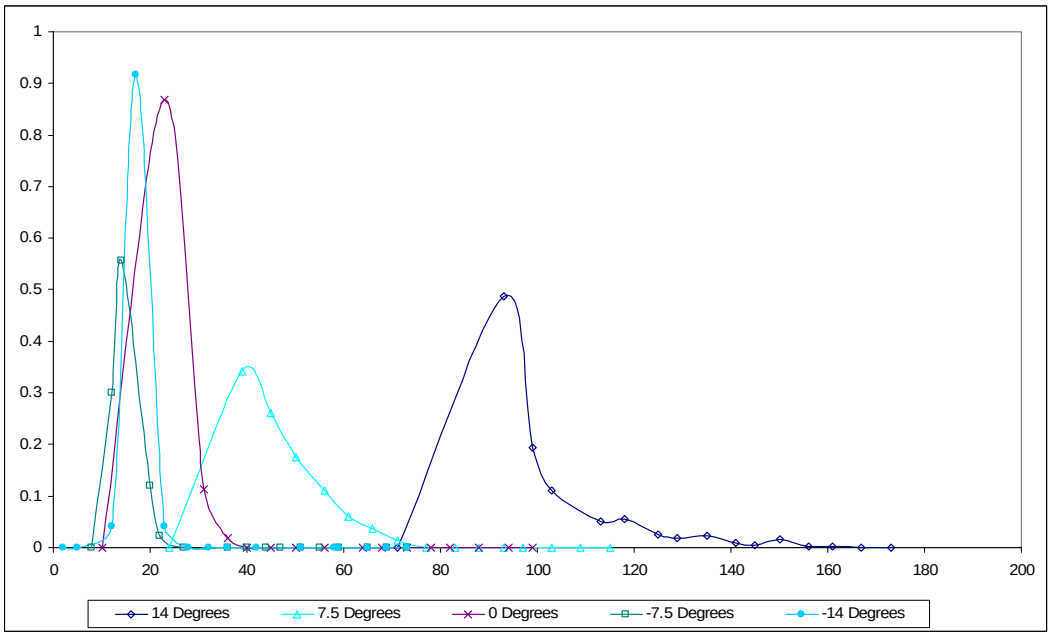

Figure 8.2: Experimental Residence Time Distributions for varying mixing angles.

In an example case study, using the five residence time distributions for different processing inclinations shown in Figure 8.4, the fluxes that "best-fit" the data were searched for the four-compartment model shown in Figure 8.1. The parameter space of the fluxes was selected to be: k_f =[0:.125:2.5], k_r=[0:.125:2.5], k_s=[0:.125:2.5]. The "best-fit" fluxes for the experimental results are shown in Table 8.1 and are shown to fit well the experimental data (Figure 8.3).

Table 8.1: Mixing Angle Flux Results for the k_f,k_r,k_s =[0:.125:2.5]

Mixing Angle	**kf**	**kr**	**ks**	**No. Points**	**Error**
Upward (+14°)	0.75	0.75	1	14	.020
Upward-Horiz. (+7.5°)	0.5	0.5	2	9	0.009
Horizontal (0°)	2.125	2.125	0.625	5	0.005
Hori-Downward (-7.5°)	1.5	1.5	0.375	6	0.058
Downward (-14°)	2.25	2.25	0.375	6	.024

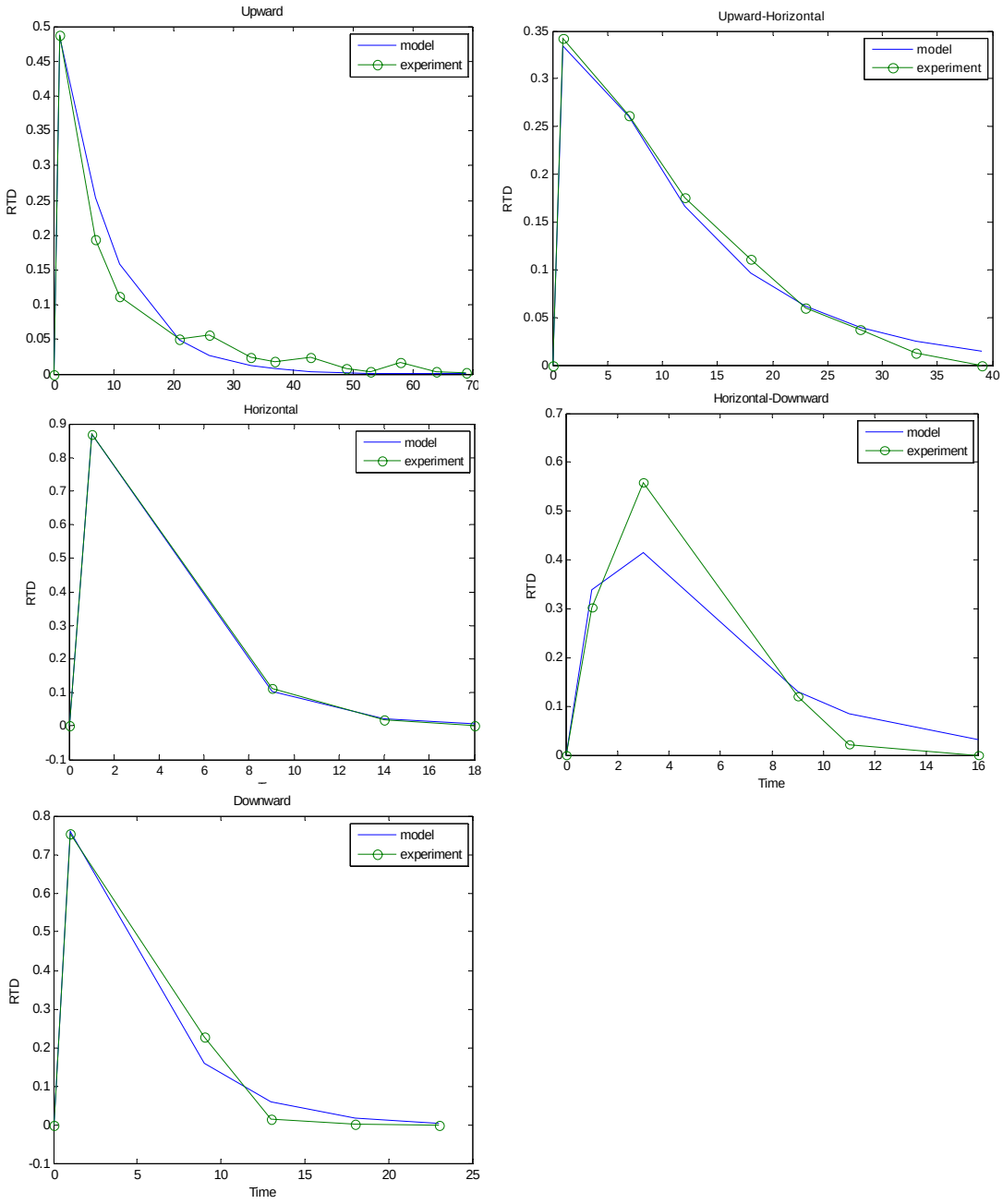

Figure 8.3: Experimental data and 4-compartment modeled (using the fluxes from **Table 8.1**) data of varying mixing inclination.

Expanding the space of fluxes k_f =[0:.125:5], k_r=[0:.125:5], k_s=[0:.125:5] slightly changes the fluxes found as shown in Table 8.2 but still results in a very small fitting error. We also decreased the interval step points to examine the subspace from 0.125 to 0.01, which resulted in the subspace k_f=[0:.01:2.5], k_r=[0:.01:2.5], k_s=[0:.01:2.5]. The

"best-fit" fluxes did change as shown in Table 8.3 but the error change remained negligible.

Table 8.2: Mixing Angle Flux Results for the k_f,k_r,k_s =[0:.125:5]

Mixing Angle	k_f	k_r	k_s	No. Points	Error
Upward	5	5	.1250	14	0.02
Upward-Horiz.	.5	.5	2	9	0.009
Horizontal	2.125	2.125	.6250	5	0.005
Hori-Downward	1.5	1.5	.375	6	0.058
Downward	2.25	2.25	.3750	6	0.024

Table 8.3: Mixing Angle Flux Results for the k_f,k_r,k_s =[0:.01:2.5]

Mixing Angle	k_f	k_r	k_s	No. Points	Error
Upward	.68	.68	2.05	14	0.019
Upward-Horiz.	2.5	2.5	.11	9	0.008
Horizontal	2.39	2.39	.54	5	0.004
Hori-Downward	1.6	1.6	.370	6	0.058
Downward	1.96	1.96	.420	6	0.023

Considering the different number of fluxes that can be obtained by utilizing this approach, finding the correct fluxes will require additional information. This additional information maybe obtained from positron emission particle tracking or discrete element methods, among other approaches. In addition to discrete element methods, other modeling frameworks that can be connected to compartment modeling exist. For example, population balance methods that account for particle agglomeration and attrition should also be investigated. Given the advantages and limitations of the existing models, a new hybrid methodology that combines more than two methods may result in an ideal modeling method for granular materials.

References

Alexander A., Muzzio F.J., 2001, Batch size increase in dry blending and mixing. (New York: Marcel Dekker.

Alexander A., Shinbrot T., Muzzio F.J., 2001, Granular Segregation in the Double-Cone Blender: Transitions and Mechanisms, Phys. Fluids, 13, 3, 578 -587.

Alexander A., Shinbrot T., Muzzio F.J., 2003, Segregation Patterns in V-Blenders, Chemical Engineering Science, 58, 487-496.

Alexander A., Arratia P., Goodridge C., Sudah O., Brone D., Muzzio F.J., 2004, Characterization of the performance of bin blenders : Part 3 Cohesive Powders, Pharm. Tech., 28, 54-74.

Alexander A.W., Chaudhuri B., Faqih A.M., Muzzio F.J., Davies C., Tomassone M.S., 2006, Avalanching flow of cohesive powders, Powder Technology, 164, 1, 13-21.

Allen T., 1981, Particle Size Measurement, 3rd ed., Chapman & Hall, London.

Arratia P.E., Duong N.-H, Muzzio F.J., Godbole P., Lange A., Reynolds S., 2006, Characterizing mixing and lubrication in the Bohle Bin blender, Powder Technology, 161, 202 - 208.

Bailey A.G., 1984, Electrostatic Phenomena during powder handling, Powder Technology, 37, 71-85.

Beaudry J.P., 1948, Blender Efficiency, Chem. Eng., 55, 112-113.

Beddow J.K., Meloy T., 1980, Testing and Characterization of Powders and Fine Particles, London: Heyden and Son Ltd.

Berntsson O., Danielsson L.G., Lagerholm B., Folestad S., 2002, Quantitative in-line monitoring of powder blending by near infrared reflection spectroscopy, Powder Technology, 123,185-193.

Berthiaux H., Marikh K, Mizonov V., Ponomarev D., Barantzeva E., 2004, Modeling Continuous Powder Mixing by Means of the Theory of Markov Chains, Particulate Science and Technology, 22, 4, 379-389.

Bertrand F., Leclaire L., Levecque G., 2005, DEM-based models for the mixing of granular materials, Chemical Engineering Science, 60, 2517-2531.

Bhattachar S.N., Hedden D.B., Olsofsky A.M., Qu X., Hsieh W.Y., Canter K. G., 2004, Evaluation of the vibratory feeder method for assessment of powder flow properties, International Journal of Pharmaceutics, 269, 385–392.

Bridgwater J., Broadbent C.J., Parker D.J., 1993, Study of the influence of blade speed on the performance of a powder mixer using positron emission particle tracking, Trans. IchemE, 71A, 675–681.

Bridson R.H., Robbins P.T., Chen Y., Westerman D., Gillham C.R., Roche T.C., Seville J.P.K., 2007, The effects of high shear blending on a-lactose monohydrate, International Journal of Pharmaceutics, 339, 84–90.

Broadbent C.J., Bridgwater J., Parker D.J., 1995, The effect of fill level on powder mixer performance using a positron camera, The Chemical Engineering Journal and The Biochemical Engineering Journal, 56, 3, 119-125.

Brone D., Alexander A., Muzzio F.J., 1998, Qualitative Characterization of Mixing of Dry Powders in V-Blenders, AICHE, 44, 271-278.

Brone D., Wightman C., Connor K., Alexander A., Muzzio F., Robinson P., 1997, Using flow perturbations to enhance mixing of dry powders in V-blenders, Powder Technology, 91, 3, 165–172.

Brone D., Muzzio F.J., 2000, Enhanced mixing in double-cone blenders, Powder Technology, 110, 179–189.

Cahn D.S., Healy T.W., Fuerstenau D.W., 1965, Blending Geometry in the Mixing of Solids, Ind. Eng. Chem. Prod. Res. Dev., 4, 318-322.

Chang R.-K., Chang S.-I, Robinson J.R., 1992, A Study of the Performance of a Modified V-Shaped Solids Mixer Using Segregating Materials, Int. J. Pharm., 80, 171-178.

Chang R.H., Badawy S., Hussain M.A., Buehler J.D., 1995, A Comparison Free-Flowing, Segregating and Non-Free-Flowing, Cohesive Mixing Systems in Assessing the Performance of a Modified V-Shaped Solids Mixer, Drug Dev. In. Pharm., 21, 3, 361-368.

Chaudhuri B., Mehrotra A., Muzzio F. J., Tomassone M. S., 2006, Cohesive effects in powder mixing in a tumbling blender, Powder Technology, 165, 2, 105-114.

Chi Square Distribution. BookRags. Retrieved 23 January 2006, from the World Wide Web. http://www.bookrags.com/sciences/mathematics/chi-square-distribution-wom.html

Chowhan Z.T., Chi L.H., 1986, Drug-excipient interactions resulting from powder mixing. IV: Role of lubricants and their effect on in vitro dissolution, J Pharm Sci., 75, 6, 542-545.

Claudel S., Fonteix C., Leclerc J.-P. Lintz H.-G., 2003, Application of the possibility theory to the compartment modelling of flow pattern in industrial processes, Chemical Engineering Science, 58, 4005-416.

Cleary P. W., Metcalfe G., and Liffman K., 1998, How well do discrete element granular flow models capture the essentials of mixing processes?, Applied Mathematical Modelling, 22, 12, 995-1008.

Cleary P.W., Sawley M.L., 2002, DEM modelling of industrial granular flows: 3D case studies and the effect of particle shape on hopper discharge, Applied Mathematical Modelling, 26, 89–111.

Cleary P.W., Prakash M., 2004, Discrete-element modeling and smoothed particle hydrodynamics: potential in the environmental sciences, Phil. Trans. R. Soc. Lond., 362, 2003-3030.

Conway S.L., Lekhal A., Khinast J.G., Glasser B.J., 2005, Granular flow and segregation in a four-bladed mixer, Chemical Engineering Science, 60, 7091–7107.

Correa S.M., 1993, Turbulence-Chemistry Interactions in the Intermediate Regime of Premixed Combustion, Combustion and Flame, 93, 41-60.

Cui Y., Van der lans R., Noorman H., and Luyben K., 1996, Compartment mixing model for stirred reactors with multiple impellers, Trans IchemE, 74, 261-271.

Cundall P.A., Strack O.D.L, 1979, A discrete numerical model for granular assemblies, Géotechnique, 47-65.

Dammer S. M., Werth J., Hinrichsen H., 2004, Electrostatically Charged Granular Matter, The Physics of Granular Media, Eds: Hinrichsen H., Wolf D.E., 253-280.

Danckwerts P.V., 1953, Continuous flow systems: distribution of residence times, Chemical Engineering Science, 2, 1–13.

DMV Product group overview, Pharmatose® milled & sieved lactose.

Einstein, H.A., 1937. Bedload transport as a probability problem. Ph.D. Dissertation (English translation: In: H.W. Shen (Ed.), 1972. Sedimentation, Water Resources Publications, Fort Collins, CO, Appendix C. 105 pp.).

EL-Hagrasy A.S., Morris H. R., D'Amico F., Lodder R. A., Drennen III J. K., 2001, Near-Infrared Spectroscopy and Imaging for the Monitoring of Powder Blend Homogeneity, Journal of Pharmaceutical Sciences, 90, 9, 1298-1307.

Fan L.T., Chen S.J., Watson C.A., 1970, Solid Mixing, Industrial and Engineering Chemistry, 62, 7, 53-69.

Faqih A.M., Chaudhuri B., Alexander A.W., Davies C., Muzzio F.J., Tomassone M. S., 2006, An experimental/computational approach for examining unconfined cohesive powder flow, International Journal of Pharmaceutics, 324, 2, 116-127.

FDA Guidance for Industry, October 2003, Powder Blends and Finished Dosage Units – Stratified In-Process Dosage Unit Sampling and Assessment, Pharmaceutical CGMP's.

Gayle J.B., Lacey O.L., and Gary J.H., 1958, Mixing of Solids-chi-Square as a Criterion, Ind. Eng. Chem., 50, 1279-1282.

Gilbertson M. A., Eames I., 2003, The influence of particle size on the flow of fluidised powders, Powder Technology, 131, 2-3, 197-205.

Gupta S. D., Khakhar D.V., Bhatia S.K., 1991, Axial segregation of particles in a horizontal rotating cylinder, Chemical. Eng. Sci., 46, 1513-1517.

Harwood C., Walanski K., Luebcke E., Swanstrom C., 1975, The Performance of Continuous Mixers for Dry Powders, Powder Technology, 11, 289-296.

Hogg R., Cahn D., Healy T., Fuerstenau D., 1966, Diffusional mixing in an ideal system, Chemical Engineering Science, 21, 1025-1038.

Hou T., Su C., Liu W., 2007, Parameters optimization of a nano-particle wet milling process using the Taguchi method, response surface method and genetic algorithm, Powder Technology, 173, 153–162.

Hutton S. R., Forsyth A. J., Rhodes M. J., Osborne C. F., 2004, Effect of interparticle force on mixing and segregation of dry granular materials, Physical Review E 70, 031301.

Iddir H., Arastoopour H., Hrenya C., 2005, Analysis of binary and ternary granular mixtures behavior using the kinetic theory approach, Powder Technology, 151, 117-125.

Ingram A., Seville J.P.K., Parker D.J., Fan X., R.G. Forster, 2005, Axial and radial dispersion in rolling mode rotating drums, Powder Technology, 158, 1-3, 27, 76-91.

Jaeger H.M., Nagel S., 1992, Physics of the Granular State, Science, 255, 1523-1531.

Jenkins J.T., Savage S.B., 1983, A theory for the rapid flow of identical, smooth, nearly elastic, spherical particles, J.Fluid Mech., 130, 187-202.

Johansen A, Schaefer T., 2001, Effects of interactions between powder particle size and binder viscosity on agglomerate growth mechanisms in a high shear mixer, Eur J Pharm Sci., 12, 3, 297-309.

Jones J.R., Parker D.J., Bridgwater J., 2007, Axial mixing in a ploughshare mixer, Powder Technology, 178, 73–86.

Jullien R., Meakin P., 1990, A mechanism for particle size segregation in three dimensions, Nature, 344, 425-427.

Kaneko Y., Shiojima T., Horio M., 2000, Numerical analysis of particle mixing characteristics in a single helical ribbon agitator using DEM simulation, Powder Technology, 108, 55–64.

Kehlenbeck V., Sommer K., 2003, Possibilities to improve the short-term dosing constancy of volumetric feeders, Powder Technology, 138, 51– 56.

Kenney J.F., Keeping E.S., 1962, Geometric Mean, Mathematics of Statistics, 3rd ed. Princeton, NJ: Van Nostrand, 54-55.

Kremmer M., Favier J.F., 2001, A method for representing boundaries in discrete element modeling, part I: geometry and contact detection, International Journal for Numerical Methods in Engineering, 51, 1407-1421.

Kuo H.P., Knight P.C., Parker D.J., Adams M.J., Seville J.P.K., 2004, Discrete element simulations of a high-shear mixer, Advanced Powder Technology, 15, 297-309.

Kuo H.P., Knight P.C., Parker D.J., Seville J.P.K., 2005, Solids circulation and axial dispersion of cohesionless particles in a V-mixer, Powder Technology, 152, 1-3, 133-140.

Laurent B.F.C, Bridgwater J., 2002a, Convection and segregation in a horizontal mixer, Powder Technology, 123, 9-18.

Laurent B.F.C, Bridgwater J., 2002b, Performance of single and size-bladed powder mixers, Chemical Engineering Science, 57, 1695-1709. …. Change it

Laurent B.F.C, Bridgwater J., 2002c, Influence of agitator design on powder flow, Chemical Engineering Science, 57, 3781-3793.

Laurent B.F.C., Bridgwater J., 2002d, Granular Flow in a Horizontal Drum Stirred by a Single Blade, AICHE, 48, 50-58.

Laurent B.F.C., 2006, Scaling factors in granular flow—analysis of experimental and simulations results, Chemical Engineering Science, 61, 4138–4146.

Lemieux M., Bertrand F., Chaouki J., Gosselin P., 2007, Comparative study of the mixing of free-flowing particles in a V-blender and a bin-blender, Chemical Engineering Science, 62, 1783 – 1802.

Lemieux M., Léonard G., Doucet J., Leclaire L.-A., Viens F., Chaouki J., Bertrand F., 2008, Large-scale numerical investigation of solids mixing in a V-blender using the discrete element method, Powder Technology, 181, 2, 205-216.

Li Y., Xu Y., Thornton C.A, 2005, Comparison of discrete element simulations and experiments for 'sandpiles' composed of spherical particles, Powder Technology, 160, 219-228.

Lim S. -Y., Davidson J. F., Forster R. N., Parker D. J., Scott D. M., Seville J.P.K., 2003, Avalanching of granular material in a horizontal slowly rotating cylinder: PEPT studies, Powder Technology, Volume 138, Issue 1, 25-30.

Li-Shin Lu a, Shu-San Hsiau, Mixing in a vibrated granular bed: Diffusive and convective effects, Powder Technol. (2007), doi:10.1016/j.powtec.2007.07.036

Liss E. D., Glasser B. J., 2001, The influence of clusters on the stress in a sheared granular material, Powder Technology, 116, 116–132.

Liss E.D., Conway S. L., Zega J. A., Glasser B.J., 2004, Segregation of Powders during Gravity Flow through Vertical Pipes, Pharmaceutical Technology, 28, 2, 78-96.

Lun C.K.K., Savage S.B.D., Jeffrey J., Chepurnity N., 1984, Kinetic theories for granular flow: inelastic particles in Couette flow and slightly inelastic particles in a general flow field, J. Fluid Mech., 140, 223-256.

Manjunath K., Dhodapkar S., Jacob K., 2004, Mixing of Particulate Solids in the Process Industries, Handbook of Industrial Mixing: Science and Practice, Ed. E. Paul, V.A. Atiemo-Obeng, S.M. Kresta, John Wiley & Sons, Inc.

Marikh K., Berthiaux H., Mizonov V., Barantseva E., 2005, Experimental study of the stirring conditions taking place in a pilot plant continuous mixer of particulate solids, Powder Technology, 157, 138-143.

Massol-Chaudeur S., Berthiaux H., Dodds J.A., 2002, Experimental study of the mixing kinetics of binary pharmaceutical powder mixtures in a laboratory hoop mixer, Chemical Engineering Science, 57, 19, 13, 4053-4065.

McCarthy J.J., Ottino J.M., 1998, Particle dynamics simulation: a hybrid technique applied to granular mixing, 97, 91-99.

Mehrotra A., Muzzio F.J., Shinbrot T., 2007, Spontaneous Separation of Charged Grains, Physical Review Letter, 99, 058001.

Metcalfe G., Lachlan G., Liffman K., Cleary P., and Shattuck M., 1998, Imaggiing of laboratory-scale industrial granular flows. World congress particle technology, vol. 3, Paper 349 ISBN 0-85295-401-8. Rugby, UK: Institution of Chemical Engineers.

Moakher M., Shinbrot T., Muzzio F.J., 2000, Experimentally validated computations of flow, mixing and segregation of non-cohesive grains in 3D tumbling blenders. Powder Technology, 109, 58–71.

Moreno-Atanasio R., Antony S.J., Ghadiri M., 2005, Analysis of flowability of cohesive powders using Distinct Element Method, Powder Technology, 158, 51-57.

Muerza S., Berthiaux H., Massol-Chaudeur S., Thomas G., 2002, A dynamic study of static mixing using on-line image analysis, Powder Technol., 128, 195-204.

Müller W., Rumph H., 1967, Powder mixing in a mixer with axial agitation, Chem. Ing. Tech., 39, 365-373.

Muzzio F.J., Llusa M., Goodridge C.L., Duong N.-H., Shen E., in press, Evaluating the mixing performance of a ribbon blender, Powder Technology, doi: 10.1016/j.powtec.2007.12.013.

Muzzio F.J, Robinson P., Wightman C., Brone D., 1997, Sampling practices in powder blending, International Journal of Pharmaceutics, 155, 2, 153-178.

Muzzio F.J., Shinbrot T., Glasser B.J., 2002, Powder technology in the pharmaceutical industry: the need to catch up fast, Powder Technology, 124, 1– 7.

Muzzio F.J., Alexander A., Goodridge C., Shen E., Shinbrot T., 2004, Solids Mixing Part A: Fundamentals of Solids Mixing. In: Paul, E.L., Atiemo-Obeng V.A., Kresta S.M. (Eds.), The Handbook of Industrial Mixing Science and Practice, Wiley, New York.

Muzzio F.J., Goodridge C.L., Alexander A., Arratia P., Yang H., Sudah O., Merge G., 2003, Sampling and characterization of pharmaceutical powders and granular blends, International Journal of Pharmaceutics, 250, 1, 51-64.

Orband J.L.R., Geldart D., 1997, Direct measurement of powder cohesion using a torsional device, Powder Technology, 92, 25-33.

Ottino J.M., Khakhar D.V., 2000, Mixing and Segregation of Granular Material, Annual Review of Fluid Mechanics, 32, 55-91.

Pandey P., Song Y., Kayihan F., Turton R., 2005, Simulation of particle movement in a pan coating device using discrete element modeling and its comparison with video-imaging experiments, Powder Technology, 79-88.

Parker D.J., Dijkstra A.E., Martin I.T.W., Seville J. P. K., 1997, Positron emission particle tracking studies of spherical particle motion in rotating drums, Chemical Engineering Science, 52, 13, 2011-2022.

Pernenkil L., Cooney C., 2006, A review on the continuous blending of powders, Chemical Engineering Science, 61, 720-742.

Porion P., Sommier N., Faugeréa A.M, Evesque P., 2004, Dynamics of size segregation and mixing of granular materials in a 3D-blender by NMR imaging investigation, Powder Technology, 141, 55–68.

Portillo P.M., Ierapetritou M.G., Muzzio F.J., 2008, Characterization of continuous convective powder mixing processes, Powder Technology, 182, 368-379.

Powell M.S., Nurick G.N., 1996, A study of charge in rotary mills. Part 2-Experimental work, Minerals Engineering, 9, 343-350.

Pyrce R. S., Ashmore P. E., 2003, The relation between particle path length distributions and channel morphology in gravel-bed streams: a synthesis, 56, 1-2, 167-187.

Ramkrishna D., Mahoney A.W., 2002, Population balance modeling. Promise for the future, Chemical Engineering Science, 57, 595 – 606.

Riley M.R., Buettner H.M., Muzzio F.J., Reyes S.C., 1995, Monte Carlo simulation of diffusion and reaction in two-dimensional cell structures, Biophys J., 68, 5, 1716–1726.

Ristow G.H., 1996, Dynamics of granular material in a rotating drum, Europhysics Letters, 34, 263-268.

Rollins D., Faust D., Jabas D., A superior approach to indices in determining mixture segregation, 1995, Powder Technology, 84, 277-282.

Ross S., 2002, A First Course in Probability, 6th Ed., Prentice Hall, Upper Saddle River, NJ.

Shah J.J., Fox R.O., 1999, Computational Fluid Dynamics Simulation of Chemical Reactors: Application of in Situ Adaptive Tabulation to Methane Thermochlorination Chemistry, Ind. Eng. Chem. Res, 38, 4200-4212.

Sinnott M., Cleary P., 2003, 3D DEM simulations of a High Shear Mixer, Third International Conf. on CFD in the Minerals and Process Industries.

Stewart R.L., Bridgwater J., Zhou Y.C., Yu A.B., 2001, Simulated and measured flow of granules in a bladed mixer, a detailed comparison, Chemical Engineering Science, 56, 5457–5471.

Sudah O.S., Coffin-Beach D., Muzzio F.J., 2002a, Quantitative characeterization of mixing of free-flowing granular material in tote (bin)-blenders, Powder Technology, 126, 191-200.

Sudah O.S., Coffin-Beach D., Muzzio F.J., 2002b, Effects of blender rotational speed and discharge on the homogeneity of cohesive and free-flowing mixtures, International Journal of Pharmaceutics, 247, 57-68.

Sudah O. S, Chester A.W., Kowalski J.A., Beeckman J.W., Muzzio F.J., 2002c, Quantitative characterization of mixing processes in rotary calciners, Powder Technology, 126, 166-173.

Thýn J., Duffek K., 1977, Powder Mixing in a Horizontal Batch Mixer, Powder Technology, 15, 193-197.

Van de Velden M., Baeyens J., Seville J.P.K. and Fan X., In Press, The solids flow in the riser of a Circulating Fluidised Bed (CFB) viewed by Positron Emission Particle Tracking (PEPT), Powder Technology.

Vrábel P, Van der lans R., Cui Y., Luyben K., 1999, Compartment model approach: Mixing in large scale aerated reactors with multiple impellers, Trans IchemE, 77, 291-302.

Walker J., Rollins D., 1997, Detecting powder mixture inhomogeneity for non-normal measurement errors, Powder Technology, 92, 9-15.

Walton O.R., Braun R.L., 1986, Viscosity, granular-temperature, and stress calculations for shearing assemblies of inelastic, frictional disks, J. Rheology, 50, 949-980.

Wang X., Dong Z., Zhang J., Zhao A., 2002, Relations between morphology, air flow, sand flux and particle size on transverse dunes, Taklimakan Sand Sea, China, 27, 5, 515 – 526.

Weinekötter R., Reh L., 1994, Characterization of Particulate Mixtures by In-Line Measurments, Particle and Particle Systems Characterization, 11, 4, 284-290.

Weinekötter R., Reh L., 1995, Continuous Mixing of Fine Particles, Particle and Particle Systems Characterization, 12, 1, 46-53.

Weinekötter R., Reh L., 2000, Mixing of Solids, Kluwer Academic Publishers, Dordrecht.

Wightman C., Muzzio F.J., Wilder J., 1996, A quantitative image analysis method for characterizing mixtures of granular materials, Powder Technology, 89, 165-176.

Wightman C., Moakher M., Muzzio F.J., 1998, Simulation of Flow and Mixing of Particles rotating and rocking cylinder, AICHE, 44, 6, 1266-1276.

Wightman C., Muzzio F. J., 1998, Mixing of granular material in a drum mixer undergoing rotational and rocking motions I. Uniform particles, Powder Technology, 98, 2, 113-124.

Williams J., Rahman M., 1971a, Prediction of the performance of continuous mixers for particulate solids using residence time distributions Part I. Theoretical, Powder Technology, 5, 87-92.

Williams J., Rahman M., 1971b, Prediction of the performance of continuous mixers for particulate solids using residence time distributions, Part II: Experimental, Powder Technology, 5, 307-316.

Williams J.C., 1976, Segregation of particulate materials--a review, Powder Technology, 15, 2, 245-251.

Williams R.A., Xie C.G., 1993, Tomographic techniques for characterizing particulate processes, Particle and Particle Systems Characteristics, 10, 252-261.

Yang R.Y., Zou R.P., Yu A.B., 2003, Microdynamic analysis of particle flow in a horizontal rotating drum, Powder Technology, 130, 138-146.

Yang Z., Fryer P.J., Bakalis S., Fan X., Parker D.J., Seville J.P.K., 2007, An improved algorithm for tracking multiple, freely moving particles in a Positron Emission Particle Tracking system, Nuclear Instruments and Methods in Physics Research A, 577, 585–594.

Yang Z., Parker D.J., Fryer P.J., Bakalis S., Fan X., 2006, Multiple-particle tracking—an improvement for positron particle tracking, Nuclear Instruments and Methods in Physics Research Section A: Accelerators, Spectrometers, Detectors and Associated Equipment, 564,1, 332-338.

Zhou Y.C., Yu A.B., Stewart R.L., Bridgwater J., 2004, Microdynamic analysis of the particle flow in a cylindrical blade mixer, Chemical Engineering Science, 59, 1343-1364.

Zhu H.P., Yu A.B., 2006, A theoretical analysis of the force models in discrete element method, Powder Technology, 161, 122-129.

Zhu H.P., Yu A.B., Wu Y.H., 2006, Numerical investigation of steady and unsteady state hopper flows, Powder Technology, 170, 3, 125-134.

CURRICULUM VITA

PATRICIA M. PORTILLO

EDUCATION

2003 B.S. Highest Honors Chemical Engineering, Rutgers School of Engineering, The State University of New Jersey, Piscataway, New Jersey

PEER-REVIEWED JOURNAL PUBLICATIONS

2006 Portillo P.M., Muzzio F.J., Ierapetritou M.G., 2006, Characterizing Powder Mixing Processes utilizing Compartment Models, International Journal of Pharmaceutics, 320, 14-22.

2007 Portillo P.M., Muzzio F.J., Ierapetritou M.G., 2007, Hybrid DEM-Compartment Modeling Approach for Granular Mixing, AICHE J., 53, 1, 119-128.

2008 Portillo P.M., Ierapetritou M.G., Muzzio F.J., 2008, Characterization of continuous convective powder mixing processes, Powder Technology, 182, 368-378.

2008 Portillo P.M., Muzzio F.J., Ierapetritou M.G., Investigation of the Mixing Behavior of a Horizontal Continuous Mixing Process, Submitted to Journal of Pharmaceutical Innovation Jan. 2008

2008 Portillo P.M., Ierapetritou M.G., Tomassone S., McDade C., Clancy D., Avontuur P.C., Muzzio F.J., Quality by Design Methodology for Development and Scale-Up of Batch Mixing Processes, Submitted to Journal of Pharmaceutical Innovation Feb. 2008

2008 Portillo P.M., Ierapetritou M.G., Muzzio F.J., Effects of Rotation Rate, Mixing Angle, and Cohesion in two Continuous Powder Mixers – a statistical approach, *Manuscript in preparation*

2008 Portillo P.M., Ingram A., Seville J.K., Ierapetritou M.G., Muzzio F.J., Investigating the effects of Speed, Flowrate, and Cohesion using PEPT on a Continuous Blender, *Manuscript in preparation*